CRYSTALLIZATION AND MELTING KINETICS

OF GERMANIUM DIOXIDE

by

PETER JOSEPH VERGANO

B.S.   Rutgers University   (1965)

A.B.   Rutgers University   (1965)

Submitted in Partial Fulfillment

of the Requirements

for the Degree of

DOCTOR OF SCIENCE

at the

Massachusetts Institute of Technology

1969

Signature of Author ____

Signature of Professor
in Charge of Research _

Donald R. Uhlmann

Signature of Chairman
of Departmental Committee
on Graduate Students _____

Philip L. de Bruyn

CRYSTALLIZATION AND MELTING KINETICS

OF GERMANIUM DIOXIDE

by

PETER JOSEPH VERGANO

Submitted to the Department of Metallurgy and Materials Science,
August 18, 1969, in partial fulfillment of the requirements for
the degree of Doctor of Science.

ABSTRACT

The effects of melting temperature and atmosphere upon the
state of reduction of germanium dioxide glass have been determined.
Glasses varying from very nearly stoichiometric to .004% reduced were
prepared; the state of reduction of these glasses was determined from
an absorption peak at 2450 Å in their ultraviolet absorption spectra.

Growth rates of hexagonal germanium dioxide crystals were
measured in four glasses of differing stoichiometries over a range of
undercooling from 3 to 416 Centigrade degrees. In air, nitrogen, and
oxygen atmospheres, the crystal thickness was found to increase linearly
with time at all temperatures studied. The measured crystal growth
rates covered a range from 10^{-8} cms/sec at 416° undercooling to a peak
of 10^{-5} cms/sec at about 75° undercooling. Crystal growth rates in all
the glasses exhibited the form of growth rate variation with temperature
typical of glassforming materials. Crystal growth rates were found to
increase with the state of reduction of the glass over the full tempera-
ture range studied. Growth rates in the .004% reduced glass were a
factor of 2 greater than those in stoichiometric glass at high under-
coolings and up to a factor of about 4 greater at low undercoolings.

No bulk nucleation was observed in any specimen; surface
nucleation was unavoidable on any glass held at room temperature before
being heated to the nucleation temperature range.

A fine thermocouple (.001") embedded in a glass indicated that
there was no detectable difference between the crystal-liquid interface
temperature and the furnace temperature as the crystal grew past the
thermocouple at a near-peak rate of 2 microns/minute.

Various extrinsic growth effects were observed. A form of rapid growth independent of specimen geometry occurring at temperatures above 950°C and a geometry-dependent type of extrinsic growth occurring at lower temperatures were both associated with sodium impurities. Extrinsic growth rates estimated to be two or three orders of magnitude greater than intrinsic growth rates were observed.

Using viscosity data of other investigators obtained on glass melted in the same way as one of the glasses studied, it was determined that the reduced growth rate

$$\frac{\text{growth rate x viscosity}}{1 - \exp\left(\frac{-\Delta H_F \Delta T}{RTT_E}\right)}$$

of GeO_2, a low entropy of fusion material, is independent of undercooling over the full range of undercooling studied, 16 to 416°C.

Melting rates were measured using a very slightly reduced glass (.002% reduced) and a very nearly stoichiometric glass over a temperature range from 5° to 23° superheat. The reduced glass exhibited faster melting in this temperature range. A plot of the growth and melting rates at temperatures near the melting temperature against temperature was found to be continuous with no change in slope through the melting temperature for both glasses whose melting rates were measured. The values of reduced growth and melting rates of these glasses were also unchanged at the melting temperature.

Melting and crystallization specimens always exhibited nonfaceted crystal-liquid interfaces. Consistent with this, an x-ray analysis of growth specimens indicated that growth was relatively isotropic.

The observed nonfaceted interface morphologies, the growth isotropy, the reduced growth rate independent of temperature, and the growth-melting rate continuity at the melting temperature all lend strong support to reasoning based on the Jackson Model of the Interface.

Thesis Supervisor: Donald R. Uhlmann

Title: Associate Professor of Ceramics

TABLE OF CONTENTS

LIST OF TABLES

LIST OF FIGURES

ACKNOWLEDGEMENTS

I. INTRODUCTION

I.1 Advantages of Glass-Forming Systems in Crystal Growth and Melting Studies

Glass-forming systems generally have properties advantageous to the study of melting and crystal growth kinetics. Such systems are unusual because their crystal growth rates in general are not controlled by heat flow effects. In a few glass-forming systems, melting also has been found not to be controlled by heat flow even when taking place at an appreciable superheat. Because of the low crystallization and melting rates intrinsic to glass-formers, the temperature of the crystal-liquid interface can be negligibly different from that of the furnace during crystal growth and melting.

Melting and crystallization, though frequently occurring at elevated temperatures, can be studied at room temperature with specimens quenched from elevated temperatures. In quenching, the melt forms a glass and the location and morphology of the crystal-liquid interface remains unchanged. For growth and melting studies at temperatures where radiative heat loss is not a problem, growth or melting measurements may be made by direct observation in hot or cold-stage microscopes. Direct observation of growth in capillary tubes is also possible. All of these techniques are simplified by the slow growth and melting rates intrinsic to glass-forming systems.

Furthermore, crystal growth rates covering several orders of magnitude can frequently be measured over a range of undercooling often in hundreds of Centigrade degrees. In contrast, in materials of high fluidity such as the metals, intrinsic crystal growth measurements are limited to a fraction of a degree undercooling in most systems. All of these advantages result directly from the fact that glass-forming materials typically exhibit a high viscosity upon melting and/or a rapid increase in viscosity with undercooling.

I.2   Purpose of This Thesis

The purpose of this thesis is to describe and to explain the processes of melting and crystal growth of hexagonal GeO_2. GeO_2 was chosen for study because it is a good glass-forming material which exhibits a low entropy of fusion. A low entropy of fusion glassformer was chosen to try to determine the relevance of the Jackson Model of the Interface and the standard models of crystal growth in predicting the variation of crystal growth rate with under-cooling and of melting rate with superheating.

At the inception of this study, this was to be the first thorough study of crystallization and melting of a low entropy of fusion glassformer. It was found that to describe completely the crystallization behavior of this material the effects of impurities, atmosphere, and the state of reduction of the glass had also to be investigated.

II. PREVIOUS RELEVANT WORK

II.1 Theories of Crystal Growth

II.1.1 General Description

The phenomena of crystallization have long been of scientific interest. J. Willard Gibbs, in 1878,(1) considered many of the characteristics of crystal growth which are still of interest. Each modern theory of crystal growth presents a picture of the crystal-liquid interface viewed on an atomic scale (with the emphasis on characterizing the crystal rather than the liquid phase), proposes a mechanism by which molecules assume their correct position in the lattice, and predicts what effects variables such as temperature, pressure, and supersaturation will have on crystal growth.

In this review, only that part of each theory pertinent to this study shall be discussed, i.e., it is limited to isothermal growth and melting of crystals in a melt of the same composition. It should be emphasized that all the standard models describing crystal growth are based on greatly simplifying assumptions. Simplification has been emphasized because of the difficulty of describing the interface structure and the relation of structure to growth and melting rates. These models are further simplified in assuming only one mechanism of growth occurring at any one time.

The first results of an attempt to describe growth and melting taking into account details of interface structure with the aid of a computer have been reported(2). This approach has led to the growth rate equations of earlier models when their proper limitations are introduced into its general equation.

II.1.2 Surface Nucleation Growth

Many early models of crystal growth(3-7) pictured the crystal-liquid interface as discontinuous. The outermost crystalline atomic layer was regarded as perfectly ordered; the next "layer" of atoms was regarded as amorphous with all the properties of atoms in the bulk liquid. From analogy with models of blocks and generally assuming only nearest neighbor interactions, it was shown that atoms most readily join a crystal along a repeatable step which sweeps over a face of a crystal to advance its growth by one atomic layer. The important obstacle to growth in this manner involves the initiation of a new layer. Each layer must start as a "surface nucleus", a group of atoms sufficient in number to overcome the surface energy barrier to the formation of a new layer.

Assuming surface nucleation controlled crystal growth, Becker and Doring(8) and Volmer and Marder(9) formulated quantitative theories relating crystal growth rates to measurable parameters. A more recent treatment(10), utilizing the Turnbull and Fisher(11) approach to nucleation is essentially the same but better suited to growth from the melt.

This approach assumes a nucleation rate equation based on absolute reaction rate theory. It is also assumed that, once nucleated, a layer of atoms will spread over the entire area of the interface before another nucleus has had time to form. Therefore, each nucleus formed results in an advancement of the interface of one interatomic spacing. Assuming that the shape of a surface nucleus of critical size is a disk one interatomic spacing, a_o high, the equation describing surface nucleation growth is (12):

$$u = \frac{N_s D''A}{a_o} \exp\left(\frac{-\pi a_o \sigma^2}{(\Delta S_F)_V k T \Delta T}\right) \qquad (\text{II.1})$$

where   u = crystal growth rate

   N_s = number of atoms per unit area

   D" = kinetic coefficient for transport at the interface

   A = area of the interface

   σ = surface free energy (isothermal work to form a unit area of surface)

   $(\Delta S_F)_V$ = entropy of fusion per unit volume

   k = Boltzmann constant

   T = temperature

   ΔT = undercooling

The undercooling dependence of the growth rate in the case of surface nucleation growth with constant surface energy has the form:

$$u \propto D'' \exp \left(\frac{- \text{constant}}{T\Delta T}\right)$$

Burton, Cabrera, and Frank(13) later concluded that surface nucleation theory could not account for the observable rates at which crystals grow at low supersaturations. Burton, Cabrera, and Frank considered the equilibrium concentrations of vacancy-adatom pairs on close-packed faces of a crystal. Treating the formation of steps as a cooperative phenomenon, they concluded that a critical temperature would divide the crystal growth temperature range into two parts. At temperatures below this critical temperature, steps would appear so rarely that growth by surface nucleation would be favored; above this temperature, steps would be so numerous that the surface becomes "essentially rough" and no nucleation barrier is encountered. They go on to point out, however, that all of these calculations apply to perfect crystals and the proven existence of dislocations in crystals renders these calculations unverifiable.

II.1.3 Normal Growth

The model of crystal growth referred to as normal growth or Wilson-Frenkel growth has evolved into a complete model by combining the work of several investigators (9,13,14-18). Wilson(14), without postulating a mechanism of crystal growth, derived an equation describing his observations on salol and other organic materials. Basically, Wilson observed that

crystal growth rates vary directly with undercooling and inversely with viscosity. Frenkel(15,16) introduced reaction rate theory in an explanation of the mechanisms of viscous flow and crystal growth. Frenkel hypothesized that both viscous flow and crystal growth required the movement of atoms through an intermediate high energy state. Assuming that the activation energy for viscous flow approximately equals that for transport across the liquid-crystal interface, Frenkel pointed out that diffusion across the interface and diffusion in the bulk liquid are very similar processes.

A more sophisticated approach to normal growth was attempted by Volmer(9), who derived a crystal growth rate equation directly from reaction rate theory. Volmer assumed that atoms in the liquid and solid phases occupy low energy sites separated by free energy barriers; atoms in a crystal occupy sites whose energy, on average, is lower than those in the liquid at temperatures below the melting temperature and higher than those in the liquid at temperatures above the melting temperature. The heat of fusion is assumed to be the difference between the activation energy needed to transfer an atom from the solid to the liquid and that for the reverse process. Volmer's equation is not used in its original form; a much more useful form is that proposed by Turnbull(18):

$$u = \frac{fD''}{a_o} \left[1 - \exp\left(\frac{\Delta H_F \Delta T}{RTT_E}\right)\right] \qquad (II.2)$$

where ΔH_F = molar heat of fusion

T_E = crystal melting temperature

R = gas constant

and f = fraction of sites on the interface where atoms can preferentially be added or removed

The site factor, f, has been added to Turnbull's original equation in order to account for the possibility of growth occurring only at some preferred fraction of sites along the interface.

The kinetic coefficient for transport at the interface, D", has not been measured in any experiment; it is assumed to have the same temperature dependence as the fluidity:

$$D'' = \frac{b}{\eta} \qquad (II.3)$$

where b = constant

and η = viscosity

The two most frequently employed estimates of the constant b in Equation II.3 are taken from the Stokes-Einstein relation and the Eyring relation, two relations which relate viscosity and self-diffusion in liquids.

Using the Stokes-Einstein relation(17):

$$b = \frac{kT}{3\pi a_o} \qquad (II.4)$$

Using the Eyring relation(19):

$$b = \frac{\lambda_1 kT}{\lambda_2 \lambda_3} \qquad (II.5)$$

where λ_1 = distance between two layers of molecules in a liquid

λ_2 = distance between neighboring molecules in the direction taken by one layer sliding over the next

and λ_3 = mean distance between adjacent molecules in a direction at right angles to the direction of sliding, but in the plane of that layer

The Eyring relation predicts a value of b greater than that of the Stokes-Einstein relation by approximately a factor of 3π.

Studies have been conducted to determine the validity of the Stokes-Einstein and the Eyring relations. Using data for viscosity and self-diffusion in pure liquid metals, Nachtrieb[20] has shown that the Stokes-Einstein relation accurately predicts ionic radii. The Eyring relation yields ionic radii about one order of magnitude too large. Nachtrieb also presents data for the variation of viscosity and self-diffusion of mercury with pressure at constant temperature. The product ηD is approximately constant over a pressure range from 1 to 8366 kg/cm^2. These results imply that viscosity and self-diffusion have the same pressure dependence and the same temperature dependence.

Ma and Swalin[21] have found that both the Stokes-Einstein and the Eyring relation predict the approximate order of magnitude of the diffusion coefficient for various metals diffusing in dilute solution in liquid tin.

Although studies such as [20] and [21] prove the utility of the Stokes-Einstein and Eyring relations in using

viscosity data to estimate approximate diffusion coefficients, the use of these equations to predict the kinetic coefficient across the interface, D", is not explicitly validated by these results. At minimum, however, these results show that viscosity and diffusion in liquids have the same temperature dependence. Studies of another process involving molecular rearrangements in liquids, dielectric relaxation, have shown that viscosity and dielectric relaxation exhibit the same temperature dependence. Denny(22) has shown that these two processes show the same temperature dependence in liquid alkyl halides, both nonassociated polar liquids and hydrogen bonded liquids, over the full range of viscosity studied, from 10^2 to 10^8 poise. Davidson and Cole(23) determined that dielectric relaxation and viscosity have the same temperature dependence in various organic liquids. A compilation of data by Litovitz et al(24) shows that the temperature and pressure dependences of dielectric and volume relaxation times are very similar in liquids, regardless of whether that behavior is Arrhenius or non-Arrhenius in form.

In sum, since diffusion, viscosity, dielectric relaxation, and volume relaxation all involve molecular reorientation in liquids and all are found to have the same temperature dependence, assuming that the molecular reorientation involved in changing the molecules near the crystal interface from an amorphous to an ordered structure has that same temperature dependence is not unreasonable,

The Stokes-Einstein relation is generally chosen over the
Eyring relation because of the better quantitative fit of
its predictions in studies such as (20) and (21). The
Eyring relation predicts values an order of magnitude
greater than Stokes-Einstein relation. Cahn, Hillig, and
Sears(25) estimate that the diffusion coefficient across the
interface should be one or two orders of magnitude greater
than that for the bulk liquid. Therefore, the Stokes-
Einstein value is probably an underestimation.

The equations describing normal growth result
from reaction rate theory without explicit reference to a
specific type of interface structure. It is clear, however,
that normal growth will not occur on any interface which
exhibits a nucleation barrier. The appropriate interface
for normal growth is that described by Burton, Cabrera, and
Frank(13) as "essentially rough". Such a rough interface is
not discontinuous in structure along a line separating two
layers of atoms. Instead, one or more atomic layers will be
composed partly of atoms fitting the crystal lattice and
partly of atoms still in amorphous array. A rough interface
can also be regarded as one having an abundance of vacancy-
adatom pairs. The starting of new layers presents no
barrier to growth on such an interface. Not all sites along
a rough interface can accomodate adatoms at a particular
time, however; hence the need for f in Equation II.2.

In normal growth, the interface is assumed to remain rough regardless of the temperature. The roughness and the site factor f are taken as independent of undercooling.

II.1.4 Screw Dislocation Growth

Frank(26) and Burton and Cabrera(27) have proposed that the presence of a screw dislocation in a growing crystal provides new steps continuously on successive atomic layers without the necessity of surface nucleation. An Archimedean spiral is taken as a simple representation of the growth morphology.

In the view of the screw dislocation theory, the crystal-liquid interface is discontinuous but the crystal is imperfect because of the presence of dislocations.

Hillig and Turnbull(28) determined the fraction of lattice sites along the interface which will be active in screw dislocation growth. It is assumed that the dislocation is an Archimedean spiral characterized by:

$$r = 2\theta r_o \qquad\qquad (II.6)$$

where r = radial distance from origin

θ = angular coordinate of the spiral

r_o = initial radius of the spiral

Assuming that the initial radius of the spiral is equal to the critical radius of a disk-shaped nucleus, $r*$:

$$r* = \sigma V_M / \Delta S_F \Delta T \qquad\qquad (II.7)$$

where V_M = molar volume

and ΔS_F = molar entropy of fusion

With the additional assumptions that: (1) growth will occur only by the addition of atoms at sites within a_O of the spiral circumference; (2) the area covered by the centers of the spirals is negligibly small; and (3) almost the entire area of the interface will be covered by growth spirals, either by one multilayered spiral or by many spirals distributed in size, the fraction of sites at which growth occurs, f', will be:

$$f' = \frac{a_O (\Delta S_F)(\Delta T)}{4\pi \sigma V_M} \qquad (II.8)$$

In crystals growing by a screw dislocation mechanism, the fraction of sites at which growth preferentially occurs, f, is equal to f'. Replacing f by f' in Equation II.2 reveals that at low undercoolings, where:

$$\left[1 - \exp\left(\frac{-\Delta H_F \Delta T}{RTT_E}\right)\right] \approx \frac{\Delta H_F \Delta T}{RTT_E} \qquad (II.9)$$

the crystal growth rate is proportional to the square of the undercooling when growth occurs by this mechanism.

II.2   The Reduced Growth Rate

Equation II.2 is applicable to normal (Wilson-Frenkel) growth and to growth by a screw dislocation mechanism. As discussed above, in the case of normal growth, the fraction of sites at which atoms preferentially join the crystal, f,

is assumed to be approximately independent of the undercooling. In the case of screw dislocation growth, the factor f is equal to f' in Equation II.8 and is directly proportional to the undercooling. The dependence of the site factor on undercooling for a particular material is determined from a plot of the reduced growth rate, u_R, against undercooling, where:

$$u_R \equiv \frac{u\eta}{[1 - \exp(\frac{-\Delta S_F \Delta T}{RT})]} \qquad (II.10)$$

In the case of normal growth and screw dislocation growth:

$$u_R = \frac{b}{a_o} f \qquad (II.11)$$

Both the Stokes-Einstein and the Eyring values for b indicate that b varies directly with temperature. However, since most crystal growth studies are conducted at relatively high temperatures, b varies little over the temperature ranges studied and is regarded as a constant. The reduced growth rate is therefore directly proportioned to the site factor and has the same temperature dependence as the site factor. It is the form of this dependence which is of interest in determining how crystals grow. According to the models discussed previously, only in the case of normal growth is the site factor independent of undercooling.

In the case of screw dislocation growth, the site factor is zero at the melting temperature and it increases linearly with undercooling.

Growth by a surface nucleation mechanism can be determined by plotting log (uη) against $(\frac{1}{T\Delta T})$. If growth occurs by this mechanism, such a plot is linear with a negative slope.

II.3   Applicability of Growth Mechanisms

Burton, Cabrera, and Frank(13) proposed general criteria for predicting under what conditions and for what materials a particular growth mechanism should occur.

Jackson(29), using a similiar treatment (Bragg-Williams treatment of cooperative phenomena(30)) and considering only the single outer layer of atoms, was able to link the type of interface expected for each particular material to its entropy of fusion. The Jackson model of the Interface describes the free energy of a crystal-liquid interface as a function of the number of adatoms on the interface. Curves showing the interfacial free energy dependence on adatom population for materials with various entropy of fusion values are presented in Figure II.1.

Each curve is derived from the equation:

$$\frac{\Delta F_s}{NkT_E} = \alpha X(1-X) + X\ln X + (1-X)\ln(1-X) \tag{II.12}$$

where

$$\alpha = \frac{\Delta S_F}{R} \left(\frac{n_1}{V}\right) \tag{II.13}$$
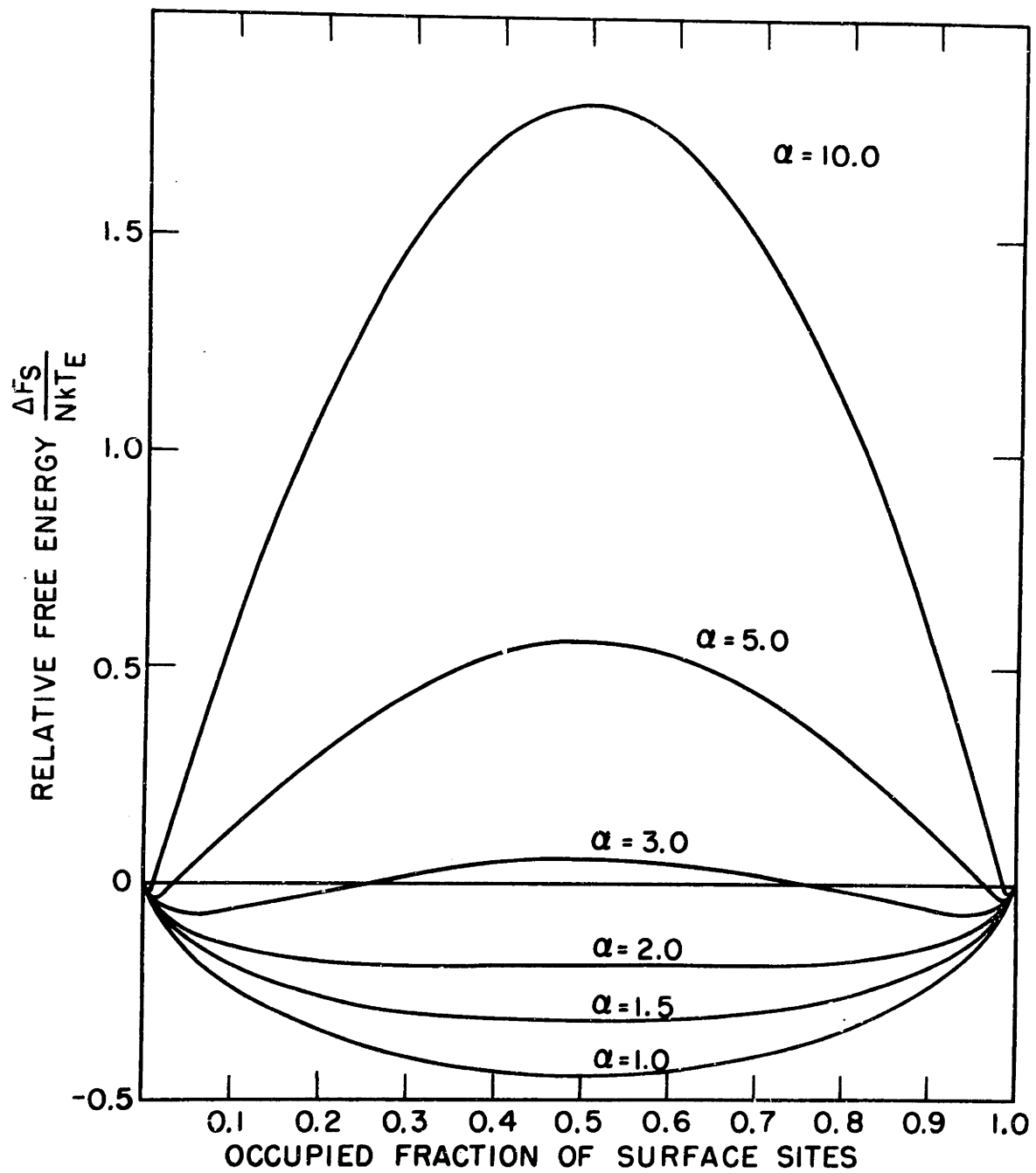
Figure II.1:   Interfacial free energy dependence on α and
              adatom population.

ΔF_s = increase in free energy due to the occupation by adatoms of a fraction X of sites

N = number of possible sites on an initially plane surface at the equilibrium temperature, T_E

X = fraction of sites occupied by adatoms

n_1 = total number of "nearest neighbor" atoms in a molecular layer parallel to the interface

V = possible total number of "nearest neighbor" atoms

As shown in Figure II.1, materials with an α factor less than two have a minimum free energy configuration when 50% of the interfacial sites are occupied by adatoms. Materials with an α factor greater than two have a minimum free energy configuration exhibiting only a few adatoms and a few vacancy sites. It is concluded that low entropy of fusion materials ($\alpha<2$) will exhibit interfaces rough on an atomic scale and non-faceted (nearly isotropic) on an observable scale. High entropy of fusion materials ($\alpha>2$) should exhibit interfaces smooth on an atomic scale and faceted (anisotropic) on an observable scale. Jackson(31) points out that this conclusion is supported by the commonly observed non-faceted interfaces of metals growing from the melt (low entropy transformations) and the faceted interfaces of solid-vapor transformations (high entropy transformations). Furthermore organic materials unusual in having a low entropy of fusion have been observed to crystallize with non-faceted morphologies(32).

The Jackson Model of the Interface does not deal directly with growth kinetics. The Jackson Model, however,

does show the relation between the entropy of fusion of a material and the type of interface it is expected to have. The various crystal growth models (Section II.1) relate the types of interfaces to the different models of crystal growth, i.e., an interface rough on an atomic scale with normal growth and an interface smooth on an atomic scale with surface nucleation or screw dislocation growth. Assuming that the crystal growth models and the Jackson Model are not too simple and not therefore invalid, the entropy of fusion and the mechanism of crystal growth may be linked. Low entropy of fusion materials will exhibit normal growth, while high entropy of fusion materials will exhibit surface nucleation or screw dislocation growth. More precisely, low entropy of fusion materials will grow with a site factor which is independent of undercooling, while high entropy of fusion materials will exhibit a site factor which increases with undercooling.

The fraction (n_1/V) in Equation II.13 is highest for close-packed planes, where $0.5 \leq (n_1/V) < 1.0$. For materials with $\Delta S_F/R \leq 2$, even the close-packed interface planes should be rough. For materials with $\Delta S_F/R \geq 4$, the most closely packed faces should be smooth, while less closely packed faces should be rough.

The relation of the α factor to interface morphology remains qualitatively the same regardless of undercooling. No transitions in growth mechanism with undercooling are

predicted with the exception of faces for which α is slightly greater than two, which may transform from a smooth to a rough morphology with undercooling.

II.4   Diffuse Interface Theory

Cahn(33) has proposed that the crystal-liquid interface is similar to ferromagnetic and ferroelectric domain walls and that crystal growth is analogous to domain wall movement. The important feature of such a "diffuse interface" is the systematic variation of free energy with the position of the advancing interface. Free energy maxima and minima occur at intervals equal to some multiple of an interatomic spacing. The diffuseness or distance between totally crystalline and totally amorphous atomic layers is a function of the material and must be determined experimentally.

Assuming a particular form for the variation of free energy with the interface position, the diffuse interface theory predicts that materials generally will have a critical undercooling which marks the transition from lateral growth (by surface nucleation or dislocation mechanism) to normal (Wilson-Frenkel) growth. The normal growth occurs at high undercoolings; lateral growth occurs at lower undercoolings. The transition will be revealed in a plot of the reduced growth rate versus undercooling.

A recent review article(34) suggested that the form of variation in free energy employed in diffuse interface theory is not applicable to first order transformations. Furthermore, the interpretation of crystal growth data(25) as supporting the diffuse interface theory has also been questioned(34).

II.5   Melting Theories

In all materials, melting is observed to begin heterogeneously at free surfaces. Temperley(35) points out that in the case of materials which expand in melting, internal melting would result in increased local pressure and a consequent increase in the melting point of the crystal surrounding the liquid. Turnbull(36) points out that the general absence of a nucleation barrier to free surface melting suggests that in all materials the sum of the free energy of the crystal-liquid interface and the liquid-vapor interface is less than or equal to the free energy of the crystal-vapor interface.

Just as liquids which are highly viscous at their melting points exhibit low crystallization rates, they also exhibit low melting rates. Whereas relatively stable undercooled liquids are commonly observed, similarly stable superheated crystals have been observed only in the case of materials which form viscous melts. The superheating of crystals of albite(37), quartz(38), cristobalite(39), phosphorus pentoxide(40) and sodium disilicate(41) has been

reported. Most materials, however, melt rapidly even at temperatures negligibly above their melting temperatures; their melting rates are governed by heat flow. Only in the case of viscous liquids are melting rates expected to be determined by interface kinetics.

If the same interface sites participate in both crystallization and melting, the plot of melting and crystallization rates versus motivating potential should be a single curve which is continuous with no abrupt change in slope through the melting temperature. This behavior would be in accord with the principle of microscopic reversibility in the limit of T_E. In the case of low entropy of fusion materials, which exhibit non-faceted interfaces during both melting and crystal growth, the sites participating in both these processes are expected to be the same. In the case of materials which are faceted during growth but non-faceted in melting, the sites participating in the two processes are not expected to be the same and a change in the slope of the crystallization-melting rate curve is expected at the melting temperature.

Theoretically, the possible mechanisms advancing a melting interface are the same as those for crystallization. Equations II.1, II.2, and II.8 are applicable with melting indicated by a negative growth rate. The ease with which atoms from the crystal find a place in the liquid, however, makes it unlikely that atoms will remain on high energy sites, such as the corners of atomic layers, for very long.

Melting by "coring" (the reverse of screw dislocation growth) might be expected to occur to a limited extent but melting limited by a surface nucleation barrier is not expected to occur.

II.6   Past Crystallization and Melting Studies

II.6.1   General Features

Due to the low fluidity and relatively slow melting and growth rates commonly encountered in glass-forming systems, the methods employed to measure melting and growth rates are uncomplicated: they are (1) direct observation using capillary tubes or a hot or cold stage microscope; and (2) quenching to room temperature and then measuring with a microscope. In general, the temperature range of the study determines the technique employed; all can yield accurate results.

Few thorough studies of melting kinetics but a great many studies of crystal growth rate variations with temperature have been made. All of the crystal growth studies have found the same general form of growth rate variation with undercooling: at low undercooling the growth rate increases rapidly with decreasing temperature, a peak growth rate is reached at 25° - 100^OC undercooling, then, the growth rate gradually decreases with greater undercooling. As demonstrated by Tammann(42), in the high undercooling region, growth is approximately proportional to the fluidity of the melt and is said to be "viscosity limited". In the

low undercooling region, the growth rate is often approximately proportional to $(\Delta T)^n$ where $1.0 \leq n \leq 2.0$ and is said to be "driving force limited".

Although the determination of crystal growth rates in glass-forming systems is straightforward, the determination of crystal growth mechanisms is not. The causes of this difficulty are two-fold: (1) the simplifications which must presently be made in attempting to mathematically describe this complex process (as discussed in II.1), and (2) the strong influence of impurities on growth rate(43) and viscosity (for example, see II.7.3). Only for those materials on which growth rate and viscosity measurements have been made using specimens similar in purity and thermal history and tested under similar conditions can growth rate theories be applied accurately. Even in these cases, the simplifications involved in these theories introduce uncertainties into the interpretation of experimental results.

Glass-forming systems whose crystallization and/or melting behavior have been studied are: glycerine(9,44), salol(34,45-48), phosphorus pentoxide(49,50), 1-2 diphenylbenzene(51), tri-α- naphthylbenzene(52), sodium disilicate(53-55), potassium disilicate(56), soda-lime-silica ternaries(57-59) and silicon dioxide(60-68). The pertinent results of these studies are discussed below.

II.6.2 Glycerine

Crystal growth rates of glycerine were measured by one group of researchers(9), while two differing viscosity determinations were made by others. Glycerine crystals were found to be faceted at all temperatures studied. Jackson et al(34) have pointed out that variability in the data allows for a number of interpretations and suggests the need of further study.

II.6.3 Salol

A critical review of salol crystallization data is included in Reference 34. Several investigations(34,45-48) of salol crystallization have been carried out; compiled they cover a temperature range down to 71.6°C undercooling. The various studies show no agreement on growth rates at small undercooling. A recent study(48) pointed out that at small undercoolings, individual crystals observed under a microscope were found to grow at their own individual rates. The measured growth rates are, therefore, probably determined by impurities.

The most recent study of salol crystallization(34) measured growth rates on samples of three differing purity levels. Observations of crystal morphology were also included. It was found that at less then 10°C undercooling the measured growth rates differed with the stage of growth, crystal perfection, and the method of study. In the range from 10° to 14°C undercooling, impurities were found to

increase the growth rate; also, a change in morphology was observed. In the undercooling range from 14° to $40^O C$, impurities still influenced growth rates and considerable scatter appeared in the growth rate data. A faceted morphology was observed over the full range of undercooling studied, $72^O C$.

Although Cahn et al(25) had interpreted the reduced growth rate variation with undercooling curve drawn with some of the early data on salol as indicating a transition from a lateral growth mechanism to a continuous one, the faceting observed at all undercoolings does not support this interpretation, as pointed out in Reference 34.

Using the latest data(34), the site factor is found to increase continuously, but with some breaks in slope, with undercooling.

II.6.4 Phosphorus Pentoxide

Turnbull et al(49) studied melting and crystallization rates of tetragonal phosphorus pentoxide, which melts with a high entropy of fusion to form a viscous melt. Melting and growth measurements were made on the same crystals, which were always faceted. Melting and growth rates were found dependent on: (1) time; (2) crystal morphology; (3) crystallographic direction;

and (4) thermal history. Using steady-state measurements
for a particular crystallographic direction on specimens
having the same thermal history, a curve continuous
through the melting temperature was drawn through the low
undercooling and low superheating data; the data,
corrected for viscosity differences, is presented in
Figure II.2. The reduced growth rate variation with
temperature, presented in Figure II.3, shows that the
scattering in the data is a serious problem. No firm
conclusions regarding continuity at the melting tempera-
ture or the dependence of the reduced growth rate on
undercooling can be made. The melting data, however, does
indicate that the reduced melting rate is independent of
temperature at small superheating. Viscosity values used
were those of the same investigators determined on the
same material(50).
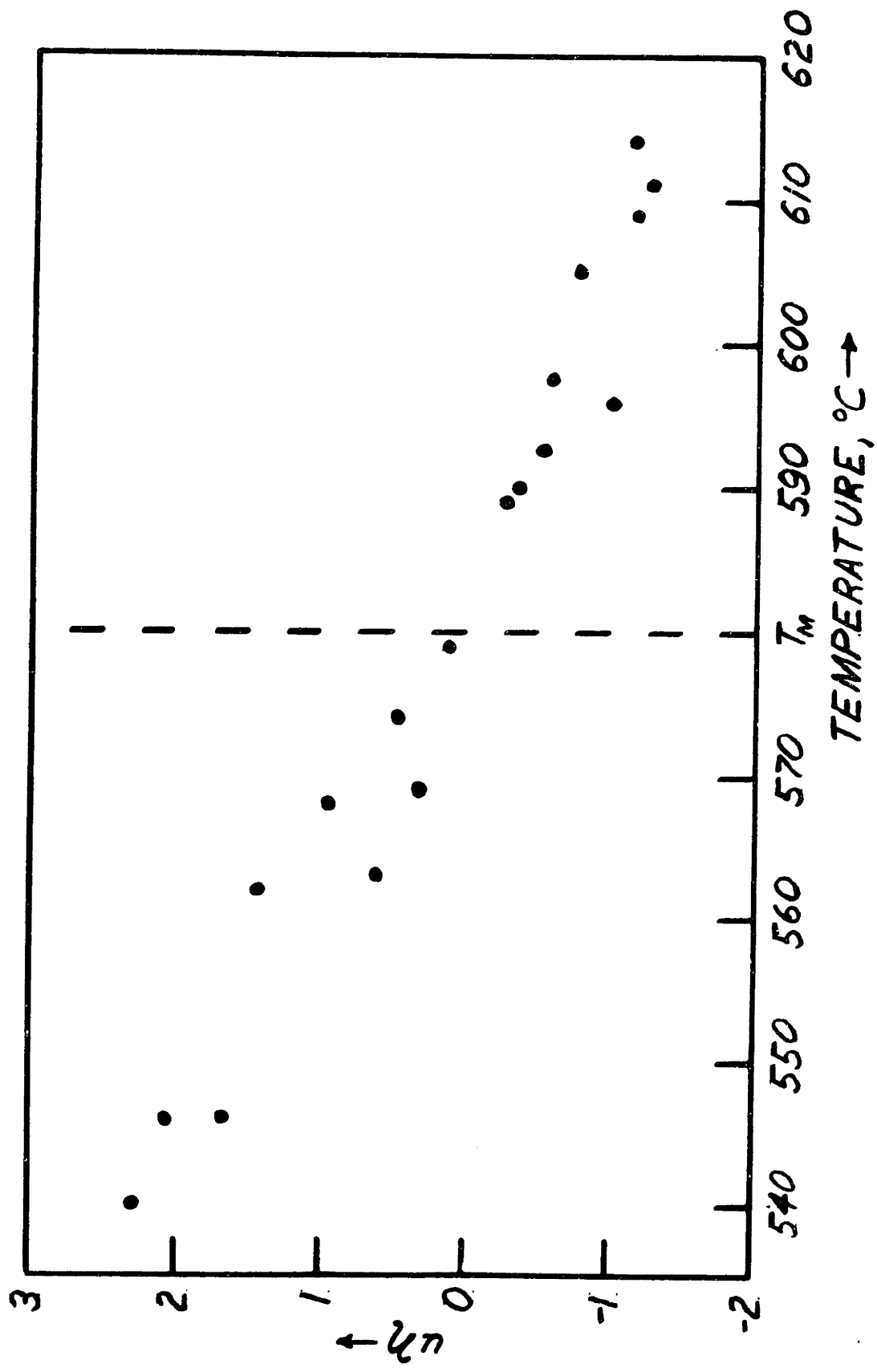
Figure II.2: P$_2$O$_5$ melting and crystallization rates (corrected for viscosity) – $u\eta$ units are cm.sec.$^{-1}$poise.
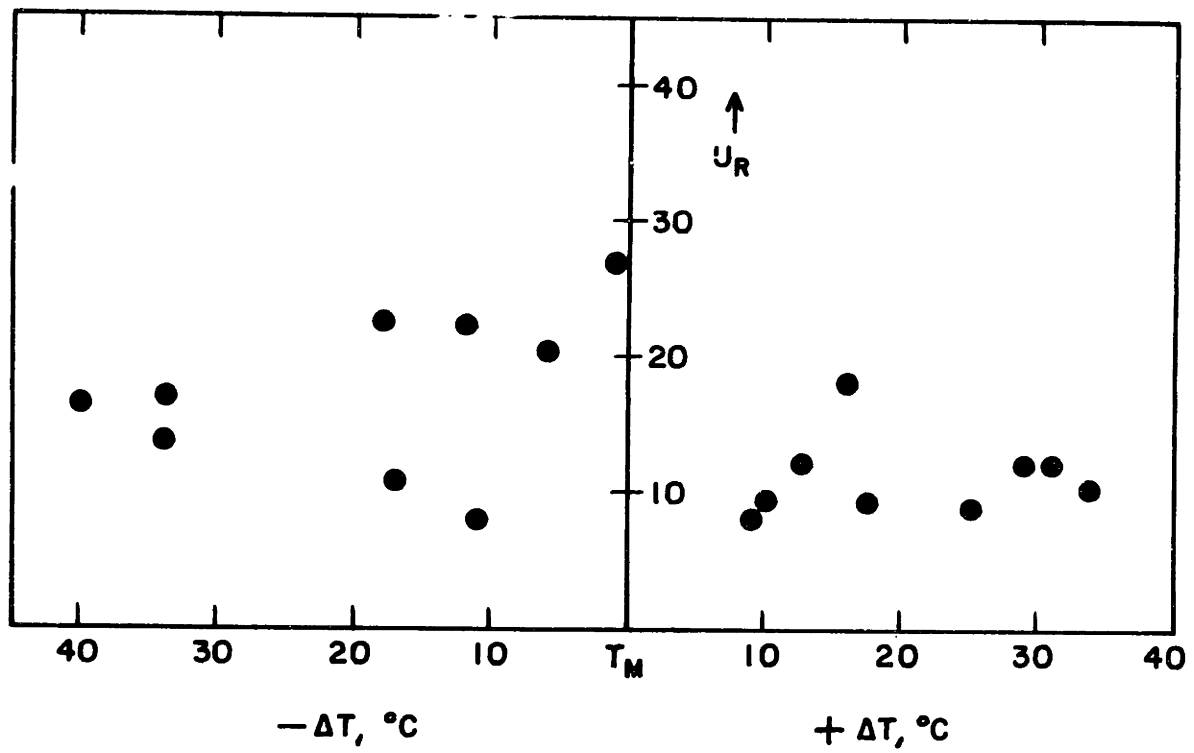
Figure II.3: P$_2$O$_5$ reduced growth and melting rates.

II.6.5 1,2 Diphenylbenzene

Greet(51) measured crystallization rates of 1,2 diphenylbenzene, an organic glass-former for which $(\Delta S_F/R)$ is 6.75. The observed interface morphology was faceted at all undercoolings studied, up to 60 Centigrade degrees. The site factor was found to increase continuously with undercooling but did not follow a form predicted by any standard growth formulation. Viscosity values were measured by the same investigators on the same material.

II.6.6 Tri-α-Naphthylbenzene

Tri-α-naphthylbenzene is a van der Waals glass-former of structurally complex molecules for which $(\Delta S_F/R)$ is approximately 10.7. Growth occurs with a faceted morphology over the full range of undercooling studied(52). The reduced growth rate increases continuously from zero at 2^O undercooling to over 100 at 105° undercooling. Magill and Plazek(52) interpreted these results as consistent with surface nucleation growth. Jackson et al(34) point out that a transition is indicated by the data at about fifty degrees undercooling, the same undercooling at which a change in crystal morphology is observed. On both sides of the break, however, the growth rate data has a form consistent with that of growth by a surface nucleation mechanism. In this study, too, both viscosity and growth rates were measured by the same group on the same material.

II.6.7 Sodium Disilicate

Sodium disilicate is a congruently melting glass-former for which $(\Delta S_F/R)$ has an intermediate value. An early study[55] and a more complete recent study[53,54] have measured essentially the same crystallization rates. The interface morphology was faceted at all undercoolings studied (up to 298 Centigrade degrees). The reduced growth rate[53,54] increases steadily with undercooling; the slope of the reduced growth rate versus undercooling curve decreases with undercooling until it reaches an undercooling of about 80 Centigrade degrees. At undercoolings from 80 to 298 Centigrade degrees, the slope of this curve is constant and positive. Extensions of this initial slope and the final slope of this curve intersect at about 40° undercooling. The form of the reduced growth rate variation with under-cooling is, therefore, unexplained. Viscosity measurements were made on the same specimens. Sodium disilicate melting rates[53,54] were significantly greater than crystallization rates at equal departures from the equilibrium temperature.

II.6.8 Potassium Disilicate

Crystal growth measurements over a range of 100 Centigrade degrees undercooling were made on potassium disilicate by Leontjewa[56]. Viscosity data for this temperature range is only available by interpolating from measurements made at higher and lower temperatures by other investigators on other potassium disilicate melts. As

pointed out by Jackson et al(34), the reduced growth rate variation with undercooling approximates that for screw-dislocation growth, but little confidence should be placed in the form of the variation due to the source of the viscosity data and also evidence of hydration problems. No morphological observations were reported on potassium disilicate.

II.6.9 Soda-Lime-Silica Glasses

Several studies(57-59) have been made of the crystal growth of devitrite (Na$_2$O·3CaO·6SiO$_2$), an incongruently melting compound whose primary field of crystallization encompasses the commonly used compositions of commercial glasses. Although these crystals grow from a melt whose composition differs from their own, initial growth is linear with time, presumably because the needle-like morphology of the crystals allows for short diffusion paths. The variation of crystal growth rate with undercooling follows the typical form. The only relevant observation, for this thesis, is the observation by Swift(57) that the melting growth rate curve is continuous through the melting temperature, with no change in slope. Photomicrographs by Milne(59) on devitrite crystals apparently show that the change in crystal morphology on melting is the reverse of that for growth.

II.6.10 Silicon Dioxide

Silicon dioxide has many properties analogous to germanium dioxide; both are good glass-forming congruently

melting oxides which exhibit low entropies of fusion. A
great deal of research has been done on silicon dioxide
crystal growth and melting. Not only has the reduced
growth rate variation with undercooling been determined(63),
but the effects of impurities, atmosphere, method of
nucleation, and state of reduction of the glass have all
been investigated.

Cristobalite, the crystalline phase invariably
observed to grow from silica glass, is normally observed to
nucleate on free surfaces only. Using slightly reduced
silica glass, Wagstaff(66,68) has been able to nucleate
cristobalite in the bulk glass and to study the growth of
these crystals without the interference of atmospheric
effects or external impurities. The center few microns of
each crystal apparently contain a second phase heterogeneity.

The growth and melting of cristobalite crystals was
studied over a temperature range from 240 Centigrade degrees
undercooling to 20° superheat. Growth and melting rates
were found to be linear with time in all instances. Over
the entire temperature range, the morphology of the
cristobalite crystals is non-faceted; at most, some crystals
show a tendency toward faceting. The growth-melting curve
was found to be continuous with no change in slope through
the melting temperature. Most importantly, the reduced
growth rate was found to be independent of temperature, as
shown in Figure II.4. The fact that the reduced growth
rate is independent of temperature is consistent with the
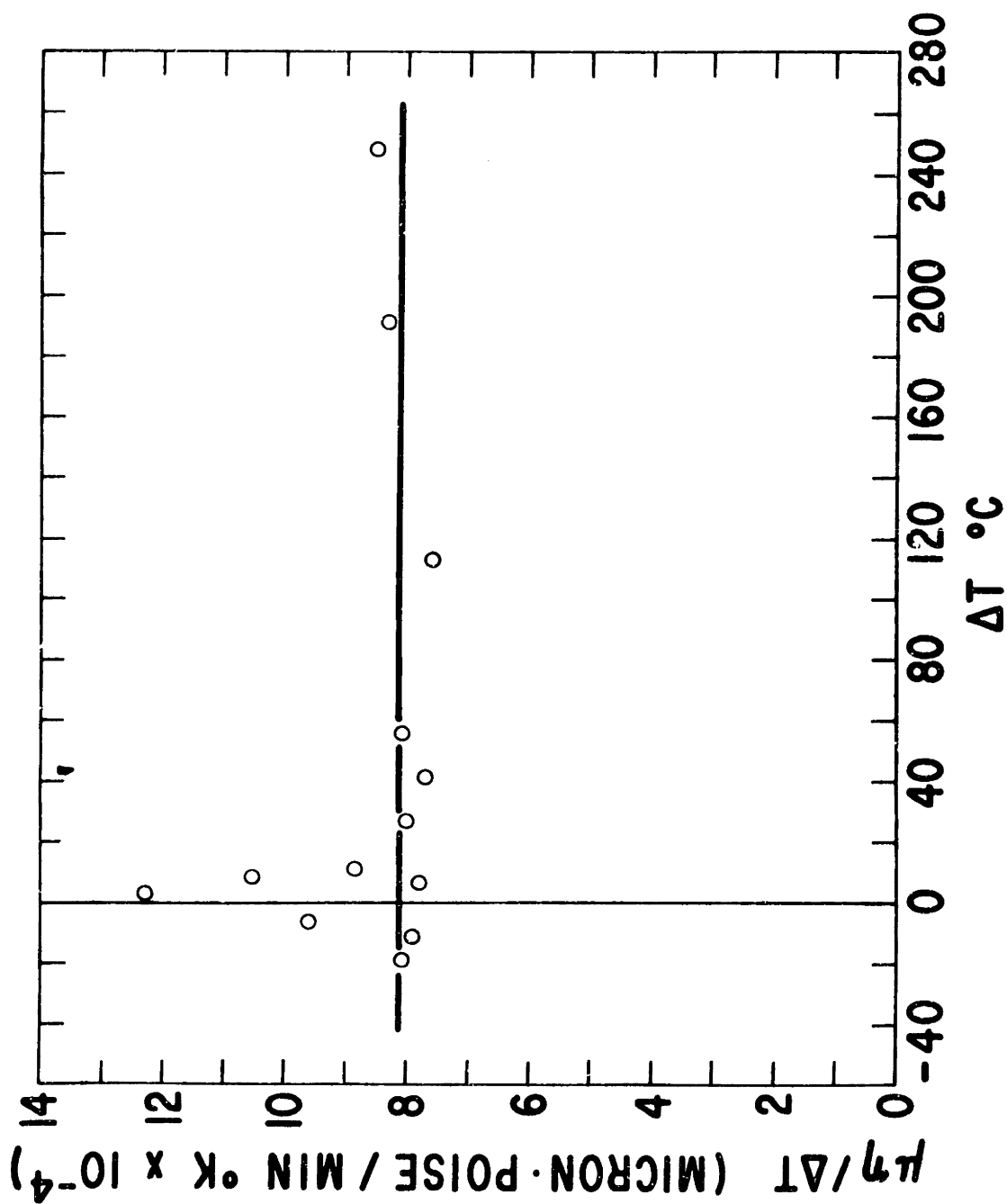
Figure II.4: SiO_2 reduced growth and melting rates.

morphology observed and the Jackson Model of the Interface(29).

An important variable affecting the rate-controlling process of cristobalite growth is the state of reduction of the glass. The state of reduction is determined from the size of an absorption peak at 2420 $\overset{o}{A}$ in the ultraviolet spectrum(69). In a neutral atmosphere, linear growth rates in a reduced glass have been shown to be more than one order of magnitude slower than those in stoichiometric glass(64,68). Surface-nucleated crystals growing in reduced glass in air exhibit diffusion-controlled growth(62-64) which is enhanced by increased oxygen or water vapor pressure in the atmosphere (the diffusion of oxygen or hydroxyl ions being the rate-controlling process).

Stoichiometric silica glass exhibits crystal growth which is linear with time, regardless of atmosphere. For stoichiometric silica glass, crystallization rates of surface-nucleated cristobalite were found to increase with atmosphere in the order: vacuum < nitrogen or argon < oxygen or water vapor. These effects have been interpreted(60) as indicating that nitrogen or argon play a neutral role in crystallization while vapors from furnace impurities (eliminated only in vacuum) enhance growth, as does oxygen and water vapor. Consistent with the observed effect of water vapor, crystal growth rates are faster in glasses of high water content(62,65).

Wagstaff(68) measured the melting rates of internally-nucleated cristobalite. The fact that the crystal growth-melting curve is continuous without change in slope through the melting temperature indicates that the same types of atomic sites are involved in both melting and growth. In this case, the continuity is observed out to significant departures from equilibrium.

II.6.11 Summary

Of all the glass-forming materials whose crystallization and/or melting behavior have been studied to date, only one, silicon dioxide, exhibits a low entropy of fusion. This is also the only material studied to date whose reduced growth rate has been found independent of temperature over a wide temperature range. The other unique aspect of cristobalite crystallization is the fact that the interface is never faceted. In all the other studies reporting crystal morphology, crystals were always observed to be faceted. In those studies not reporting crystal morphology, it is assumed that the crystals are faceted since most investigators regard non-faceted crystals as an interesting anomaly(70).

The unique characteristics of cristobalite crystallization are consistent with the reasoning of Jackson(29), i.e., a low entropy of fusion material has an interface rough on an atomic scale and a site factor independent of undercooling. The morphological observations

and the site factor dependence on undercooling of all high entropy of fusion materials studied to date are also consistent with predictions based on the Jackson Model of the Interface.

The data collectively suggest the need for greater refinement of crystal growth models. It also shows that transitions in growth mechanisms have not been observed in any material.

Important to this thesis and other crystal growth studies are the observed effects of impurities, atmosphere, state of reduction, and method of nucleation on cristobalite crystal growth. Atmosphere has been shown to have no effect on sodium disilicate growth, but the variability of the data in all studies suggests that impurity effects are commonly encountered. Only for salol and cristobalite have some of these impurity effects been determined.

For those materials whose crystallization and melting have both been studied, the evidence indicates that the crystallization-melting curve is continuous without change in slope through the melting temperature only in the case of silicon dioxide and devitrite. This result can be attributed to a low entropy of fusion in the case of silicon dioxide. In the case of devitrite, where the crystal and glass differ in composition, the situation is more complex.

II.7   Properties of Germanium Dioxide

II.7.1   Forms of Germanium Dioxide

Germanium dioxide occurs in two crystalline forms, one having a rutile (tetragonal) structure[71], the other an α-quartz (hexagonal) structure[72]. Tetragonal germanium dioxide is insoluble in water and is not readily attacked by HF or HCl[73]; hexagonal germanium dioxide is soluble in water and is readily attacked by HF and HCl[71]. The density of tetragonal germanium dioxide is 6.239 gms/cm^3 at 25°C; hexagonal germanium dioxide has a density of 4.228 gms/cm^3 at 25°C[71].

Hexagonal germanium dioxide is the form invariably appearing in growth from the melt or from solution[74] although it is thermodynamically stable only over the temperature range from 1033°C to 1116°C[71]. The estimated accuracy of the melting point determination of 1116°C is ± 4°C[71]. The tetragonal form is stable at temperatures below 1033°C[71]; however, it is obtained only through transformations of the hexagonal form under pressure or through the use of mineralizers[71,74].

The germanium-germanium dioxide phase diagram exhibits only a single eutectic point, at 912°C, with a composition of 88% germanium dioxide-12% germanium[75]. Although not thermodynamically stable, solid germanium monoxide has been grown from the vapor and its properties determined[76].

Hexagonal germanium dioxide melts congruently at $1116^{\circ}C$ to a viscous liquid; it has a low entropy of fusion with the factor $(\Delta S_F/R)$ equal to 1.3(77). The glass transition range for germanium dioxide extends approximately from 450° to $575^{\circ}C$(78). Although the glass is resistant to crystallization at temperatures below this transition range, surface crystallization occurs readily in the presence of water even at room temperature(78). Germanium dioxide glass has a density of 3.637 gms/cm^3 at $25^{\circ}C$ and a hardness of less than 5 on the Moh's scale(78). The liquid is a network liquid, composed of GeO$_4$ tetrahedra with a germanium-oxygen spacing of 1.65 $\overset{\circ}{A}$(79) and a bond strength of about 100 Kcal/mole(80). Like the hexagonal crystalline form, the glass is soluble in water and is readily attacked by HF and HCl.

References 77 and 81 comprise a complete study of the thermodynamic properties of germanium dioxide from $298^{\circ}K$ to $2000^{\circ}K$.

II.7.2 The Absorption Spectrum of Germanium Dioxide Glass

The absorption spectrum of germanium dioxide contains three peaks which vary with the melting conditions and the atmosphere in which the glass is held. These peaks occur at approximately 2080 $\overset{\circ}{A}$, 2450 $\overset{\circ}{A}$, and 2.86 microns.

The peak at 2080 $\overset{\circ}{A}$ is a fundamental one, attributed to absorption by valence electrons of oxygen(82). This peak

does increase slightly in glasses treated in reducing conditions and is diminished by treatment in oxidizing conditions. Generally, only the long wavelength side of this peak is observed, appearing as the ultraviolet cutoff, since specimens of a thickness in the range of microns are needed to observe the short wavelength side of the peak at approximately 1850 $\overset{o}{A}$ (83,86).

The peak at 2.86 microns is attributed to the hydroxyl ion concentration in the glass(84) by analogy with the source of peaks at approximately this wavelength in other oxide systems. The infrared absorption cutoff occurs at approximately 6.15 microns(85). In thin specimens (100 microns) the final infrared cutoff is observed at about 15 microns(84).

The absorption peak at 2450 $\overset{o}{A}$ has unusual properties and has been extensively studied(74,87,88,90). This peak appears in germanium dioxide glass melted in air at temperatures above $1300^{o}C$; its size increases with increasing melting temperature. In reducing atmospheres, the peak appears at even lower temperatures; in hydrogen, it can be induced at $400^{o}C$(74). The peak can be bleached out by heat treatments in oxygen. Diffusion studies(87,88) conducted on thin laths (<100 μ's thick) in an oxidizing atmosphere have shown the source of the peak is an oxygen deficiency in the glass. Germanium dioxide glass deficient in oxygen can also be regarded as a reduced glass; i.e., it has an excess of germanium atoms. The exact form of the

color center is believed to be an oxygen vacancy with two associated electrons(74). Paramagnetic resonance studies supporting this conclusion have shown that paramagnetic resonance peaks first appear when this peak is bleached with ultraviolet radiation. If the absorption peak is reformed by thermal treatments, the paramagnetic resonance peaks disappear(74).

In silicon dioxide glass, the absorption peak at 2429 $\overset{O}{A}$ appearing in glass melted under reducing conditions has been shown to vary with the concentration of germanium impurity(89). This peak is therefore analogous to the germanium dioxide peak at 2450 $\overset{O}{A}$.

A part of this thesis previously reported(90) noted that a peak at 2450 $\overset{O}{A}$ appears in the absorption spectrum of germanium dioxide glass melted at elevated temperatures (>1300°C) in pure oxygen or even in vacuum. The degree of reduction of germanium dioxide glass increased with atmosphere in the order: vacuum or oxygen < air << dry nitrogen.

The visible absorption spectrum of germanium dioxide glass contains no peaks(85). The glass is normally colorless; however, the long wavelength tail of the 2450 $\overset{O}{A}$ peak does produce a brown tint in reduced germanium dioxide glasses.

II.7.3 Viscosity of Germanium Dioxide

At least six independent studies have been conducted on the viscosity of liquid germanium dioxide (91-96). In total, measurements cover the temperature range from 500°C to 1750°C, with data in the crystallization range (700 - 1116°C) very limited. The data from all six studies are collected in Figure II.5. The causes for the lack of agreement among the results reported are primarily differences in: (1) chemical purity; (2) melting procedures; and (3) measuring techniques.

In the low temperature range, there are marked differences in the results of the studies. The data of Kurkjian and Douglas (92) agree quite well with those of Nemilov and Ivanov (93), but the viscosity values are substantially larger than those obtained by Fontana and Plummer (96) and by Bruckner (95).

The data of Mackenzie (91) are the only exceptions to the close agreement of the data of all other investigations at high temperature. This result might be attributed to the 0.1% calcium impurity reported by Mackenzie; however, the addition of CaO to the melt would be expected to lower, not increase, viscosity. Moreover, impurity effects are difficult to ascertain since two investigations did not include impurity measurements (93,95). Melting conditions and atmospheres also differed in the other studies. Probably the most important difference in Mackenzie's study was the fact that the measurements were made in a pure oxygen
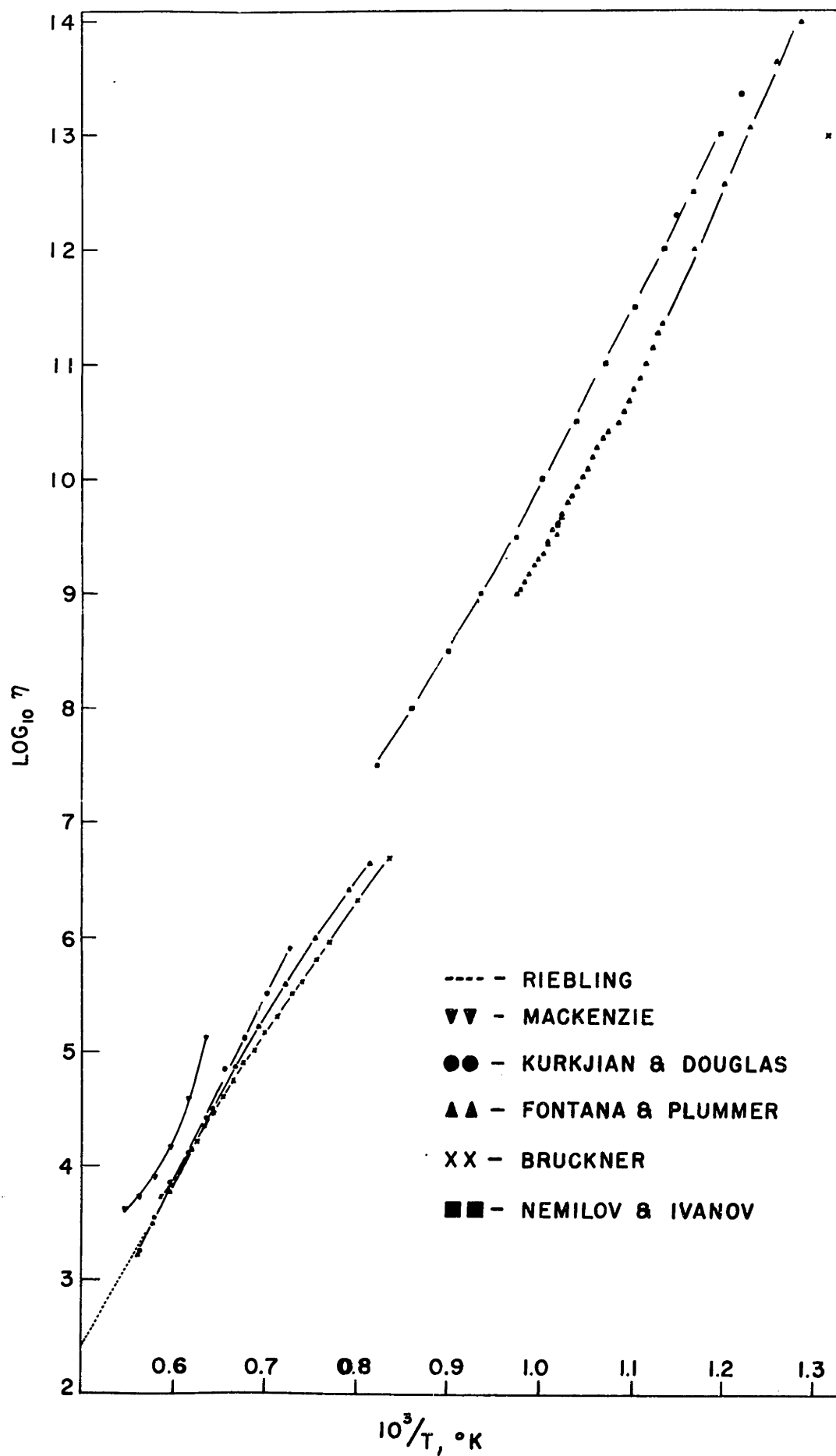
Figure II.5: Viscosity of GeO_2.

atmosphere on a glass which had been exposed only to oxygen atmospheres when at elevated temperatures. Mackenzie's glass was thus more nearly stoichiometric than the somewhat more reduced glasses on which viscosity measurements were made in air in all the other studies (see II.7.2).

A recent study(97) has shown that the viscosity of germanium dioxide glass is lowered with the addition of germanium. Thus the more reduced glasses produced by exposure to air rather than pure oxygen at elevated temperatures should exhibit lower viscosity values, as seen in Figure II.5.

Although little viscosity data are available for temperatures in the crystallization range, both Kurkjian and Douglas and Fontana and Plummer found that their own data on both sides of the crystallization range could be expressed by one equation. The results of Kurkjian are described to a reasonable accuracy by the equation:

$$\log_{10}\eta = -5.8 + \frac{16,300}{T}$$

η = viscosity

R = gas constant

T = temperature

The data of Nemilov and Ivanov, some of it taken in the crystallization range, fit this equation with somewhat less accuracy.

The data of Fontana and Plummer along with that of
Riebling over the range from 250 to 5×10^{10} poises (from
$1720^{\circ}C$ to $650^{\circ}C$) are expressed by the equation:

$$\log_{10}\eta = -4.543 + \frac{13,938}{T}$$

In the present study, germanium dioxide glasses
were melted from the same raw material and with melt
schedules the same as or similar to the Fontana and Plummer
melt schedule. Their viscosity data are therefore most
relevant to this study.

III.   <u>OUTLINE AND PLAN OF WORK</u>

This study involved the preparation of germanium dioxide glasses of several different states of reduction, the growth and melting of hexagonal germanium dioxide crystals in those glasses, and an analysis indicating how the results obtained are related to theories of crystal growth and melting.

IV. EXPERIMENTAL PROCEDURES

The experimental procedures employed in this study divide themselves into six parts: (1) melting of germanium dioxide glasses; (2) preparation of glass and crystalline laths; (3) measurement of the kinetics of crystallization; (4) measurement of the kinetics of melting; (5) determination of the state of reduction, the water content, and the purity of the glasses; and (6) additional minor experiments included as appendices.

IV.1   Melting of Germanium Dioxide Glasses

Thirteen batches of germanium dioxide glass, each weighing about one hundred grams, were prepared from Eagle-Pitcher Electronic Grade germanium dioxide crystals. No additives were included in these melts.

The glasses were melted in a horizontal mullite tube furnace heated by silicon carbide resistor elements. The bottom of the 2" diameter mullite tube was covered with a 1/4" thickness of refractory brick to protect it from thermal shock as the glass was removed from the furnace. Each end of the 30" long mullite tube contained a 9" long fireclay refractory brick for insulation. The center 7" of the tube was the hot zone. The ends of the mullite tube were sealed by brass plates and silicone rubber gaskets with ports of copper tubing to allow for the control of atmosphere and the entry of a thermocouple. One or two ports through the end seals were connected by rubber

tubing to a mechanical vacuum pump, a mercury manometer, a thermocouple vacuum gauge, and one or two gas cylinders.

Temperature was monitored in the furnace with a Pt (10% Rh)-Pt thermocouple placed within the mullite tube either at the top or bottom center.

The glasses were melted in a platinum boat approximately 4" long by 1-3/4" wide by 1/2" deep. This boat was formed of platinum foil 4" x 5" x .004" folded so that the sides extended to partially cover the glass in melting. The boat slid into and out of the furnace on a mullite slab cut from 3" diameter mullite tubing. Bubbled alumina on this slab provided a flat surface supporting the boat.

Five different melt schedules were used to produce glasses of different states of reduction. Series 1 glasses (1A - 1E) were melted following the schedule of Fontana and Plummer(96) as closely as possible. This schedule involved: (1) holding overnight at a vacuum of from 1000 to 200 microns of mercury at approximately $100^{\circ}C$; (2) heating in the same vacuum to $1150^{\circ}C$ in about five hours; (3) holding in vacuum at $1150^{\circ}C$ for four hours; (4) raising the temperature to $1400^{\circ}C$ in about one hour with dry nitrogen introduced to a back pressure of a few centimeters of mercury at $1300^{\circ}C$; (5) soaking overnight at $1400^{\circ}C$ in dry nitrogen; (6) quenching to room temperature.

Glass 2A was melted using the same schedule with the exception that the overnight soak was made at $1360^{\circ}C$. Glass

2B was produced following the first five steps of the Fontana and Plummer schedule and then soaking for six hours at $1200^{O}C$ in a pure oxygen atmosphere before quenching to room temperature. Glass 2C was melted according to the Fontana and Plummer schedule; instead of sealing the furnace during the overnight soak, however, dry nitrogen was flowed through the furnace at a rate of 4 ft^3/hour.

Series 3 glasses (3A - 3D) duplicated the Fontana and Plummer melt schedule, with the exception that a pure oxygen atmosphere was substituted in steps 4 and 5.

Series 4 glasses (4A and B) had the same melt schedule as Series 3 glasses and also additional heat treatments. Before these additional heat treatments, these glasses were cut into pieces about 1/2" wide x 4" long x 1/4" thick. Each of these pieces was held in air at $1150^{O}C$ for forty-eight hours in a platinum boat. Each piece was then removed from the platinum boat, turned over, and again treated in air at $1150^{O}C$ for forty-eight hours. The important features of the various heat treatments are listed in Table IV.1.

After quenching to room temperature, all of the glasses were annealed at $480^{O}C$ in air for two hours.

The procedure for providing a one atmosphere gas pressure over the glass during most of the melts involved backfilling through the same port used in evacuating the furnace. The furnace was then left sealed with a connection to the gas tank maintaining about 5 cms. Hg positive pressure.

Table IV.1

Glass Melting Procedures

glass	soak temp. ($^{\circ}$C)	soak atmosphere	additional heat treatment
Series 1	1400	N_2	-
2A	1360	N_2	-
2B	1400	N_2	6 hrs in O_2 at 1200°C
2C	1400	flowing N_2	-
Series 3	1400	O_2	-
Series 4	1400	O_2	96 hrs in air at 1150°C

An improved procedure used in melting the last few glasses involved backfilling with gas through a port at the end of the tube opposite the exhaust port and flowing the gas through the furnace.

IV.2   Preparation of Glass and Crystalline Laths

After annealing, each glass was freed from the platinum boat by bending the overlapped foil at the corners of the boat to break free the glass at these points and then peeling away the foil. The glass slab was cut into laths averaging about 1/2" square by .050" thick. Cutting was done in a kerosene bath with a diamond saw; the glass was mounted on a talc block with balsam.

The two large faces of each lath were ground and polished in three steps: (1) grinding on a lap wheel with a kerosene slurry of American Optical M $302\frac{1}{2}$ Abrasive; (2) the same procedure with M $303\frac{1}{2}$ Abrasive; and (3) polishing in a Syntron Vibratory Polisher with a kerosene slurry of M 309 W Abrasive. Steps 1 and 2 required a few minutes each; Step 3 required at least 6 hours. The glass laths were mounted on brass weights with balsam during grinding and polishing.

After grinding and polishing, each lath had to be cleaned in acetone, wiped off with paper towels, and the unpolished ends scraped with a small knife.

The melting study required the fabrication of laths composed of crystals 100 microns or greater in diameter. These crystalline laths were produced by putting glass laths through melting and growth cycles in which the glass was crystallized, then melted back, leaving only a few crystal remnants, then growing these remnants to form larger crystals. The cycling procedure used required six crystal growth periods at approximately $1050^{\circ}C$ for at least one hour each alternating with melting periods at $1120^{\circ}C$ of 8, 16, and 24 minutes and at $1130^{\circ}C$ of 16, 24, and 30 minutes. The final step was a crystal growing period of at least one hour at approximately $1050^{\circ}C$. A nitrogen atmosphere was held over Series 1 glasses crystallized by this procedure; Series 4 glasses were crystallized in air.

IV.3   Measurement of Kinetics of Crystallization

Hexagonal germanium dioxide crystals were grown in the polished glass laths by subjecting the laths to heat treatment which produced nucleation on the glass surfaces and then growth of the crystals into the glass. The crystals thus produced formed a layer around the glass.

The crystallization procedure involved first inserting a clean glass lath into a Vycor test tube 19 mm in diameter and 18 inches long. The lath was placed at the bottom of the test tube; for runs made at $1100^{\circ}C$ or higher, the lath was held in a small platinum foil boat. The top of the test tube was sealed with a rubber stopper protected

from radiation by a lump of Kaowool. A short piece of glass tubing connected to rubber tubing passed through the rubber stopper. When an atmosphere other than air was required, the test tube was evacuated down to a pressure of about 200 microns Hg, filled to one atmosphere with the required gas, evacuated again, then filled to a pressure of about 20 cms. Hg and sealed. This gas pressure produces approximately one atmosphere pressure in the crystallization range.

Crystals were nucleated and grown by inserting the sealed test tube containing the glass lath into a horizontal tube furnace. The furnace used was a Kanthal-wound mullite tube furnace 30" long with an inner diameter of 2-1/2". An Inconel sleeve 7" long and about 3/8" thick was placed at the center of the tube to produce a uniform hot zone of that length. The furnace was heavily insulated and powered by a saturable core reactor-magnetic amplifier unit with which its temperature was controlled. The temperature was recorded by an expanded-scale strip chart recorder. The hot zone temperature was held within a maximum fluctuation of $\pm 0.1^\circ C$. The temperature in the hot zone of the furnace was determined to within $0.1^\circ C$ using a Pt (10% Rh)-Pt thermocouple in a Vycor tube in place of a specimen before each set of crystallization runs. The thermocouple used throughout the study was calibrated against a secondary standard thermocouple whose calibration is traceable to N.B.S. Test # 189571-A,

Each glass lath was first inserted into the cooler
part of the furnace at a temperature between $500^{o}C$ and
$800^{o}C$, in each case approximately $300^{o}C$ cooler then the
hot zone of the furnace. Each glass lath was held at this
point for two minutes to assure nucleation and to lessen
the warmup time in the hot zone. The lath was then inserted
into the hot zone, reaching within $5^{o}C$ of the hot zone
temperature in less than two minutes. The lath was held in
the hot zone for a measured length of time, then quenched to
room temperature. The crystallization experimental condi-
tions and glasses are listed in Table IV.2.

The depth to which a lath had crystallized was
determined with a Filar eyepiece on an optical microscope.
For most of this study, the optical system of an LL Tukon
Hardness Tester was used; at a magnification of 566X, the
Filar eyepiece read directly in microns. When this instrument
was unavailable, an American Optical Metallographic Micro-
scope was used at a magnification of 500X. On this
instrument, the Filar eyepiece was calibrated using a stage
micrometer.

After heat treatment, each lath was broken in half
and one or both halves were mounted vertically in plastic,
allowing a cross-section of each lath to be viewed. The
procedure for grinding and polishing the mounted laths was
the same as that used to polish the glass laths
(Section IV.2).

Table IV.2

Crystallization Experiments

glass	temp. $^\circ$C	atmosphere	times (minutes)
1A	1100	dry N_2	$3\frac{1}{2}$,4,5,5
1A	1050	"	6,9,12,15
1A	1000	"	4,5,6,7,8
1A	950	"	4,5,6,7,8
1A	900	"	4,6,8,10,12
1A	850	"	10,14,18,22,26
1B	850	"	10,14,18,22,26
1B	800	"	30,45,60,75,90
1B	750	"	60,90,120,150,180
1B	700	"	6,9,12,15,18 hours
2A	1107	dry N_2	6,12,18,24,30
2A	1102	"	4,8,12,16,20
2A	1097	"	4,6,8,10,12
2A	1093	"	4,6,8,10,12
2A	1050	"	4,6,8,10,12
2B	1000	"	4,5,6,7,8
2B	950	"	4,6,8,10,12
2B	900	"	8,10,12,14
2B	850	"	10,18,26,34
2B	800	"	45,60,75,90,120
3A	1110	dry N_2	10,15,20,25
3B	1110	"	6,10,12,14
3A	1106	"	4,8,12,16,20
3A	1101	"	4,6,8,10
3C	1100	"	6,12,18
3B	1100	"	4,6,8,10,12
3A	1050	"	4,6,8,10,12
3B	1050	"	4,6,8,10,12
3C	1050	"	4,6,8,10,12
3A	1000	"	4,6,8,10,12
3B	1000	"	4,6,8,10,12
3C	1000	"	4,6,8,10
3A	950	"	4,6,8,10,12
3B	950	"	4,6,8,10,12
3C	950	"	4,6,10
3B	900	"	8,12,16,20,24
3D	850	"	20,40,60,70,80
3D	800	"	1,2,3,4,5 hours

Table IV.2 (cont'd)

glass	temp. $^\circ$C	atmosphere	times (minutes)
4A	1111	O_2	5,10,15,20,25
4A	1105	"	5,10,15,20,25
4A	1099	"	4,6,8,10,12
4A	1094	"	5,10,15,20,25
4A	1050	"	4,6,8,10,12
4A	1000	"	4,4,5,6,8,10,12
4B	1000	"	4,6,8,10,12
4B	950	"	4,6,8,10,12
4B	900	"	5,10,15,20,25
4A	850	"	20,40,60,80,80
4A	800	"	1,2,3,4,5 hours
2C	900	dry N_2	5,10,15,20,25
2C	900	N_2 + water vapor	5,10,15,20,25
2C	900	O_2	5,10,15,20,25

Thicknesses down to one micron could be measured reproducibly with the Filar eyepiece with an accuracy of ±0.1 micron. Measurements were made at intervals of 500 or 1000 microns, depending on specimen size, along each of the lath faces which had been initially polished. Typically, ten to twelve measurements were made on each of the two long sides of the lath. Separate averages were computed for each side, yielding two data points for each lath.

IV.4   Measurement of Kinetics of Melting

The procedure used to measure melting kinetics was basically the same as that used to measure crystallization kinetics; the equipment was identical. No nucleation step was needed in melting the crystalline laths; however, they were held for five minutes at about 1050°C in the furnace before being inserted into the hot zone in order to minimize the warming time. The conditions under which specimens were melted are listed in Table IV.3.

During melting, the crystalline laths remained in the platinum foil boats in which they had been cycled. The foil was peeled off before the melted laths were mounted in plastic.

In addition to a layer of glass formed around the perimeter of each specimen, melting also occurred at grain boundaries. Observation of the melt specimens under an

Table IV.3

Melting Experiments

glass	temp. ^{o}C	atmosphere	times (minutes)
1C and 1D	1122	dry N_2	4,6,8,10,12
"	1127	"	2,4,6,8,10,12,14
"	1132	"	2,4,5,6,7,8,10,12
"	1137	"	2,3,4,5,6,7,8
4A	1119	O_2	6,9,12
"	1125½	"	4,6,8,10
"	1131	"	3,4,6,8,10
"	1136	"	2,4,6,8

optical microscope also revealed that the crystal sizes were distributed over a range from about 10 microns to about 500 microns in diameter. Some regions of melted laths became completely glassy during melting runs because of the small size of the crystals in those regions. Measurement of the thickness of the peripheral melt layer, therefore, could not be made at uniform intervals around the entire perimeter of most specimens. Instead, measurements of the thickness of the peripheral melt layer were made only in those areas where this layer was bordered by large crystals.

IV.5   Determination of Glass Properties

The state of reduction of each glass was computed from the size of the absorption peak at 2450 $\overset{o}{A}$ in its ultraviolet absorption spectrum. Ultraviolet absorption spectra were determined with a Cary 14 Spectrophotometer using specimens approximately .010" thick. Neutral density filters were used to extend the absorption measurable from two to five orders of magnitude. Specimens .010" thick were prepared by mounting glass laths on the end of a brass cyclinder whose center had been milled down .012", then grinding and polishing the glass down to this thickness using procedures described in Section IV.2.

The hydroxyl ion contents of the glasses were determined from an absorption peak at 2.85 microns in the

infrared spectrum. A Perkin-Elmer 237 B or 337 Grating Infrared Spectrophotometer was used with specimens approximately 1/4" thick; specimen surfaces were either "as-melted" or ground and polished.

Spectographic analyses of some of the glasses were made under the direction of Mr. D. L. Guernsey of M.I.T. using standard techniques. For these analyses, glasses were crushed in plastic ball mills to avoid contamination. Chlorine determinations were made by wet chemical analyses. In both of these cases, analyses were made on glasses from batches in which crystallization and melting kinetics had been determined. Specimens had been ground, polished, and cleaned in exactly the same way as the glass laths in which crystals were grown, before being submitted for impurity analyses.

IV.6   Additional Experiments

An investigation determining the effects of glass melting conditions on the state of reduction of germanium dioxide glass is discussed in Appendix C.

V. RESULTS

V.1 State of Reduction of GeO_2 Glass and Crystals

The effects of atmosphere and temperature upon the state of reduction of germanium dioxide glasses, as determined here, are discussed in some detail in Appendix B.

The glasses used in the study of melting and crystallization divide themselves into four groups according to their state of reduction. The most reduced glasses have been labeled Series 1; the groups continue in arithmetic order from the most reduced to Series 4 which is very nearly stoichiometric. The state of reduction of each glass was determined by applying Smakula's Equation, assuming an oscillator strength of unity, to the peak at 2450 $\overset{o}{A}$ in the ultraviolet absorption spectrum of each glass. The assumptions involved in the use of Smakula's Equation and a typical calculation are presented in Appendix B. The degree of reduction of each glass, along with its linear absorption coefficient at the peak, k_{max}, and the peak width at half maximum, H, are listed in Table V.1.1. The peak height is measured taking the absorption of stoichiometric glass at 2450 $\overset{o}{A}$ as zero. A representative absorption spectrum for each of the four series of glasses is presented in Figure V.1.1.

Table V.1.1

State of Reduction of GeO_2 Glasses

glass	K^*_{max} (cm^{-1})	H** (eV)	$\overset{o}{A}$	N_o defects $\overline{cm^3}$	state of reduction GeO_{2-X} X
1A	151	0.670	320	9.11×10^{17}	4.4×10^{-5}
1B	134	0.620	300	7.50×10^{17}	3.6×10^{-5}
1C	142	0.682	320	8.72×10^{17}	4.2×10^{-5}
1D	137	0.682	320	8.41×10^{17}	4.1×10^{-5}
2A	120	0.545	260	5.90×10^{17}	2.9×10^{-5}
2B	75.4	0.855	400	5.80×10^{17}	2.8×10^{-5}
2C	89.7	0.521	250	4.21×10^{17}	2.0×10^{-5}
3A	35.8	0.496	240	1.60×10^{17}	7.7×10^{-6}
3B	38.4	0.472	236	1.63×10^{17}	7.9×10^{-6}
3C	24.0	0.496	240	1.07×10^{17}	5.2×10^{-6}
3D	44.2	0.545	260	2.17×10^{17}	1.0×10^{-5}
4A	2.00	0.409	200	7.37×10^{15}	3.6×10^{-7}
4B	0.909	0.334	160	2.74×10^{15}	1.3×10^{-7}

* K_{max} = linear absorption coefficient at the peak.

** H = peak width at half height.
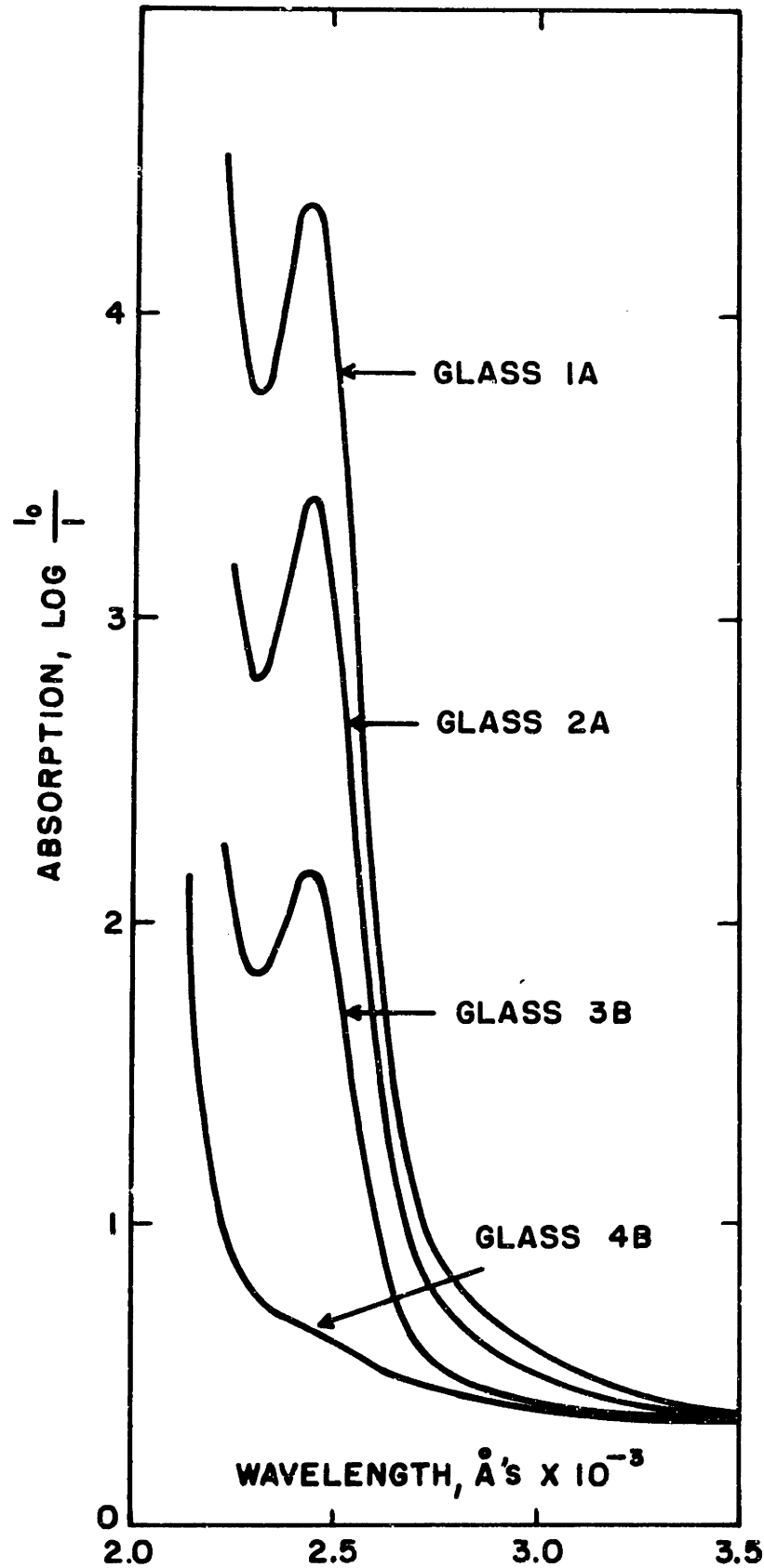
Figure V.1.1: Representative ultraviolet absorption spectra of Series 1-4 glasses.

Ultraviolet absorption spectra of hexagonal germanium dioxide crystals were measured on thin laths approximately .002" thick. These laths were formed by crystallizing glass laths supported by a frame of platinum foil. The crystal laths were not removed from the platinum foil; they were mounted in the Cary 14 spectrophotometer using the foil for support. One lath of Glass 4B was crystallized at $1000^{O}C$ in oxygen; a lath of Glass 1A was crystallized at $1000^{O}C$ in nitrogen. The crystals grown from the stoichiometric glass (4B) had only a single absorption peak, at 2050 $\overset{O}{A}$, in their ultraviolet absorption spectrum. The crystals grown from the reduced glass (1A) exhibited a broader peak at 2050 $\overset{O}{A}$ and a "shoulder" at 2150 $\overset{O}{A}$. The appearance of the ultraviolet absorption spectra of the two crystals is the same as that of a stoichiometric and a reduced glass shifted 300 $\overset{O}{A}$ lower in wavelength. It was assumed that the "shoulder" appearing in the spectrum of the crystal grown from the reduced glass is produced by oxygen vacancies in the crystal. Applying Smakula's equation, it was determined that the state of reduction of the crystal grown from the reduced glass (1A) was .0006%. The degree of reduction of Glass 1A is .0044%.

V.2 Nucleation

No bulk or homogeneous nucleation of germanium dioxide crystals was observed in any of the specimens examined in this study. Surface nucleation was found to occur without exception on any glass specimen which had been cooled to room temperature for any length of time and then heated to a temperature in the crystallization range. No special seeding or other surface treatment was necessary to produce surface nucleation. There was no evidence of any delay time or incubation period preceding nucleation.

The only specimens in which surface nucleation was avoided were those glass laths in which crystals were grown by cycling. After the crystals were melted back from the surface at temperatures above the melting point, no crystals nucleated on the surface during the following crystal growth cycle. This observation is very likely associated with the fact that the samples were not cooled down to the nucleation temperature range between treatments. This effect was observed microscopically during the development of the cycling schedule used in this study.

V.3 Crystallization Kinetics

The crystal growth data for the glasses in which crystallization rates were measurable are presented in Table A.1 of Appendix A. Typical plots of growth data

(crystal thickness versus time) are presented in Figures V.3.1 - V.3.3.

At all temperatures studied and in all the atmospheres employed, the intrinsic growth was always linear with time, i.e., the thickness of the crystalline layers increased linearly with time. Crystals growing in Glass 1A at 1100°C grew linearly with time until a crystalline layer about fifteen microns thick was formed; growth then proceeded erratically. The early crystallization rate was taken as the intrinsic rate in this case.

For the most part, two data points were obtained from each specimen, one for each polished surface. In instances where only one point is reported for a given time at a given temperature, no measurements could be made on the other surface due to surface cleaning problems or because of fracture along that surface caused by the lath's sticking to the platinum foil in which it was held during crystallization.

The lines drawn through the data in Figures V.3.1 - V.3.3 were determined by least squares analyses in which no intercepts with the time axis were specified. The time plotted is time in the furnace hot zone. The crystal growth rates were determined in all cases from the slope of the line fit to the data by a least squares analysis. The crystal growth rates measured are presented in Table V.3.1.
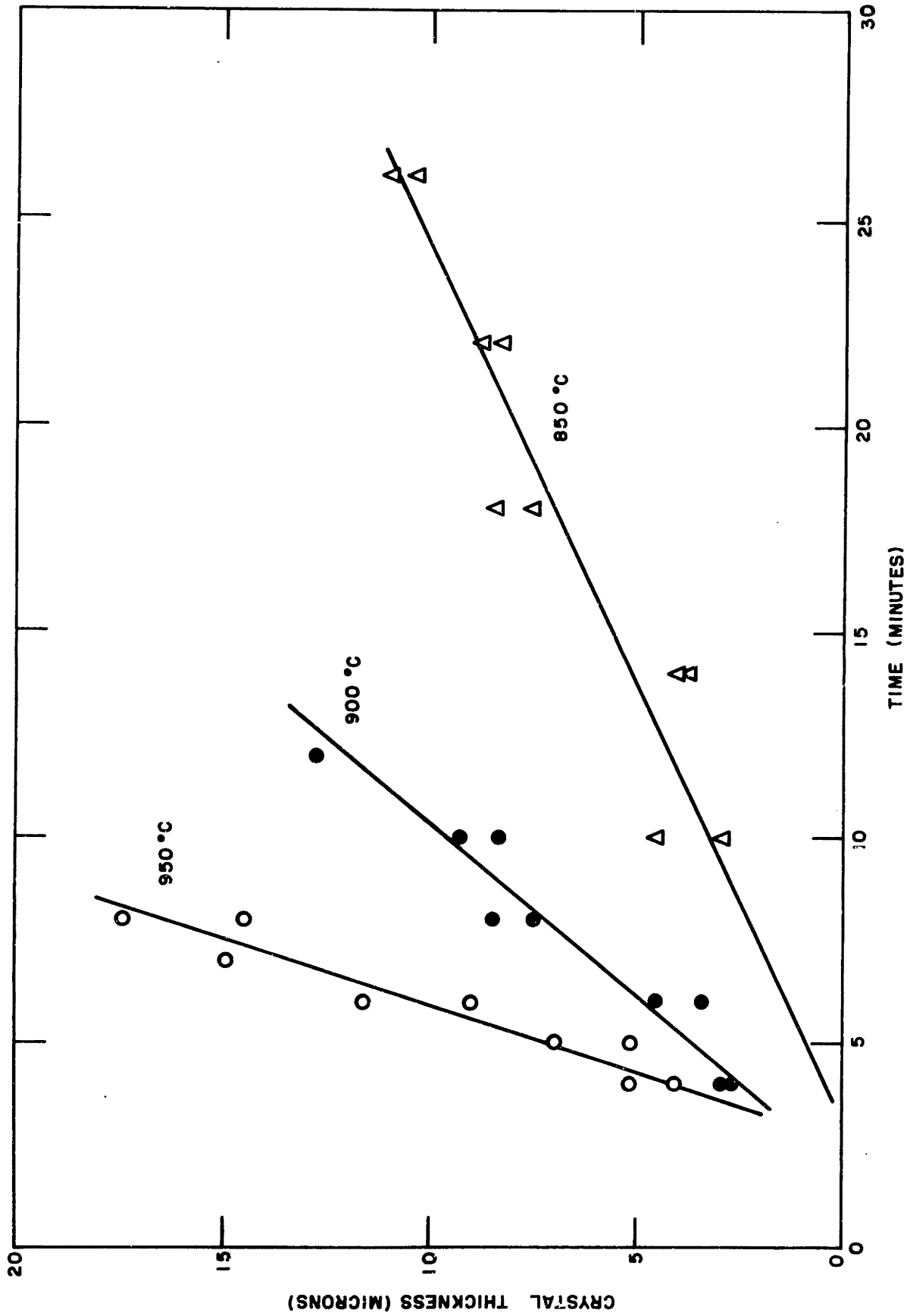
Figure V.3.1: Crystal growth in Series 1 glasses at 850°, 900°, and 950°C.
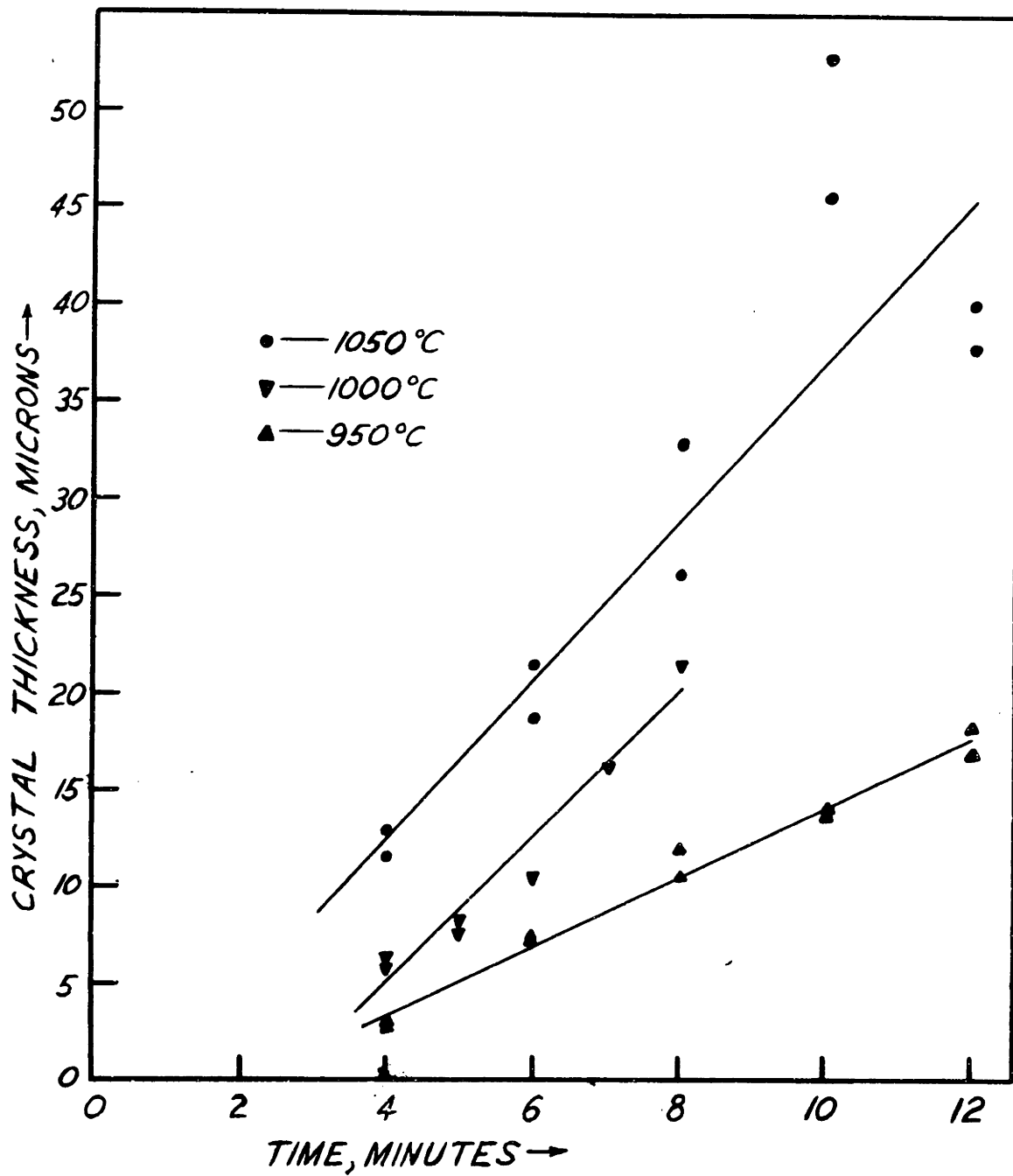
Figure V.3.2: Crystal growth in Series 2 glasses at 950°, 1000°, and 1050°C.
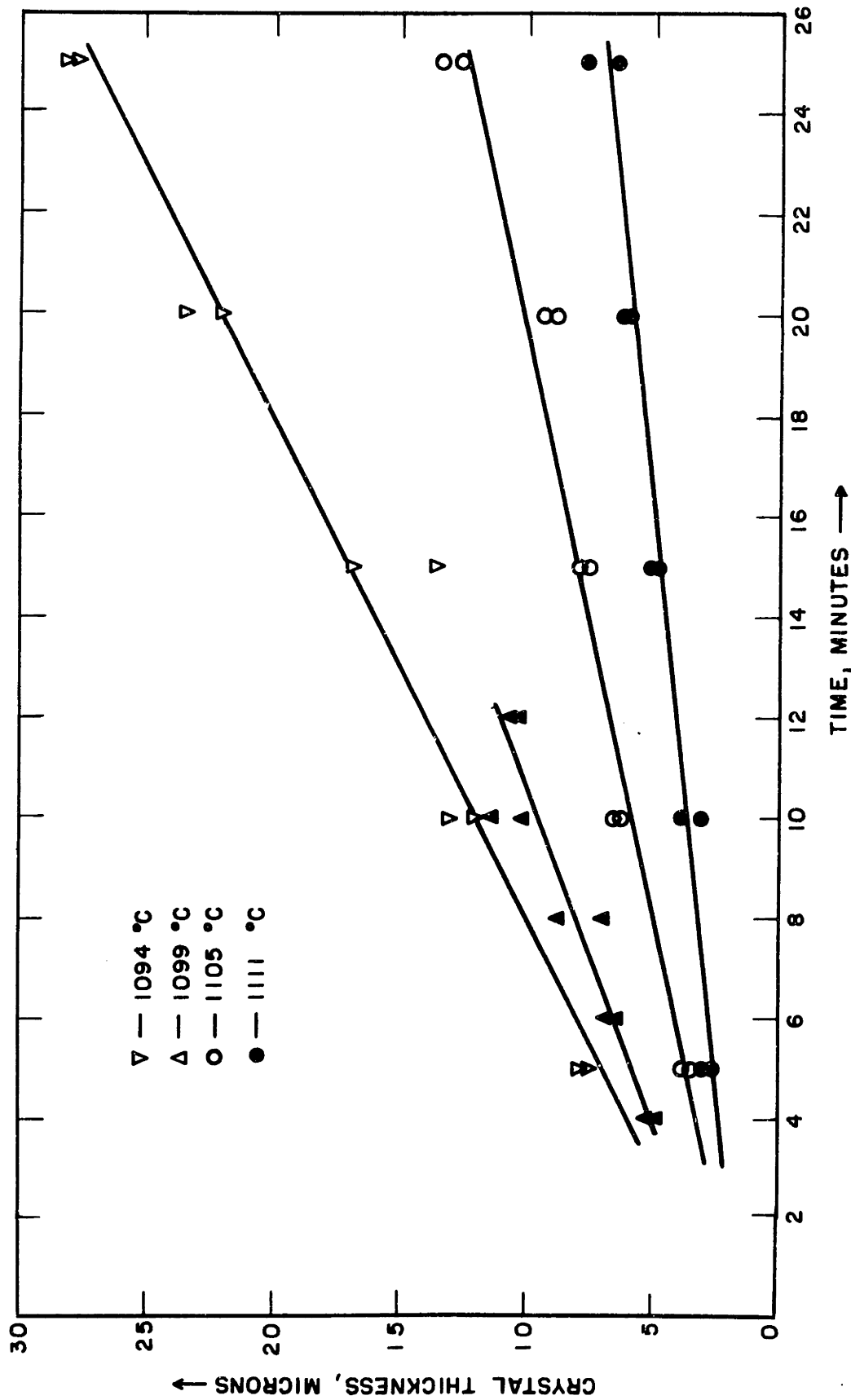
Figure V.3.3: Crystal growth in Series 4 glasses at low undercoolings.

Table V.3.1

Crystal Growth Rates

glass	atmosphere	temperature $^{\circ}C$	growth rate (cms./sec.)
1A	N_2	1100	6.39×10^{-6}
1A	"	1050	1.05×10^{-5}
1A	"	1000	9.96×10^{-6}
1A	"	950	5.08×10^{-6}
1A	"	900	1.99×10^{-6}
1A	"	850	7.75×10^{-7}
1B	"	850	6.87×10^{-7}
1B	"	800	1.91×10^{-7}
1B	"	750	5.97×10^{-8}
1B	"	700	1.33×10^{-8}
2A	"	1107	2.28×10^{-6}
2A	"	1102	3.70×10^{-6}
2A	"	1097	3.75×10^{-6}
2A	"	1093	5.00×10^{-6}
2A	"	1050	6.83×10^{-6}
2B	"	1000	6.27×10^{-6}
2B	"	950	2.97×10^{-6}
2B	"	900	1.79×10^{-6}
2B	"	850	4.58×10^{-6}
2B	"	800	1.51×10^{-7}

Table V.3.1 (cont'd)

glass	atmosphere	temperature $^\circ$C	growth rate (cms./sec.)
3A	N_2	1110	5.14×10^{-7}
3B	"	1110	7.20×10^{-7}
3A	"	1106	7.44×10^{-7}
3C	"	1102	1.71×10^{-6}
3A	"	1101	1.83×10^{-6}
3B	"	1101	8.85×10^{-7}
3A	"	1050	3.32×10^{-6}
3B	"	1050	4.40×10^{-6}
3C	"	1050	6.40×10^{-6}
3A	"	1000	3.98×10^{-6}
3B	"	1000	2.25×10^{-6}
3C	"	1000	4.12×10^{-6}
3A	"	950	2.34×10^{-6}
3B	"	950	1.15×10^{-6}
3C	"	950	1.84×10^{-6}
3B	"	900	1.01×10^{-6}
3D	"	850	3.33×10^{-7}
3D	"	800	7.88×10^{-8}

Table V.3.1 (cont'd)

glass	atmosphere	temperature $^{\circ}C$	growth rate (cms./sec.)
4A	O_2	1111	3.67×10^{-7}
4A	"	1105	7.09×10^{-7}
4A	"	1099	1.23×10^{-6}
4A	"	1094	1.69×10^{-6}
4A	"	1050	3.54×10^{-6}
4A	"	1000	3.65×10^{-6}
4B	"	1000	4.88×10^{-6}
4B	"	950	2.96×10^{-6}
4B	"	900	9.88×10^{-7}
4A	"	850	4.93×10^{-7}
4A	"	800	1.36×10^{-7}
2C	N_2	900	1.67×10^{-6}
2C	N_2 + water vapor	900	1.54×10^{-6}
2C	O_2	900	1.78×10^{-6}

The crystal growth rate dependence on temperature of each series of glasses (i.e., of approximately equal state of reduction) is plotted in Figures V.3.4 - V.3.7. The curves drawn through these data points are simply drawn by eye. Crystal growth rates in Series 3 glasses exhibited the greatest amount of scatter. At temperatures for which two or more growth rate values were measured, the curve was drawn as closely as possible through the average of these values. In Series 1, 3, and 4, different glasses were run at the same temperature to assure that grouping according to state of reduction was relevant. In Figure V.3.8, the curves drawn through the crystallization data for all the runs made in nitrogen are compiled. All of the curves show the same form with a peak at approximately 75° undercooling. The growth rates cover approximately three orders of magnitude, from a minimum of 10^{-8} cms/sec at $416^{\circ}C$ undercooling to a maximum of 10^{-5} cms/sec at $75^{\circ}C$ undercooling.

The crystal growth rates in oxygen in stoichiometric GeO_2 glass (Series 4) are plotted in Figure V.3.7. Within experimental error, crystal growth rates in Series 4 glasses are the same as those in Series 3 glasses over the entire temperature range studied, even though the Series 3 glasses are approximately .001% reduced.
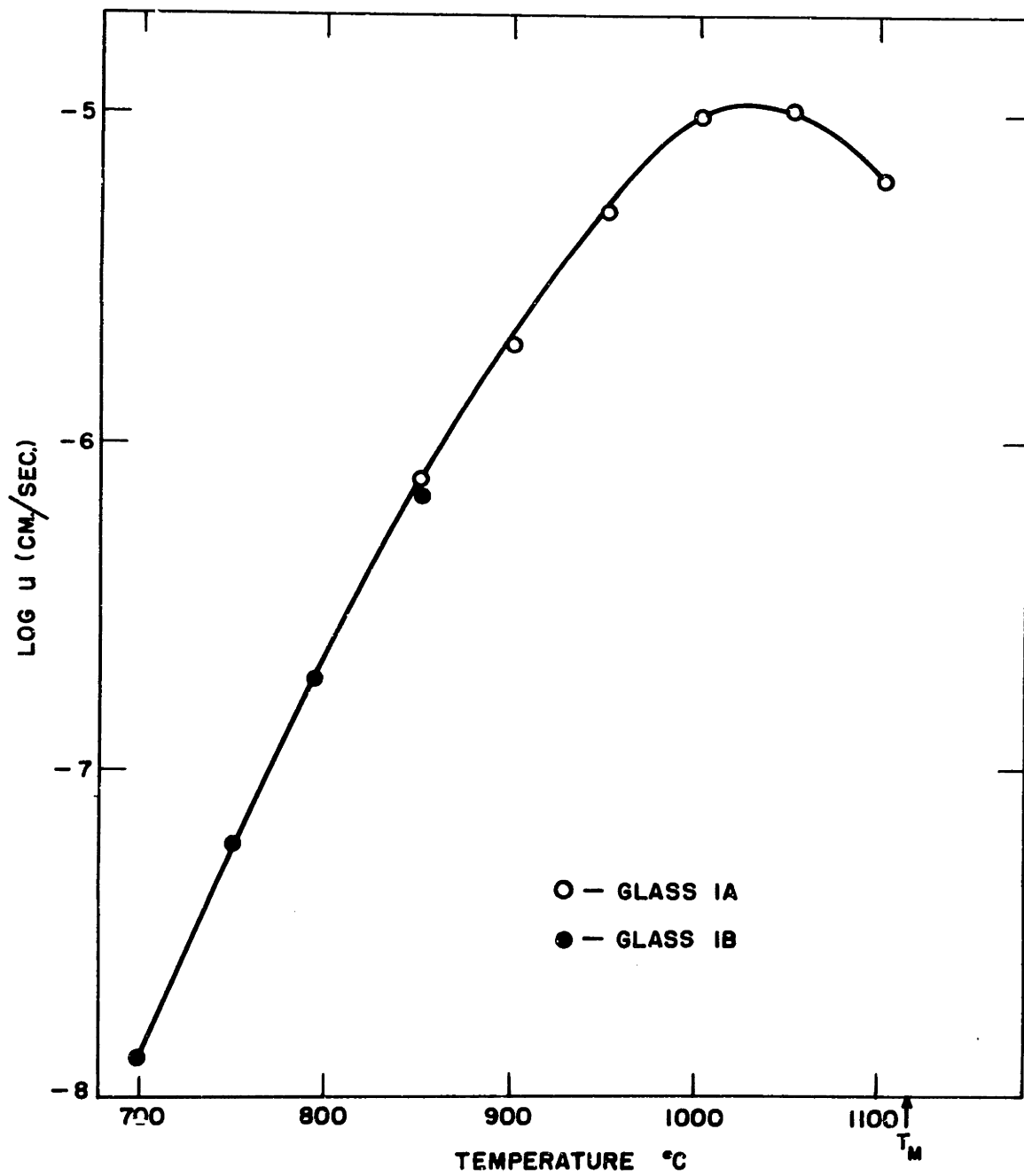
Figure V.3.4:   Crystal growth rates in Series 1 glasses.
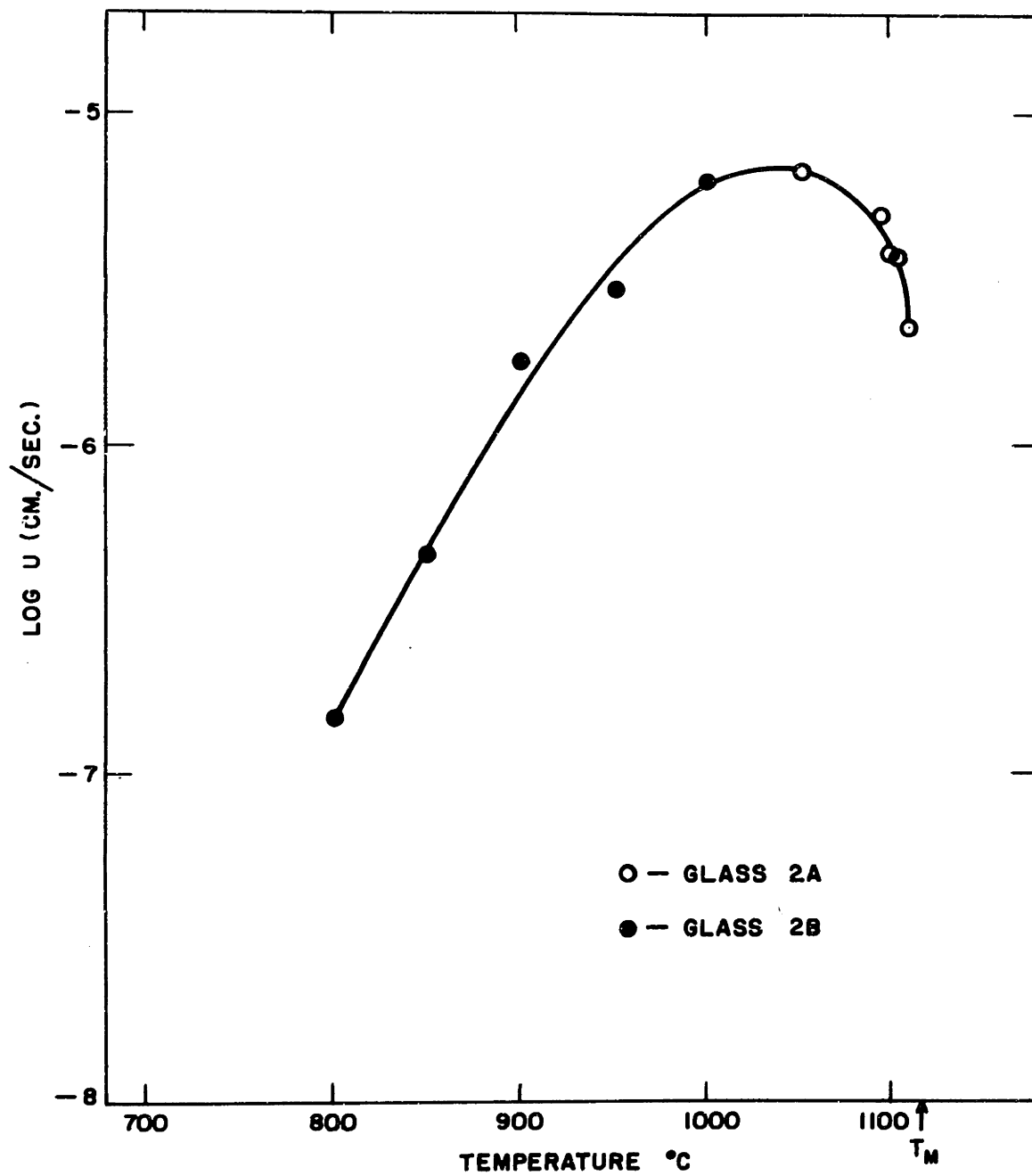
Figure V.3.5: Crystal growth rates in Series 2 glasses.
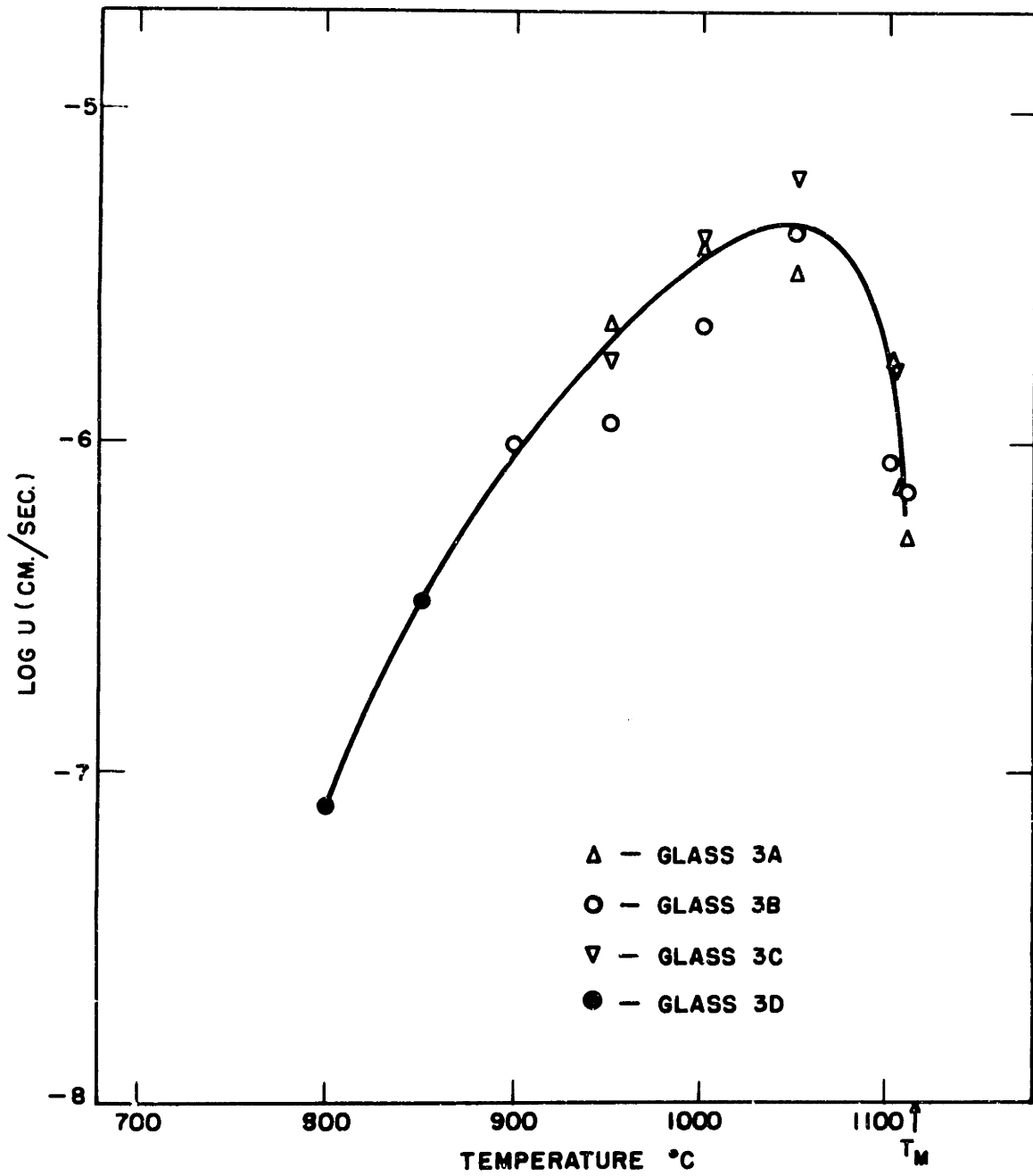
Figure V.3.6: Crystal growth rates in Series 3 glasses.
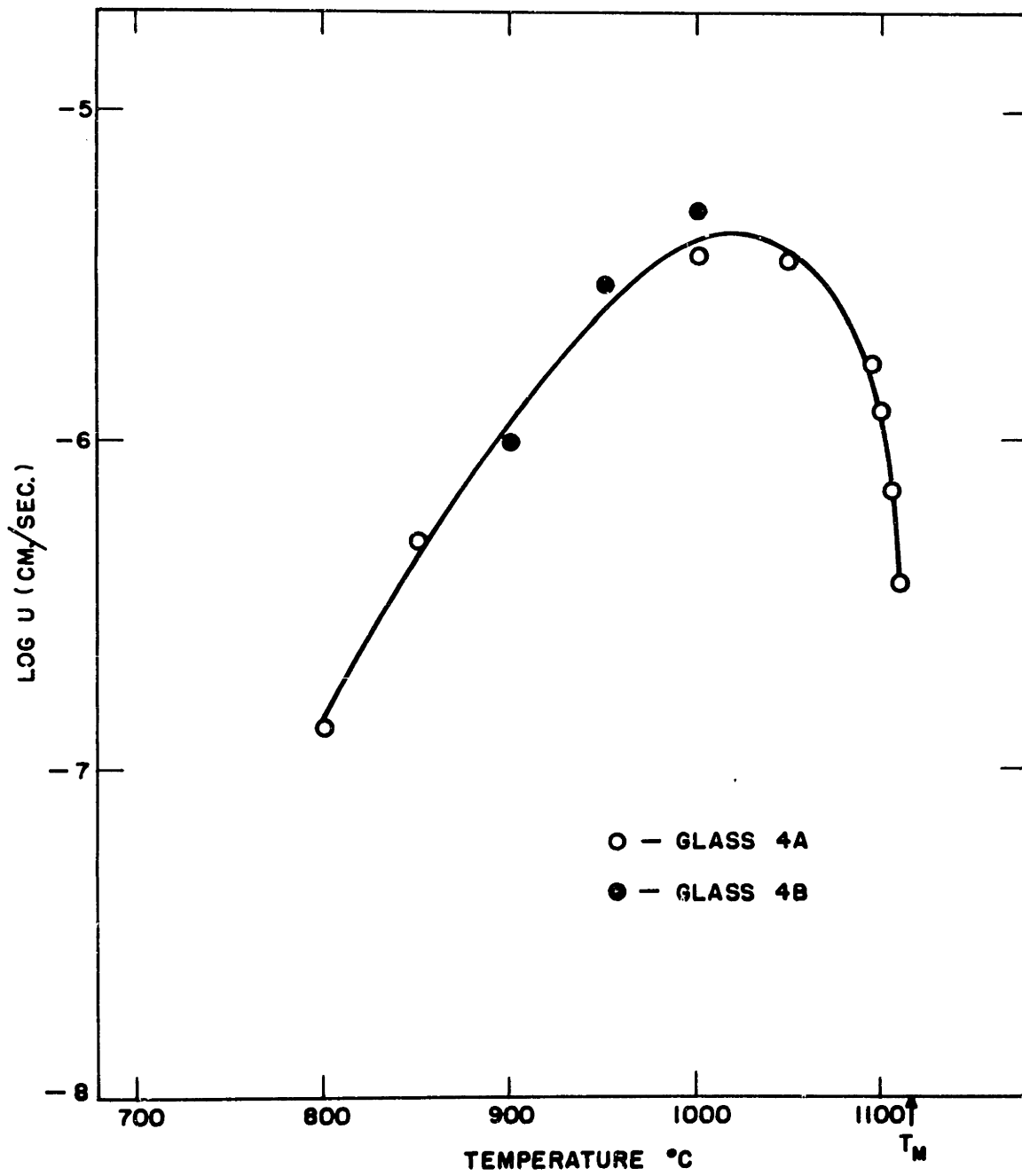
Figure V.3.7: Crystal growth rates in Series 4 glasses.
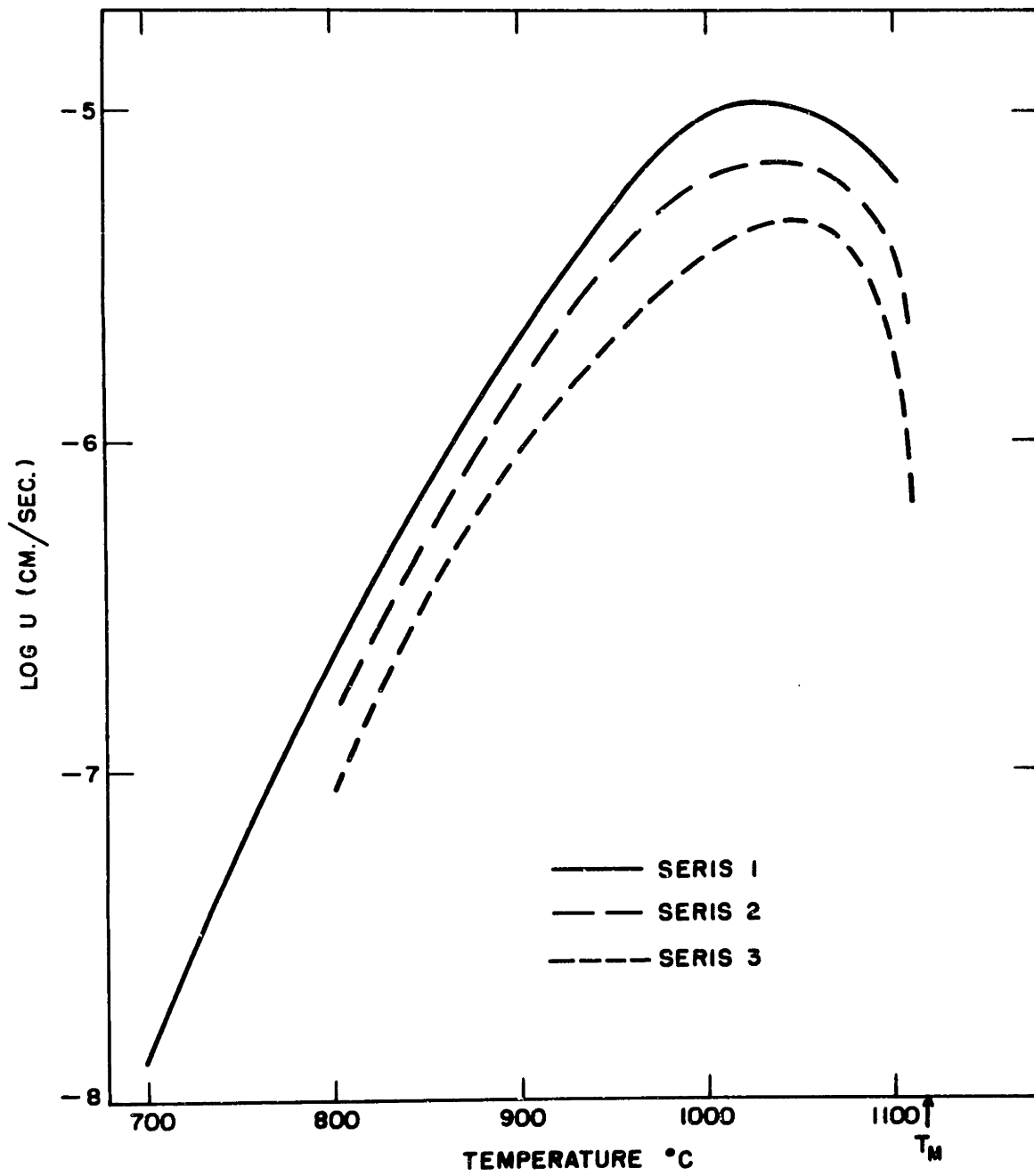
Figure V.3.8: Crystal growth rates in glasses of differing
states of reduction.

The minimum undercooling at which measurements could be made was found to be about 4°. At this point, the glass viscosity was low enough to allow the flat surfaces of the laths to become curved in the time needed to build up a measurably thick crystal layer. The crystal layers were fragmented and sometimes found scattered in the glass as a result.

Crystal growth measurements were limited also to minimum growth rates in the range of 10^{-8} cms/sec because of geometric effects. In this growth rate range, the surfaces of the specimens become scalloped (in cross-section), and the growth rate varied with the size of the scallops - being fastest in the smallest scallops. An example of this effect is seen in Figure V.3.9.

V.4   Melting Kinetics

The melting data for crystals grown from Series 1 and Series 4 glasses are presented in Table A.2 of Appendix A. Typical plots of melting data (melt layer thickness versus time) are presented in Figure V.4.1. The thickness of the melted layers increased linearly with time at all temperatures studied and in both oxygen and nitrogen atmospheres. Melting rates, determined from the slopes of lines fit to the data by least squares analysis, are listed in Table V.4.1.
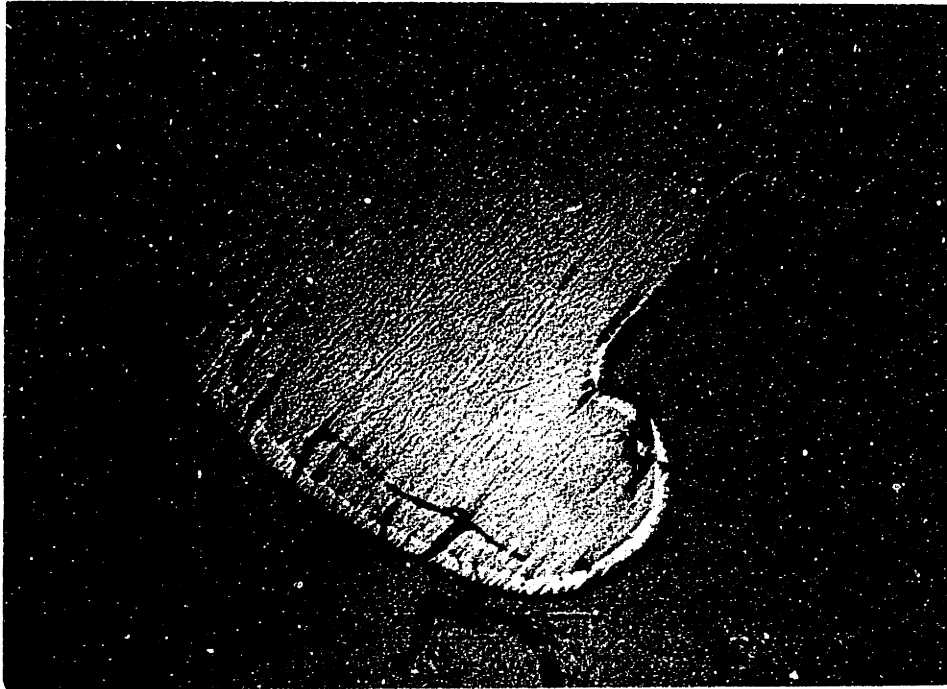
Figure V.3.9: Scalloped crystal growth at 750°C in a
Series 2 glass (100X). Crystal is
white border between light gray glass
and dark gray mount.
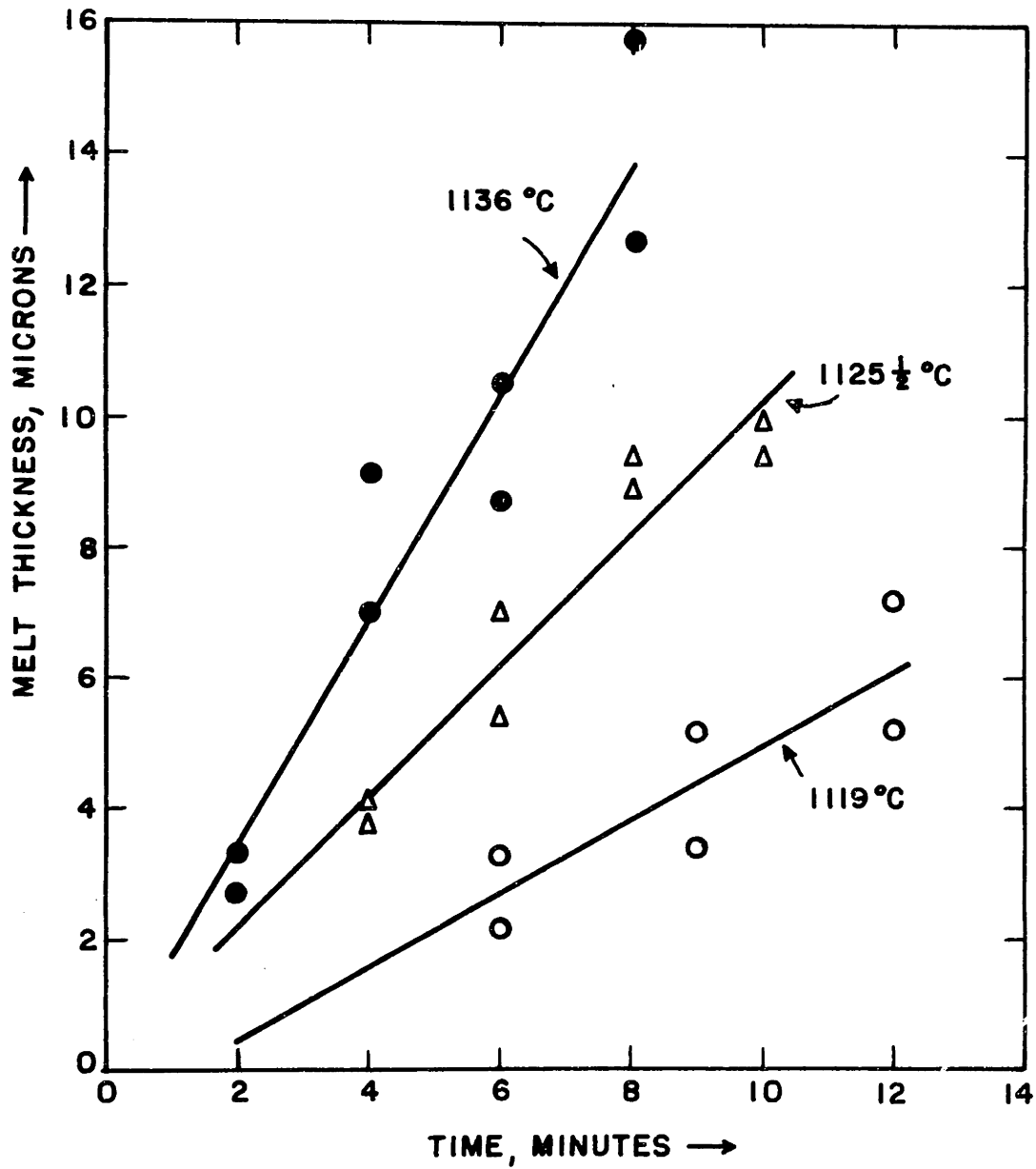
Figure V.4.1: Melting in Series 4 glasses.

Table V.4.1

Melting Rates

$T,^{\circ}C$	glass	atmos.	μ/min.	cm./sec.
1122	1C and 1D	N_2	1.52	2.52×10^{-6}
1127	"	"	3.38	5.11×10^{-6}
1132	"	"	4.19	6.95×10^{-6}
1137	"	"	6.75	1.12×10^{-5}
1119	4A	O_2	0.47	9.54×10^{-7}
1125½	"	"	1.01	1.68×10^{-6}
1131	"	"	1.55	2.56×10^{-6}
1136	"	"	1.77	2.93×10^{-6}

Table V.5.1

Impurity Concentrations in Some Glasses Used in Crystal Growth Rate Determinations (Weight %)

element	Glass 1A	1B	3B
Cl	0.15	0.13	0.14
Ag	< .0001	-	-
Al	.001 - .01	.001	.001
Ca	.001	.001	.0001 - .001
Cu	.0001	< .0001	< .0001
Fe	.001	.001	.0001
Mg	.001	.0001 - .001	.0001 - .001
Si	.001 - .01	.001 - .01	-
Ti	.0001 - .001	-	.001

element	3D	2A	3C
Cl	0.04	0.02	0.01
Ag	-	< .0001	-
Al	.001	.001 - .01	.0001 - .001
Be	-	< .0001	-
Ca	.0001 - .001	.0001 - .001	.0001 - .001
Cr	-	.0001 - .001	-
Cu	< .0001	.0001 - .001	.001 - .01
Fe	.0001	.0001 - .001	< .0001
Mg	.0001 - .001	.0001 - .001	.0001 - .001
Si	.001	.001	.0001 - .001
Ti	.0001 - .001	.0001 - .001	-

Table V.5.2

Impurity Analysis of Three Glasses
Exhibiting Extrinsic Crystal Growth
(weight %)

element	Glass #1	Glass #2	Glass #3
Cl	0.20	0.11	0.14
Ag	<.0001	<.0001	<.0001
Al	.0001 - .001	-	<.0001
Ca	.0001 - .001	-	.0001 - .001
Cu	.001 - .01	<.0001	<.0001
Fe	.0001 - .001	.0001 - .001	.0001 - .001
Mg	<.0001	-	<.0001
Mn	-	-	.0001 - .001
Na	.01	-	.01
Si	.0001 - .001	-	.0001 - .001
V	.0001 - .001	.0001 - .001	.0001 - .001

V.6 X-Ray Analysis of Hexagonal GeO$_2$ Crystal Growth Planes

Preferred growth planes of crystals grown intrinsicly and extrinsicly (Section V.8) from the surfaces of glass laths were determined from the X-ray diffraction patterns of two specimens of intrinsicly grown crystals and two specimens of extrinsicly grown crystals. An indication of the preferential appearance of each particular set of planes in each specimen was obtained from the relation(98):

$$p(hkl) = \frac{\dfrac{I(hkl)}{I'(hkl)}}{\dfrac{1}{n} \sum_{n} \dfrac{I(hkl)}{I'(hkl)}}$$

where p(hkl) = ratio of volume fraction diffracting from a non-random specimen to the volume fraction diffracting from a random specimen

   n = number of reflections observed

   I = intensity reflected by a preferentially oriented specimen

   I' = intensity reflected by a randomly oriented specimen.

p(hkl) was computed for each reflection of each specimen; these values are listed in Table V.6.1.

Table V.6.1

p(hkl) Values for GeO_2 Crystal Growth

hkl	intrinsic #1	intrinsic #2	extrinsic #1	extrinsic #2
100	0.49	0.34	0.21	0.52
101	2.18	0.17	0.14	0.26
110	0.85	0.16	0.44	0.78
102	0.60	1.03	0.12	0.43
111	0.49	0.57	0.35	0.49
200	0.62	0.52	0.19	0.40
201	0.32	-	-	-
003	0.31	-	-	-
112	0.78	1.91	4.32	3.70
103	0.29	-	-	-
202	1.22	1.29	1.05	1.05
210	0.98	0.78	0.70	-
211	0.85	0.65	0.26	0.61
113	1.46	2.06	0.70	0.70
203	0.98	1.16	-	-
212	0.98	0.41	0.23	0.58
301	2.44	1.03	-	0.70
104	1.22	2.72	3.30	2.42
302	1.46	0.52	-	1.39
114	-	2.06	-	-
221	-	1.03	-	-
310	-	0.78	-	-
312	-	0.78	-	-
105	-	-	2.09	1.56
214	-	0.78	-	-
006	-	-	1.57	1.22
411	-	-	0.35	0.17

V.7   Interface Morphology

The GeO_2 crystals grown in this study exhibited nonfaceted interfaces at all temperatures studied. The GeO_2 crystals which were melted also exhibited a nonfaceted interface morphology at all temperatures. Occasional facets appeared along otherwise nonfaceted interfaces in many of the crystal growth specimens. The number of these facets was greater in crystals growing near the melting temperature. The number of facets also was greater in specimens held for longer times at these temperatures. Glass 2A exhibited the greatest number of facets, with some areas of some specimens appearing largely faceted but apparently growing at the same rate as adjacent nonfaceted areas. Glass 3B exhibited interfaces which had the fewest facets and which appeared to be the least damaged in grinding and polishing and was the most free from pullouts and cracking at the interface. In most specimens which were mounted and polished, cracks occur in the glass ten to fifty microns in front of the interface and run parallel to the interface for much of its length.

A photomicrograph of a typical nonfaceted interface appears in Figure V.7.1; one of a region of Glass 2A which appears faceted appears in Figure V.7.2.

Mount Crystal Glass

Crack in Glass

~20µ

Nonfaceted Interface

Original Polished Surface
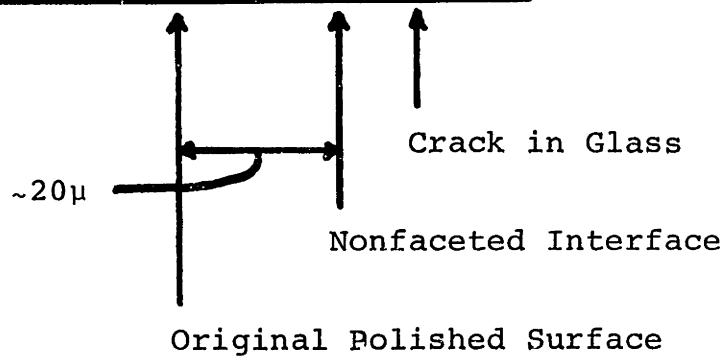
Figure V.7.1: Typical nonfaceted interface.
(1000X, Glass 3B, 1000°C, 12 mins.)
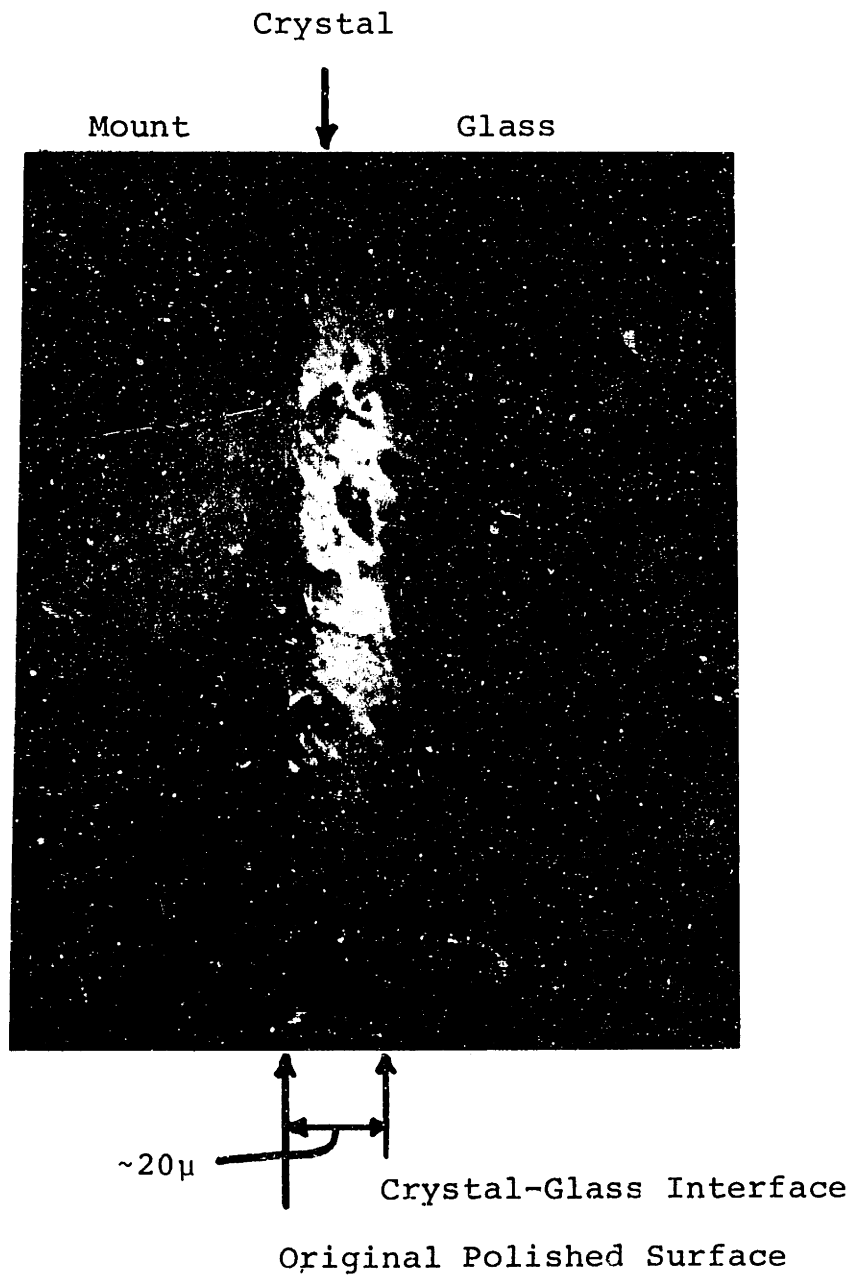
Figure V.7.2: Facets along an interface in Glass 2A. (500X, 1107°C, 18 mins.)

V.8   Extrinsic Growth Effects

The thirteen glasses whose crystallization and/or melting rates are recorded in this thesis were the only glasses of more than sixty melted which exhibited growth and/or melting which was both self-consistent and reproducible and which therefore was considered intrinsic. All of the other glasses melted exhibited crystal growth rates which varied greatly both among specimens heat treated in identical fashion and within individual specimens. All of these glasses exhibited crystal growth rates at least a factor of three greater than any measured intrinsic growth rates; typically, crystal growth was two or three orders of magnitude faster in these glasses. Due to the inconsistency of growth in these glasses, only such rough estimates of growth rates were possible.

Extrinsic growth effects take two distinctly different forms: at temperatures below about $950^{\circ}C$, extrinsic growth is affected by specimen geometry, with rapid growth proceeding from the four thin edges of the glass laths; above $950^{\circ}C$, extrinsic growth proceeded from all faces of the laths. The viscosity at $950^{\circ}C$ is 2×10^{6} poises.

Some typical results of attempts to measure extrinsic crystal growth at a temperature above $950^{\circ}C$ are presented in Figure V.8.1, which contains photomicrographs of crystals
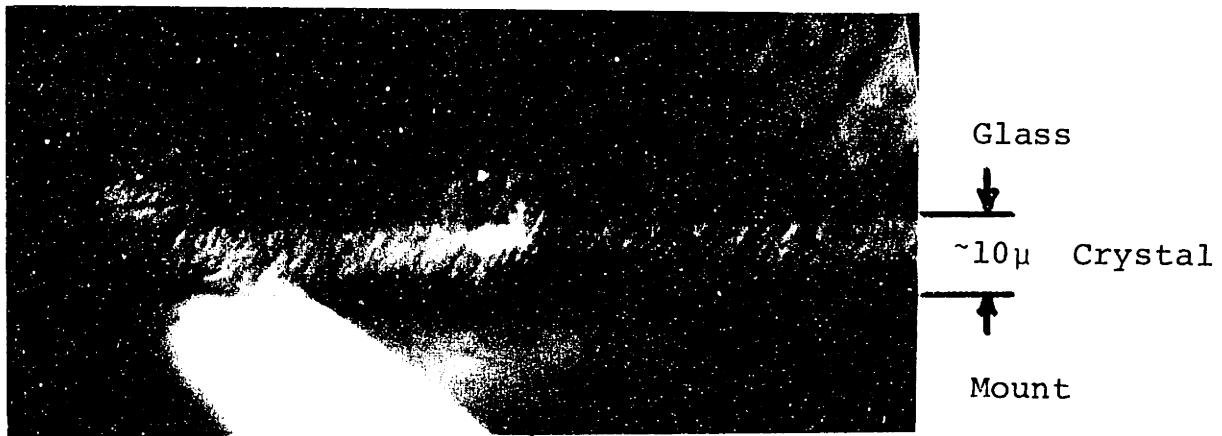
Figure V.8.1.A: Extrinsic crystal growth, 2 mins. at 1000°C (1000X).
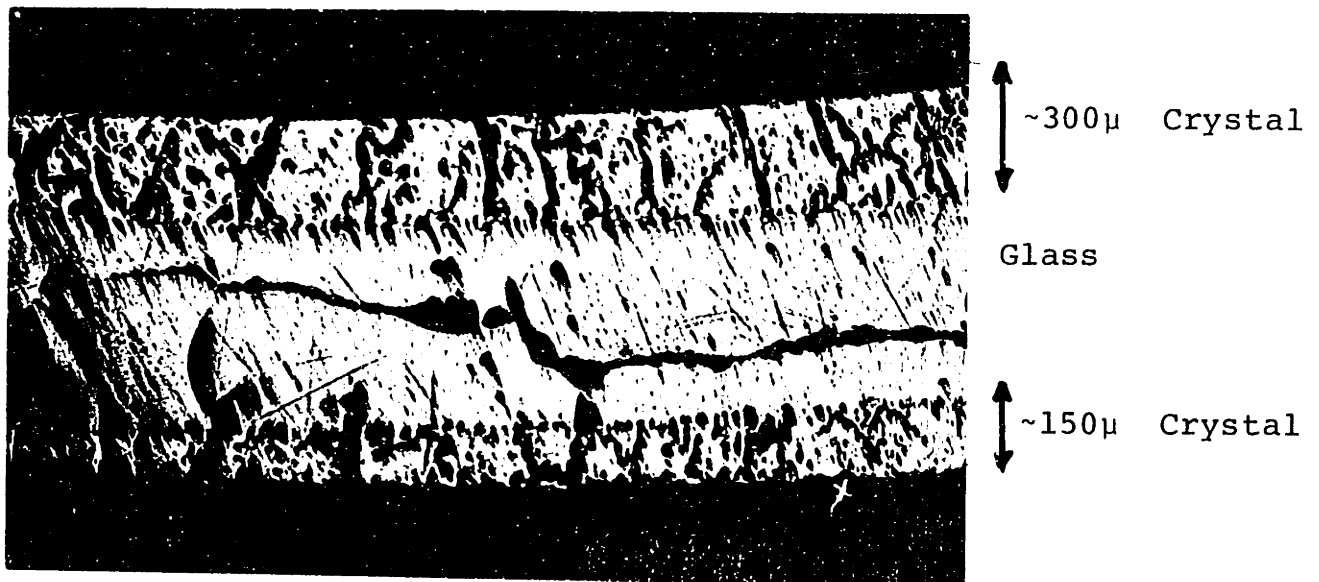
Figure V.8.1.B: Extrinsic crystal growth, same glass, 2¼ mins. at 1000°C (50X).

which were grown at 1000°C. The two minute specimen had

a crystalline layer only a few microns thick (Figure

V.8.1.A); specimens held for 2¼ minutes or longer each had

crystal layers hundreds of microns thick. Figure V.8.1.B

is a photomicrograph of the 2¼ minute specimen. Figure

V.7.1 is a photomicrograph of intrinsic growth in a glass

as reduced as the glass of Figure V.8.1.

Figure V.8.2 consists of photomicrographs showing

the typical form of extrinsic crystal growth which occurs

below 950°C. Although very rapid growth from the large

faces of the glass laths is sometimes seen in this tempera-

ture range, the specimen geometry apparently favors growth

from the edges of the lath. Figures V.8.2A-D are photo-

micrographs of laths approximately 1 mm thick magnified 50X.

The times of treatment are respectively 2, 2½, 3, and 3½

mins. in a furnace set at 900°C. Growth apparently is

initiated at corners in this case. Crystal spheres grow

from opposite corners and link as seen in Figure V.8.2.A.

The crystals then grow rapidly through the glass behind a

concave interface (Figure V.8.2.B and C), until the entire

specimen is crystallized and a void is formed near the center

of the lath (Figure V.8.2.D). In this type of extrinsic

growth, growth on the large faces of the lath far enough from

the corners to be uninfluenced by that faster growth is

rather reproducible. However, even these growth rates are at

least a factor of three greater than those measured in glasses

which do not exhibit rapid growth from the lath corners.

A

2 minutes

B

2½ minutes
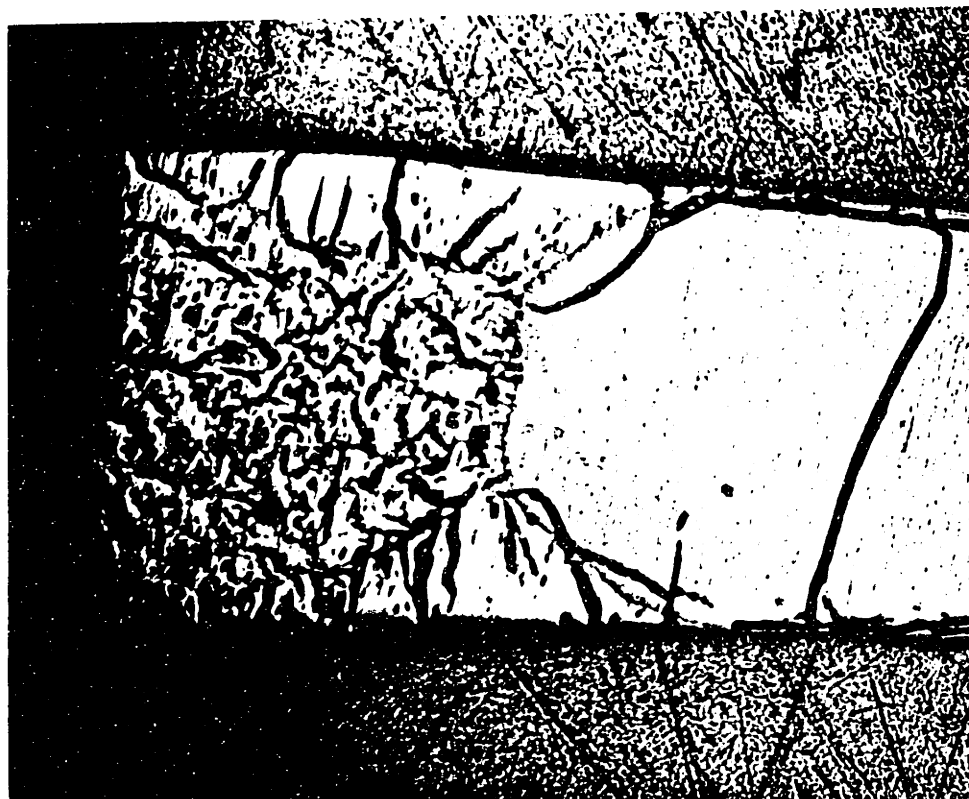
Figure V.8.2: Extrinsic growth at 900°C.

C

3 minutes

D

3½ minutes
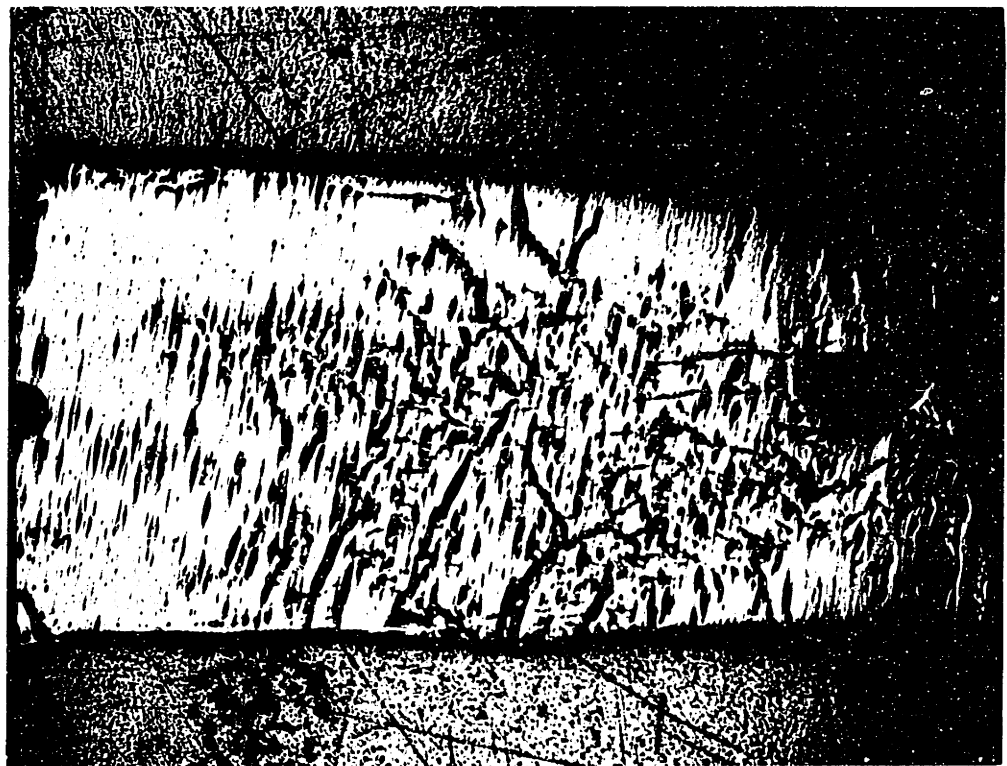
Figure V.8.2 (cont'd)

Figure V.8.3 contains photomicrographs of glasses crystallized at 900°C. The crystal layer in Figure V.8.3.A was grown in a specimen exhibiting the type of extrinsic growth shown in Figure V.8.2. Figure V.8.3.B is a photomicrograph of intrinsic crystal growth in a glass free of extrinsic growth effects. Both interfaces exhibit the same nonfaceted morphology.

V.9 Hydroxyl Ion Concentration

The hydroxyl ion concentrations of the glasses melted in this study were all very low ($<10^{-4}$%). The concentrations were determined by applying Smakula's equation, assuming an oscillator strength of unity (an example of this calculation appears in Appendix B) to the absorption peak at a wavelength of 2.8 microns. Some typical infrared absorption spectra are presented in Figure V.9.1; the absorption spectrum for the glass with the highest hydroxyl ion concentration (0.4 ppm), Glass 3A, is presented in Figure V.9.2.

In order to determine whether the absorption peak at 2.8 microns resulted from surface-absorbed water or hydroxyl ions in the bulk glass, spectra were determined for two different thicknesses of each of two different glasses. The size of the absorption peak increased in proportion with thickness in both cases, indicating that the source of this peak is hydroxyl ions in the bulk glass.
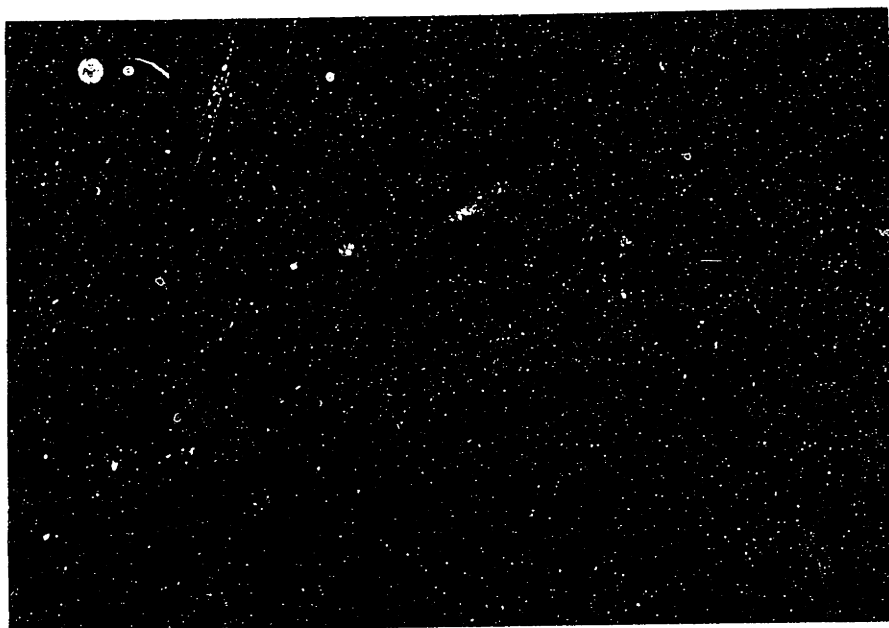
Figure V.8.3.A: Extrinsic growth (3½ minutes, 1000°C,
                   1000X).
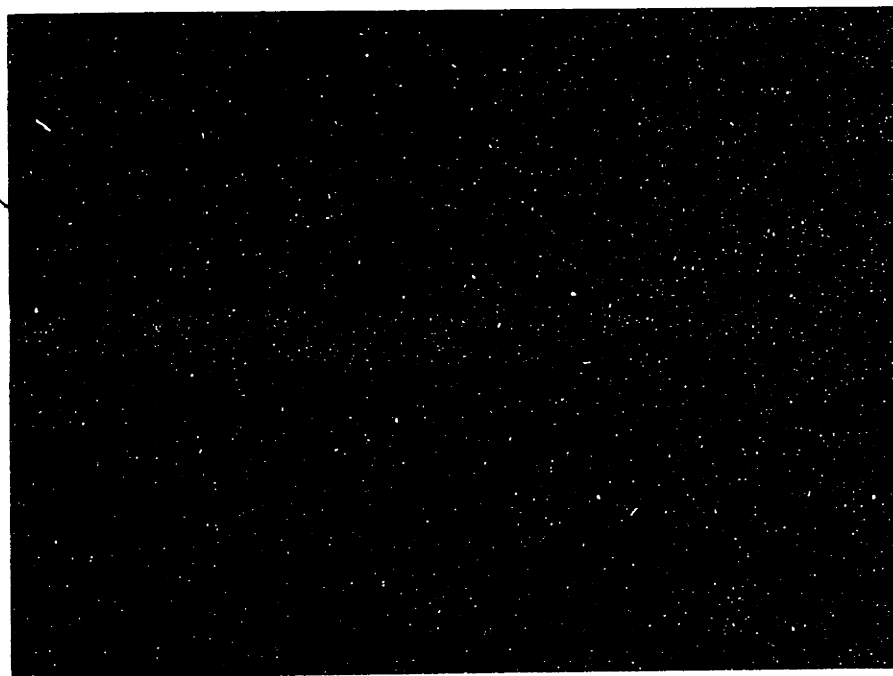
Figure V.8.3.B: Intrinsic growth (Glass 1A, 12 minutes,
                   900°C, 800X).

97.
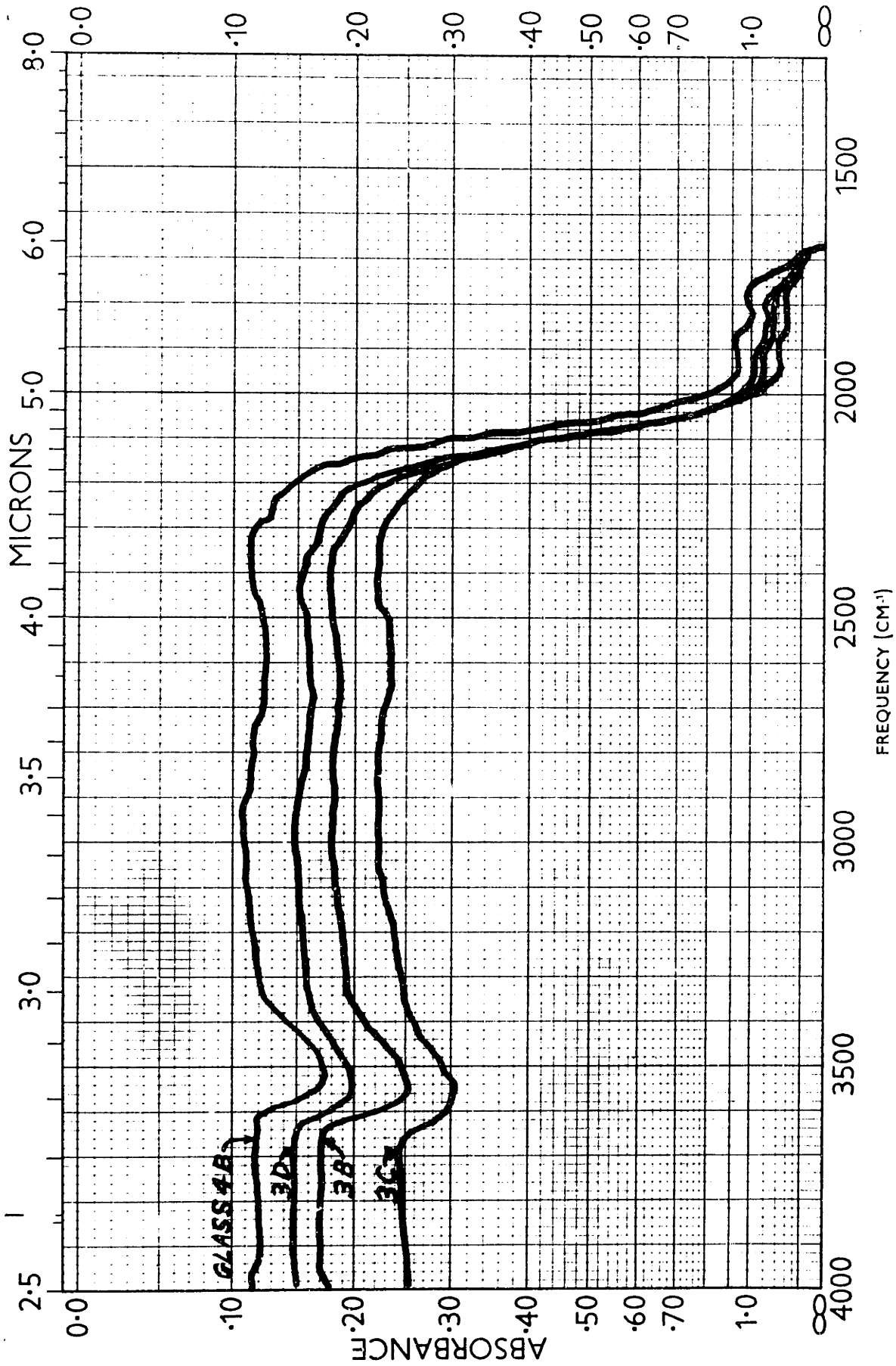
Figure V.9.1: Infrared absorption of Glasses 4B, 3D, 3B, and 3C (all .20" thick).
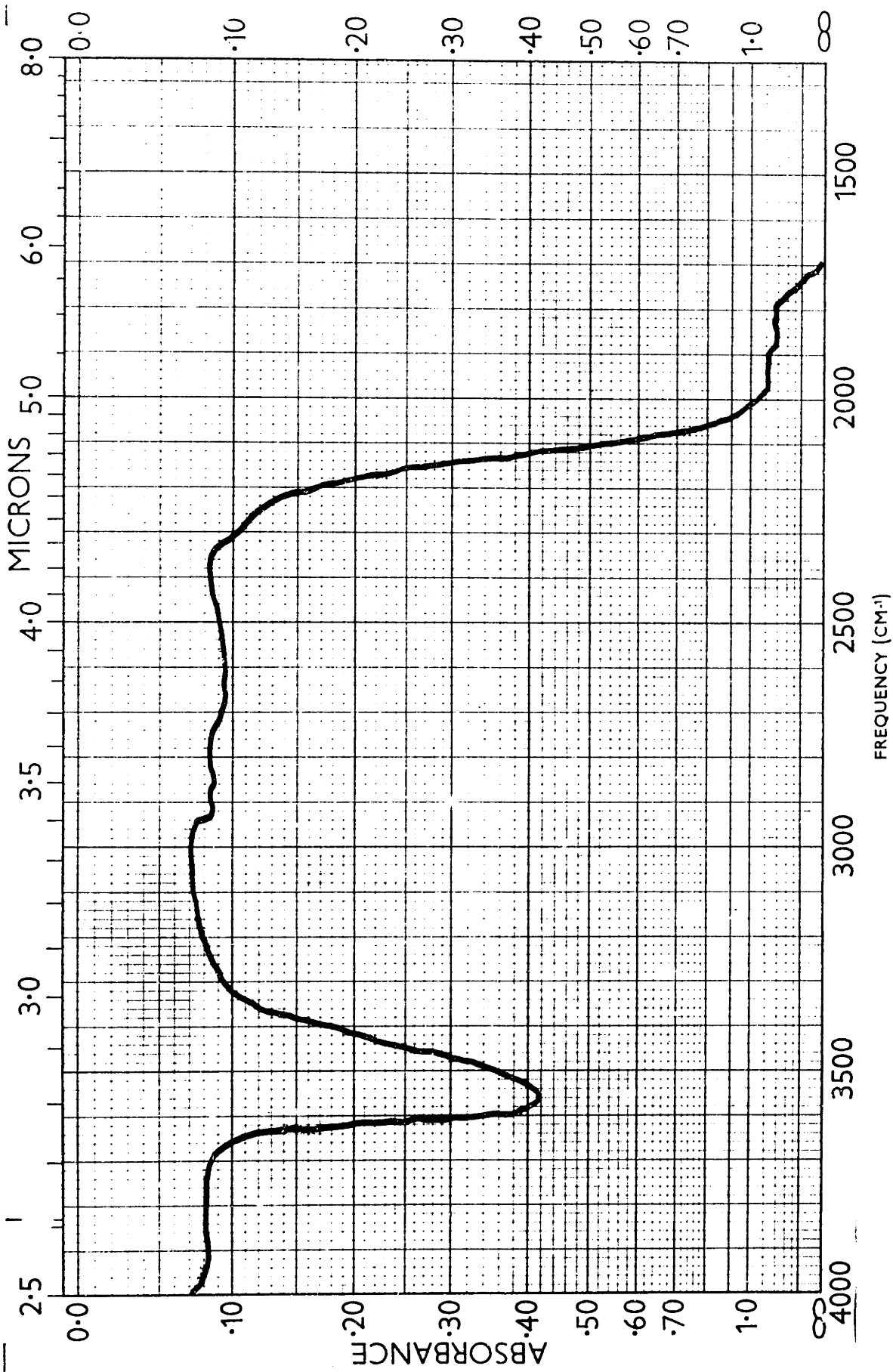
Figure V.9.2: Infrared absorption of Glass 3A (.25" thick).

V.10   Atmosphere Effects

In order to determine how atmosphere affects crystallization of germanium dioxide, specimens of Glass 2C were crystallized at $900^{\circ}C$ in dry nitrogen, wet nitrogen, oxygen, and hydrogen atmospheres. The crystal growth rates of crystals growing in oxygen, wet nitrogen, and dry nitrogen, were found to be the same, well within the limits of experimental error, as listed in Table V.3.1. The crystals grown in hydrogen grew at faster but not reproducible rates; the glass and crystal were blackened during crystallization, indicating reduction by the hydrogen.

Glass 2C specimens also were crystallized at $750^{\circ}C$ in air, dry nitrogen, and oxygen. No crystallization rates could be determined since scalloping of the surface occurred and the thickness of crystal layers in these specimens varied with the size of the scallops formed. It might be noted that this effect was the same in all of the specimens, regardless of atmosphere.

VI. DISCUSSION

VI.1 The Influence of the State of Reduction on Crystal Growth and Melting Rates

Within experimental error, Series 3 (.0008% reduced) and Series 4 (stoichiometric) glasses exhibit the same crystallization rates over the full temperature range studied. As shown in Figure V.3.8, however; crystallization rates increase with increasing state of reduction in glasses reduced more than .0008%. Series 1 glasses exhibit crystal growth rates greater than those of Series 3 and 4 glasses by a factor of two at high undercoolings and by a factor of about four at low undercoolings. Series 3 glasses also exhibit the greatest amount of scatter in their measured crystal growth rates.

The amount of scatter in the Series 3 measurements and the fact that Series 3 and 4 glasses exhibit about the same crystal growth rates may be explained by considering the concentrations of oxygen vacancies (excess Ge) and cation impurities in these glasses. The oxygen vacancy concentrations of Series 3 glasses are about at the midpoint in the cation impurity concentration ranges determined for Glasses 3B, 3C, and 3D (Table V.5.1). The oxygen vacancy (excess Ge) concentrations of Series 4 glasses are lower than their impurity concentrations. The impurities in Series 3 and 4 glasses may therefore determine their crystallization

rates; the scatter in the Series 3 measurements may result from differences in impurity levels in the glasses and possible interactions of the different types of defects when they are present in approximately equal concentration.

The direction of the change in growth rates with the state of reduction is consistent with the observed lowering of the bulk viscosity of the melt with increasing state of reduction(97). The extent of the change in growth rate with changing stoichiometry seems, however, far too great to be associated with this effect. The departures from stoichiometry cover a range of only .004%, and from the work of de Neufville(97), at $1100^O C$, excess germanaium concentrations of 0.3% were required to decrease the viscosity by a factor of 1/2. Similarly, Kurkjian and Douglas(92) found that a concentration of .045 mole % Na_2O was needed to decrease GeO_2 viscosity by a factor of 1/3 at $1100^O C$; an equal addition of Ge would not be expected to have as great an effect.

Although the oscillator strength of unity employed in computing oxygen vacancy (excess Ge) concentrations is believed to be the correct value, it is the upper limit on the range of possible oscillator strengths. The use of an oscillator strength of 0.1, for example, would have resulted in computed oxygen vacancy concentrations more nearly consistent with the observed differences in crystal growth rates.

Available data on the effects of additives on GeO_2 viscosity were all obtained at high temperatures. The viscosity data for pure GeO_2 for low temperatures exhibits greater scatter than that for high temperatures, as discussed below (Section VI.8). This suggests that the effects of additives on viscosity may be greater at low temperatures, and might account for the factor of two difference in crystal growth rates at low temperatures; however, it would not account for the greater difference observed at higher temperatures.

A possible mechanism increasing crystal growth rates of slightly reduced glasses could be the pileup of oxygen vacancies (excess Ge) ahead of the advancing interface. Such a pileup occurs because the crystals growing from the glass are closer to stoichiometry than the glass itself, as indicated by the ultraviolet absorption spectra of the crystals (see Section V.1). The region ahead of the advancing interface, rich in excess germanium, has a lower viscosity than the bulk glass and may result in faster growth rates.

Melting rates were measured for crystals grown from Series 1 and Series 4 glasses. The laths of Series 1 glasses which were held at temperatures between $1050^{\circ}C$ and $1130^{\circ}C$ in nitrogen while being cycled to grow large crystals were oxidized from .004% reduced state to a state of reduction of about .002%. Melting rates determined on these

Series 1 glasses were therefore measured on crystals in glasses only .002% reduced, a state of reduction in the range of Series 2 glasses.

The degree of reduction of these Series 1 melt specimens was determined using a specimen of Glass 1C prepared along with and in exactly the same way as the specimens used to measure the melting rate at $1132^{\circ}C$. This one specimen was held for thirty minutes at $1132^{\circ}C$, about twice the time of the longest melting run, to remove all but the smallest crystals remnants. The state of reduction was determined from its ultraviolet absorption spectrum.

The crystallization and melting rates of the .002% reduced glasses and the nearly stoichiometric (Series 4) glasses are plotted in Figure VI.1.1. The more reduced glass exhibits faster melting, as well as faster crystal growth rates. Crystal growth and melting rates increase linearly with undercooling and superheating in this temperature range near the melting temperature. At equal departures from the melting temperature, the melting rates of both glasses are greater than their respective crystallization rates. As will be seen below, this difference may be associated with the lower viscosity under conditions of melting.

The fact that melting is faster in the .002% reduced glass by a factor equal to the difference in the growth
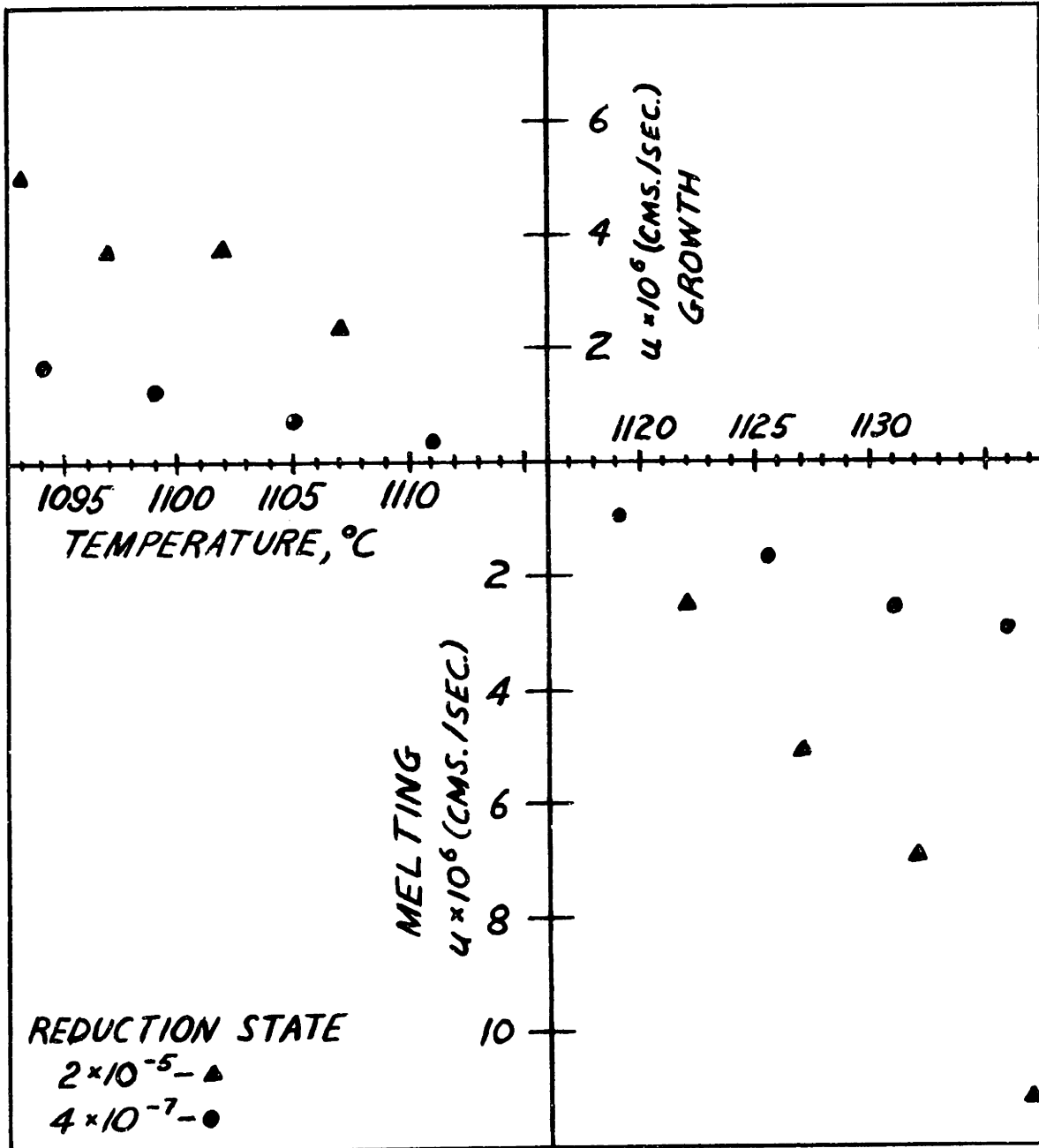
Figure VI.1.1: Crystallization and melting rates near the melting temperature.

rates in these glasses indicates that the difference in growth rates is not due to a pileup of oxygen vacancies (excess Ge) before an advancing interface. This type of pileup cannot occur in melting since the solubility of excess Ge in glass is greater than that in the crystals.

VI.2 Crystallization-Melting Rate Continuity at the Melting Temperature

Because of possible viscosity effects, it is not clear whether the crystallization and melting rates plotted in Figure VI.1.1 are continuous without change in slope through the melting temperature. To determine the continuity of crystallization and melting rates through the melting temperature with measurements covering a temperature range of $40^{\circ}C$, it is necessary to take into account the change in viscosity of the melt. Figure VI.2.1 is a plot of the product of the growth rate times the viscosity ($u\eta$) against temperature using the data of Figure VI.1.1 and the viscosity data of Fontana and Plummer(96). Although this viscosity data is not directly appropriate for these glasses, the form of its variation with temperature over the relatively small 40° range is probably not dissimilar to that of the correct viscosity data, and its use here probably introduces only a small error.

In Figure VI.2.1 it is clear that the melting and crystallization rates of both glasses are continuous without
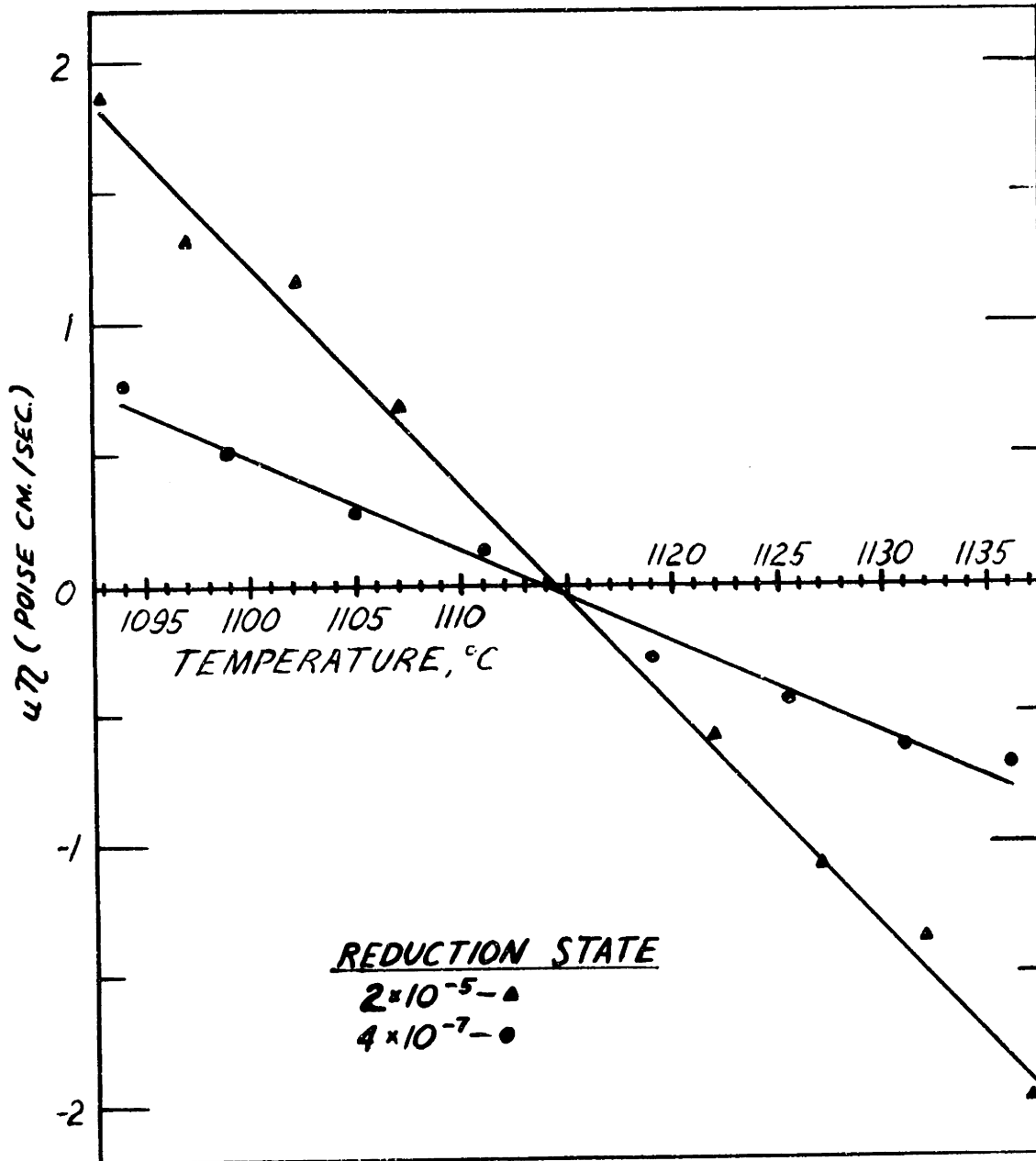
Figure VI.2.1: Crystallization and melting rate
continuity at the melting temperature.

change in slope through the melting temperature. The lines
drawn through the data in Figure VI.2.1 are fit by least
squares analyses. The intercepts with the temperature axis
indicate that the melting temperature is between 1113° and
1115^OC, within the accuracy range ($\pm$ 4^OC) of the generally
accepted value of the melting temperature, 1116^OC.

To further elucidate this point, a lath of crystals
grown from Glass 1C was held overnight in the furnace at
1115^OC. This lath was completely melted, indicating that
the melting temperature is below 1115^OC; based on the
present results, a value of 1114^OC is probably a better
estimate than the literature value. It should also be
noted that the melting temperature of the crystals grown in
this study is not a result of the chlorine impurity
concentration, since chlorine appears in equal concentration
in both the glass and crystals studied.

VI.3   Reduced Growth and Melting Rates

Table VI.3.1 lists the reduced growth rates and the
data used to compute them for all the crystallization runs
of Series 1 glasses. Tables D.1 and D.2 in Appendix D list
the reduced growth rates of Series 2-4 glasses and the
reduced melting rates of Series 1 and Series 4 glasses.

The reduced growth rate data which is relevant in
determining how the site factor varies with undercooling
is that of Series 1 glasses, which were melted in the same

Table VI.3.1

Reduced Growth Rates of Series 1 Glasses

glass	temperature $^{\circ}$C	u (cms/sec)	η (poises)	$[1-\exp(\frac{-L\Delta T}{RTT_E})]$	u_R
1A	1100	6.39×10^{-6}	4.37×10^{5}	0.0152	184
1A	1050	1.05×10^{-5}	1.07×10^{6}	0.0630	179
1A	1000	9.99×10^{-6}	2.69×10^{6}	0.112	239
1A	950	5.08×10^{-6}	7.59×10^{6}	0.161	239
1A	900	1.99×10^{-6}	2.24×10^{7}	0.212	211
1A	850	7.75×10^{-7}	7.76×10^{7}	0.265	227
1B	850	6.87×10^{-7}	7.76×10^{7}	0.265	201
1B	800	1.91×10^{-7}	2.76×10^{8}	0.318	166
1B	750	5.97×10^{-8}	1.23×10^{9}	0.364	202
1B	700	1.33×10^{-8}	6.02×10^{9}	0.419	191

way as the glass on which viscosity measurements were made

by Fontana and Plummer(96). The reduced growth rate

variation with undercooling for Series 1 glasses is

presented in Figure VI.3.1. Over the full range of

undercooling studied, from 16° to 416^OC, the reduced growth

rate is approximately constant, with random scatter of $\pm$ 15%

about a value of 210.

Theoretical reduced growth rate values, computed

using the Stokes-Einstein value for b in Equation II.3,

are indicated by a dotted line in Figure VI.3.1. The actual

reduced growth rates are about one order of magnitude

greater than these theoretical values, close to the values

predicted using the Eyring relation. These results are

consistent with the estimate of Cahn et al(25) that the

kinetic coefficient for transport across the interface should

be one or two orders of magnitude faster than that for

diffusion in the liquid.

The viscosity data used to compute the reduced growth

rates of Series 1 glasses can be accurately applied only to

those glasses since they are in the same state of reduction

as the glass on which viscosity was measured. The viscosity

measurements were made in air, creating the possibility that

the glass became less reduced during the course of the

viscosity measurements. However, the viscosity measurements

at high temperatures ($>950^O$C) were made by cycling the

glass three times in eight hour periods from a temperature of

about 1400^OC down to about 950^OC then up above 1500^OC.
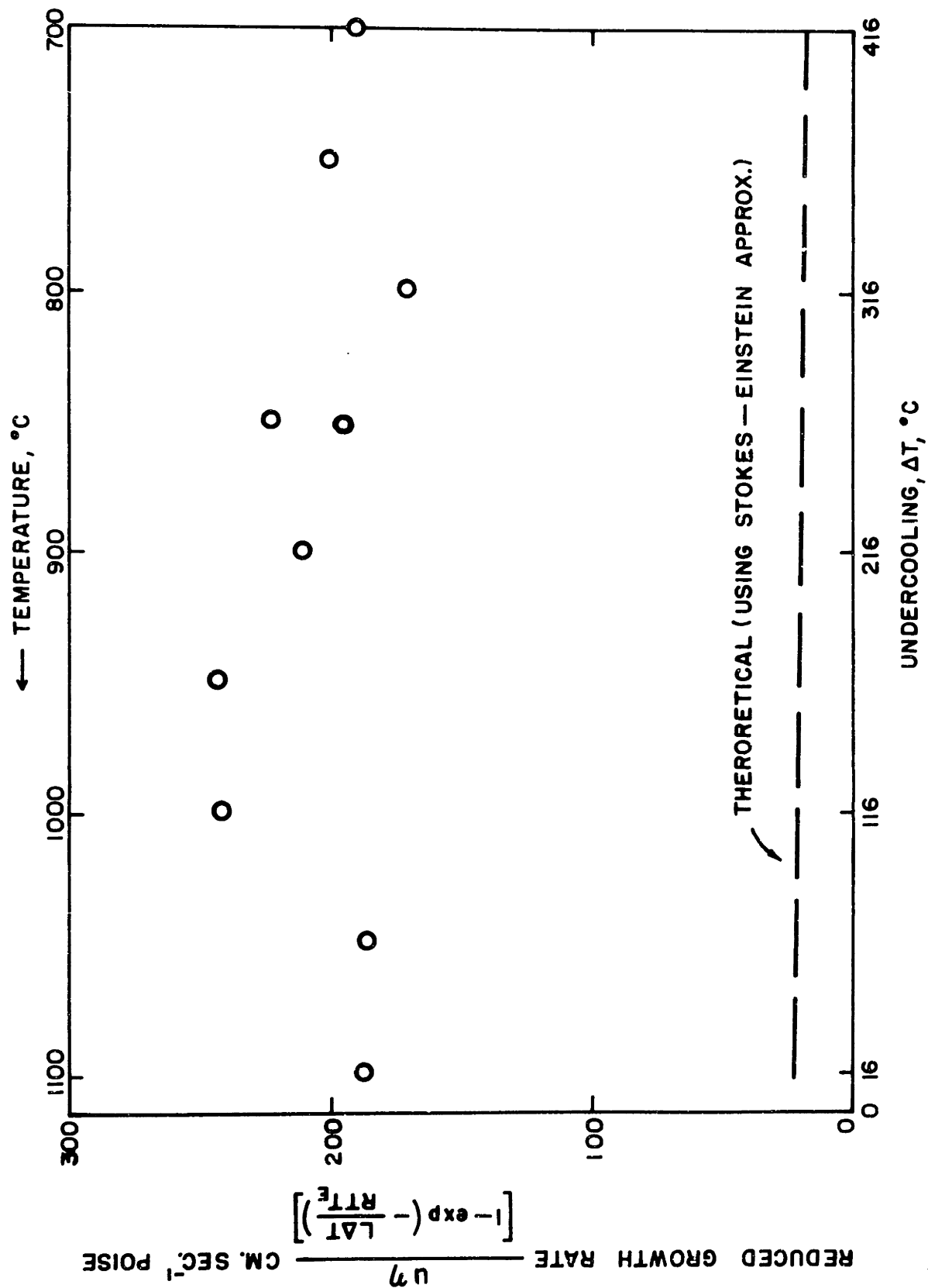
Figure VI.3.1: GeO_2 reduced growth rate variation with undercooling.

Figure C.3 of Appendix C indicates that glasses melted in air at temperatures between $1400^{\circ}C$ and $1500^{\circ}C$ are about as reduced as those melted in nitrogen at $1400^{\circ}C$. Because of the depth of the glass in the Margules viscometer employed in these high temperature viscosity measurements and the fact that the stoichiometry of the glass is changed by diffusional processes, it is unlikely that the state of reduction of the glass changed significantly during the viscosity determinations. The low temperature ($<760^{\circ}C$) viscosity data also can be assumed to be that for a glass in the same state of reduction as the Series 1 glasses because of the slowness (relative to the time of the experiment) of diffusional processes in highly viscous ($>10^9$ poises) glasses.

The reduced growth rate values for Series 2-4 glasses listed in Table D.1 were computed using the Fontana and Plummer viscosity values even though these values are known to be incorrect for these glasses since no viscosity data on glasses prepared as these were is available. Although the reduced growth rates computed for these glasses are approximately independent of temperature in each case, the amount of departure from a reduced growth rate independent of temperature increases with the difference in state of reduction between these glasses and the Series 1 glasses. This trend in the data suggests that these departures from reduced growth rates perfectly independent of temperature are due to an increasing error in the form

of the temperature dependence of the viscosity data used.

Plots of the reduced growth rate variation with temperature

for Series 2-4 glasses are included in Appendix D.

New batches of stoichiometric glass have been

prepared by the authors and sent to Dr. E. Fontana, who

has graciously offered to determine their viscosity-

temperature relations.

Figure VI.3.2 is a plot of the reduced growth and

melting rates near the melting temperature for glasses of

two different states of reduction. The continuity of the

growth and melting rates of these glasses at the melting

temperature was discussed in Section VI.2 and is clearly

seen in Figure VI.2.1. The reduced growth and melting

rates plotted in Figure VI.3.2 were computed taking $1114^{\circ}C$

as the melting temperature. $1114^{\circ}C$ is assumed to be the most

accurate value of the melting temperature of GeO_2 for the

reasons discussed in Section VI.2. Table VI.3.2 lists the

values of the reduced growth and melting rates plotted in

Figure VI.3.2 and the data used to compute them.

The reduced growth and reduced melting rates are

much more sensitive indicators of continuity than the

product $(u\eta)$. In Figure VI.3.2, it is clear that the

reduced melting rates of both glasses are independent of

temperature. The reduced growth and melting rates of both

glasses are also continuous through the melting temperatures.
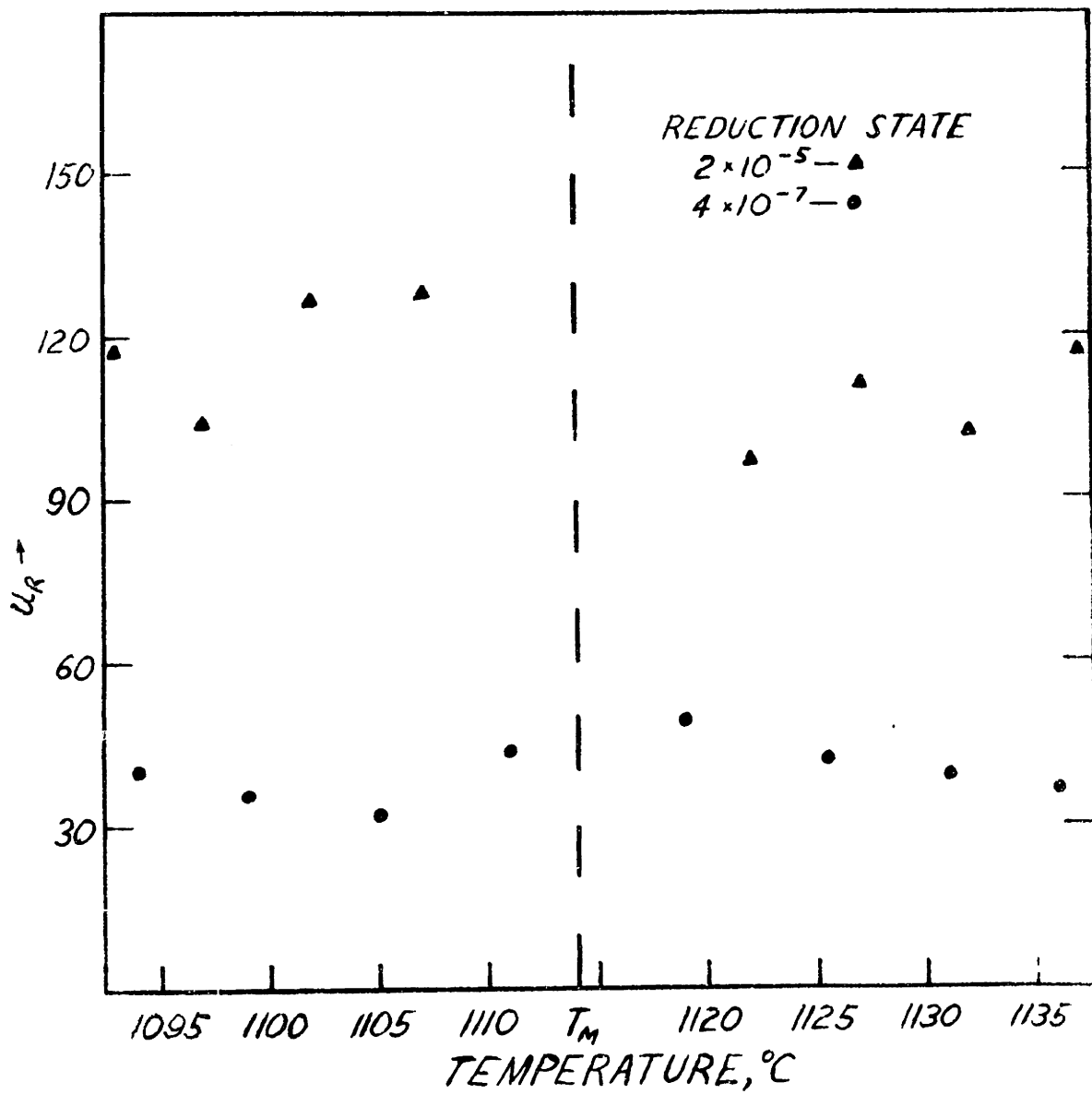
Figure VI.3.2: Reduced growth and melting rate continuity through the melting temperature.

Table VI.3.2

Reduced Growth and Melting Rates Near the Melting Temperature

state of reduction	temperature °C	$\|u\|$ (cms./sec.)	η (poises)	$[1-\exp(\frac{-L\Delta T}{RTT_E})]$	u_R
2 x 10⁻⁵	1093	5.00 x 10⁻⁶	4.68 x 10⁵	.020	117
=	1097	3.75 x 10⁻⁶	4.47 x 10⁵	.0161	104
=	1102	3.70 x 10⁻⁶	3.89 x 10⁵	.01135	127
=	1107	2.28 x 10⁻⁶	3.71 x 10⁵	.00660	128
2 x 10⁻⁵	1122	2.52 x 10⁻⁶	2.86 x 10⁵	.00745	97
=	1127	5.11 x 10⁻⁶	2.60 x 10⁵	.0120	111
=	1132	6.95 x 10⁻⁶	2.42 x 10⁵	.0165	102
=	1137	1.12 x 10⁻⁵	2.21 x 10⁵	.0212	117
4 x 10⁻⁷	1094	1.69 x 10⁻⁶	4.49 x 10⁵	.0190	40
=	1099	1.23 x 10⁻⁶	4.20 x 10⁵	.0142	36
=	1105	7.09 x 10⁻⁷	3.81 x 10⁵	.0085	32
=	1111	3.67 x 10⁻⁷	3.35 x 10⁵	.00282	44
4 x 10⁻⁷	1119	7.75 x 10⁻⁷	2.95 x 10⁵	.00467	49
=	1125½	1.68 x 10⁻⁶	2.69 x 10⁵	.01070	42
=	1131	2.56 x 10⁻⁶	2.42 x 10⁵	.0157	39
=	1136	2.93 x 10⁻⁶	2.28 x 10⁵	.0185	36

The viscosity data listed in Table VI.3.2 is that of Fontana and Plummer(96); its use here probably introduces only a small error, as discussed in Section VI.2.

VI.4   Hydroxyl Ion Concentrations

All of the glasses melted in this study had a very low concentration of hydroxyl ions; by far the highest concentration was that of Glass 3A, 0.4 ppm. Series 3 glasses differed by as much as one order of magnitude in their hydroxyl ion concentration; however, no systematic differences in crystal growth behavior were observed which could be attributed to variations in the hydroxyl ion concentration. The hydroxyl ion concentrations were at least two orders of magnitude lower than the impurity concentrations in all of the glasses.

VI.5   Interface Morphology

The occurrence of facets on the crystal-liquid interface in the higher temperature crystal growth specimens was random. The glass exhibiting the greatest number of facets and the most perfectly formed facets was Glass 2A. The first spectrographic analysis of this glass measured a high concentration of Al impurity (0.01-0.1%); the second analysis detected a concentration of only 0.001-0.01%.

Interpreting the results of the two spectrographic analyses as indicating either that this glass had a concentration of Al impurity somewhat greater than any cation impurity concentration in any of the other glasses studied, or that it contained some regions of higher Al concentration, these results suggest the faceting is due to Al impurities. The mechanism by which faceting occurs may be a preferential adsorption of impurities on crystals growing in particular crystallographic directions, which introduces greater anisotropy of growth. Why no difference in growth rate is observed between the faceted and nonfaceted areas of crystals growing in Glass 2A is not known. Whether Al is the only impurity producing these effects is also not known, but other impurity species are likely to behave similarly.

VI.6   Extrinsic Growth Effects

Spectrographic analysis of three batches of glass which exhibited extrinsic crystal growth revealed a concentration of .01% of sodium impurity in two of the three glasses (see Table V.5.2). This concentration is close to the lower limit at which sodium can be detected spectrographically. Extrinsic growth effects were less pronounced in the glass in which no sodium was detected; possibly this glass contained slightly less sodium than the other two glasses. The remainder of the cation impurity concentrations in these three glasses were the same as those

whose analyses are listed in Table V.5.1 (glasses exhibiting intrinsic crystallization).

The melting procedures followed to avoid sodium contaimination are discussed in Appendix E. Use of the melt schedule included in Appendix E completely eliminated sodium contamination problems. The last five batches of glasses, melted in this way for this study and for viscosity measurements, exhibited no extrinsic crystal growth effects.

The form of intrinsic growth observed below $950^{\circ}C$ is particularly interesting because of the appearance of crystals growing at two greatly differing rates in a single very small specimen. Because of the small size of the specimens, temperature and/or impurity differences are ruled out. Differences in surface treatment are ruled out because the same effect was observed in laths polished on all six faces. The geometry and time dependence of the faster crystal growth, however, do suggest that the faster crystal growth may result from stresses built up in the amorphous phase during crystallization. The faster crystal growth does not begin before a layer of crystal at least ten microns or so thick has formed on the surfaces of the glass. This crystal layer may prevent the rapid release of stress in the glass in front of the advancing concave interface.

The phenomenon mentioned in Section V.3 concerning the erratic crystal growth in Series 1 glasses at $1100^{\circ}C$ after a layer of crystal fifteen microns or so thick had

formed appears to be an impurity effect. This effect was observed in both the Series 1 glasses crystallized at 1100°C. After a layer of crystal about fifteen microns thick had formed, the scatter in measured crystal layer thicknesses increased to the point that no reliable data could be taken, with the majority of the data points falling below the extension of the initial linear growth line. The type of impurity and the mechanism involved are not known.

VI.7   Isotropy of Crystal Growth

The parameter p(hkl), defined in Section V.6, is an indication of the preferential occurrence of the (hkl) set of planes relative to their occurrence in a randomly oriented powder. The planes with the highest value of p(hkl) in Table V.6.1 are, therefore, not necessarily the planes on which most of the crystals are growing. A p(hkl) value of 2, for example, indicates only that the intensity of the x-ray beam diffracted by this set of planes in the crystal growth specimen was greater than that in the powder pattern; it does not provide a direct measure of the frequency of appearance of that particular set of planes.

The intrinsicly grown crystals used in this analysis have no highly preferred growth planes. The two most preferred sets of growth planes are different in the two

specimens. The same type of results have been observed
for a variety of other intrinsicly grown crystals whose
x-ray diffraction patterns have been determined.
Intrinsic crystal growth of hexagonal germanium dioxide
is therefore nearly isotropic.

The high values of $p(112)$ determined in both
extrinsicly grown crystal specimens indicate that this
set of low index planes is preferred in extrinsic growth.
Extrinsic crystal growth is therefore somewhat less
isotropic than intrinsic crystal growth in this material.

VI.8   Viscosity or Impurity Controlled Growth

In sections of the discussion above, different
observed phenomena are attributed to differences in
viscosity or differences in impurity levels, as if these
two properties were independent. Of course, the phenomenon
of viscosity decreasing with the state of reduction of the
glass can be viewed as an impurity effect, the impurity
species being oxygen vacancies (excess Ge) rather than some
species not introduced by the glass itself. In this light,
this study can be taken as an analysis of the sensitivity
of crystal growth to impurity concentrations. More
importantly, it raises the question of the sensitivity of
viscosity to impurity concentrations, since it has been
shown that a difference of .004% in the state of reduction
of a glass can produce a four-fold increase in the crystalli-
zation rates of that glass at some temperatures.

In general, it would not be expected that a bulk property, such as viscosity, would be as sensitive to impurities as a phenomenon occurring at an advancing interface. The viscosity of germanium dioxide glass is, however, apparently sensitive to differences in the state of reduction of the glass. The viscosity data of Nemilov and Ivanov(93), the only available extensive low temperature data other than that of Fontana and Plummer(96), shows viscosity values greater than the Fontana and Plummer values by a factor of about five over a wide temperature range. A few low temperature values determined by Bruckner(95), whose viscosity values agree with those of Fontana and Plummer at high temperature, are at least one order of magnitude lower than an extension of the Fontana and Plummer data to the temperature range of the Bruckner data. Typical data from each of these investigations is presented in Figure II.5.

Each of these viscosity investigations used glasses of different purity and prepared in different ways. It is hoped that the further study, on the stoichiometric glass, will clarify the source of the discrepancy in the data of earlier studies and determine the sensitivity of the viscosity to the state of reduction of slightly reduced amorphous germanium dioxide.

VI.9   Comparison with Results of Other Studies

To put the results obtained in this study in perspective, it is useful to compare them with the results of previous crystallization studies. Melting and crystallization studies of sodium disilicate, a glass-former with an intermediate entropy of fusion value, and silicon dioxide, the only other low entropy of fusion glassformer studied to date, are quite complete and provide results relevant for comparison.

The 400°C range of undercooling in which crystal growth rates of Series 1 glasses were measured is the widest temperature range in which crystal growth rates have been measured, although both SiO_2 and $Na_2O \cdot 2SiO_2$ crystal growth rates have been measured over a range of hundreds of Centigrade degrees. Silicon dioxide and germanium dioxide both exhibit continuity of crystallization and melting rates at the melting temperature, while $Na_2O \cdot 2SiO_2$ exhibits faster melting rates at equal departures from equilibrium. The two low entropy of fusion glass-formers exhibit nonfaceted interfaces during both melting and crystallization; $Na_2O \cdot 2SiO_2$ crystals are faceted during growth, but melt with a nonfaceted interface morphology. These results indicate that the sites participating in growth and melting are the same only in the case of the low entropy of fusion materials.

The variation of crystal growth rates with temperature has approximately the same form in all three of these materials; however, only the low entropy of fusion materials exhibit a reduced growth rate which is independent of undercooling.

Germanium dioxide crystallization rates increase with the state of reduction of the glass, while silicon dioxide crystallization rates decrease with the state of reduction. This difference in behavior can be attributed to the difference in hydroxyl ion concentration in the glasses studied. Turnbull and Uhlmann([99]) have attributed the slow crystal growth in reduced silicon dioxide glasses to the association of the hydroxyl ions and the reduced species. In SiO_2 glasses, hydroxyl ions may be present in concentrations as low as the present GeO_2 glasses or in concentrations as high as 0.1%, depending on the preparation methods employed. If the effect of excess network forming cation tying up hydroxyl ions does occur in germanium dioxide glasses, it would not be seen in the glasses studied here, since the highest hydroxyl ion concentration in any glass measured was only 4×10^{-4}%.

VII. CONCLUSIONS

The conclusions of this study, stated briefly
and in approximately the order in which they were
discussed are:

1.   Bulk nucleation has not been observed in germanium
      dioxide glass; surface nucleation occurs readily
      on glasses heated from room temperature to the
      crystallization temperature range.

2.   The state of reduction of germanium dioxide glasses
      varies with melting conditions; at temperatures
      above $1400^{\circ}C$, regardless of atmosphere, all
      germanium dioxide glass is slightly reduced.

3.   The extents of crystal growth and melting in the
      intrinsic region are linear with time at all the
      temperatures studied.

4.   The intrinsic crystal growth rates vary with
      temperature in a manner typical of crystal growth
      in glass-forming materials, with a peak growth
      rate of approximately 10^{-5} cms/sec at 75°
      undercooling.

5.   Crystal growth and melting rates increase with
      increasing reduction of the glass over the full
      range of temperature studied so long as the defect
      concentration associated with reduction is greater
      than the impurity concentration.

6.   Combining crystal growth rate and viscosity data,
the reduced growth rate is independent of
undercooling - over the full range of undercooling
between 16 and 416 Centigrade degrees - for the
material melted in the same way as that on which
viscosity measurements were made.

7.   The morphology of growing and melting crystals was
nonfaceted at all temperatures studied. The
random appearance of facets on some of the
crystals seems to be associated with the impurities
present in the glass, particularly Al.

8.   The reduced growth rate-reduced melting rate plot
is continuous through the melting temperature for
glasses of the same state of reduction.

9.   The plot of melting and crystal growth rates
against temperature is continuous with the same
slope through the melting temperature. When
corrected for the temperature dependence of the
viscosity, these rates vary linearly with
temperature.

10.   Crystal growth in germanium dioxide is sensitive
to impurities. Extrinsic growth rates, attributed
to sodium impurities, are relatively independent of
time and temperature (in the crystallization range)
and generally orders of magnitude greater than
intrinsic growth rates.

11.   Intrinsic crystal growth in amorphous germanium
dioxide is relatively isotropic, with no highly
preferred growth directions.

12.   Crystal growth and melting of stoichiometric and
slightly reduced germanium dioxide glasses occur
at the same rates in air, oxygen, and nitrogen.
Hydrogen increases crystallization but also
reduces the glass.

13.   Predictions concerning the growth of crystals of
materials with low entropies of fusion based on
the Jackson Model of the Interface have received
support from the results of this study. These
include observations of nonfaceted interface
morphologies, a reduced growth rate independent of
temperature, melting-crystallization rate continuity
through the melting temperature, and relatively
isotropic growth.

VIII. <u>SUGGESTIONS FOR FUTURE WORK</u>

Germanium dioxide glass is a material in which hydroxyl ion concentration, impurity concentrations, and the state of reduction can each be independently controlled. The effects on crystal growth of each of these variables, in much greater concentration ranges than studied here, are of interest.

A determination of the oscillator strength for the absorption peak at 2450 $\overset{o}{A}$ may be made by independently measuring defect concentrations from measurements of electrical conductivity.

REFERENCES

1. *The Scientific Papers of J. Willard Gibbs*, Vol. 1, *Thermodynamics*, Dover Publications, New York (1961), pp. 324-326.

2. K. A. Jackson, "On The Theory of Crystal Growth": "The Fundamental Rate Equation", J. Cryst. Growth, 5 (1969), pp. 13-18.

3. I. N. Stranski, Z. Phys. Chem., 136 (1928), p. 259.

4. I. N. Stranski and R. Kaischew, Z. Phys. Chem., (B)26 (1934), p. 100.

5. M. Volmer, *Kinetik der Phasenbildung*, Dresden and Leipzig: Steinkopff (1939).

6. W. Kossel, Nachr. Akad. Wiss. Gottingen Math-physik Kl. (1927), p. 135.

7. I. N. Stranski, Z. Phys. Chem., 11B (1931), p. 342.

8. R. Becker and W. Doring, Ann. Phys. Lpz., 24 (1935), p. 719.

9. M. Volmer and M. Marder, Z. Physik Chem., A154 (1931), pp. 97-112.

10. J. D. Hoffman, Soc. Plastics Engrs. Trans., 4 (1956), pp. 323-324.

11. D. Turnbull and J. C. Fisher, "Rate of Nucleation in Condensed Systems", J. Chem. Phys., 17 (1) (1949), pp. 71-73.

12. Course Notes, M.I.T. Subject 3.61 (Prof. D. R. Uhlmann).

13. W. K. Burton, N. Cabrera and F. C. Frank, Phil. Trans. R. Soc., A243 (1951), p. 299.

14. H. A. Wilson, Phil. Mag., 50 (1900), p. 238.

15. J. Frenkel, Physik Z. Sov., 1 (1932), p. 498.

16. J. Frenkel, Zeit. fur Phys., 35 (1926), p. 652.

17. A. Einstein, Ann. Physik, 17 (1905), p. 549.

18.   D. Turnbull, "On the Relation Between Cyrstallization Rate and Liquid Structure", J. Phys. Chem., 66 (1962), pp. 609-613.

19.   S. Glasstone, K. Laidler, and H. Eyring, The Theory of Rate Processes, McGraw-Hill Book Co., New York (1941), pp. 516-519.

20.   H. H. Nachtrieb, "Transport Properties in Pure Liquid Metals", pp. 49-55 in Liquid Metals and Solidification, American Society for Metals, Cleveland (1958).

21.   C. H. Ma and R. A. Swalin, "A Study of Solute Diffusion in Liquid Tin", Acta Met., 8 (6) (1960), pp. 388-395.

22.   D. J. Denny, "Viscosities of Some Undercooled Liquid Alkyl Halides", J. Chem. Phys., 30 (1) (1959), pp. 159-162.

23.   D. W. Davidson and R. H. Cole, "Dielectric Relaxation in Glycerol, Propylene Glycol, and n-Propanol", J. Chem. Phys., 19 (1951), pp. 1484-1490.

24.   T. A. Litovitz and G. E. McDuffie, Jr., "Comparison of Dielectric and Mechanical Relaxation in Associated Liquids", J. Chem. Phys., 39 (3) (1963), pp. 729-734.

25.   J. W. Cahn, W. B. Hillig, G. W. Sears, "The Molecular Mechanism of Solidification", Acta Met., 12 (12) (1964), pp. 1421-1439.

26.   F. C. Frank, Disc. Faraday Soc., 5 (1949), pp. 48 & 67.

27.   W. K. Burton and N. Cabrera, Disc. Faraday Soc., 5 (1949), p. 33.

28.   W. B. Hillig and D. Turnbull, J. Chem. Phys., 24 (1956), p. 914.

29.   K. A. Jackson, "Mechanism of Growth", pp. 174-186 in Liquid Metals and Solidification, Amer. Soc. Metals, Cleveland (1958).

30.   W. L. Bragg and E. J. Williams, Proc. Roy. Soc., (A) 145 (1934), p. 699; Proc. Roy. Soc., (A) 151 (1935), p. 540.

31.   K. A. Jackson, "Interface Structure", pp. 319-323 in Growth and Perfection of Crystals, edited by R. H. Doremus, D. Turnbull, and B. W. Roberts, John Wiley, New York (1958).

32. K. A. Jackson and J. D. Hunt, "Transparent Compounds that Freeze Like Metals", Acta Met., $\underline{13}$ (1965), pp. 1212-1215.

33. J. W. Cahn, "Theory of Crystal Growth and Interface Motion in Crystalline Materials", Acta Met., $\underline{8}$ (1960), pp. 554-562.

34. K. A. Jackson, D. R. Uhlmann and J. D. Hunt, "On the Nature of Crystal Growth from the Melt", J. Cryst. Gr., $\underline{1}$ (1) (1967), p. 1.

35. H. Temperley, Changes of State, p. 107, Cleaver-Hume Press Ltd., London (1956).

36. D. Turnbull, Solid State Physics 3, p. 292, Academic Press, New York (1956).

37. A. L. Day and E. T. Allen, Carnegie Inst. Wash. Publ., p. 31 (1905).

38. J. D. Mackenzie, J. Am. Cer. Soc., $\underline{43}$ (1960), p. 615.

39. N. G. Ainslie, J. D. Mackenzie, and D. Turnbull, J. Phys. Chem., $\underline{65}$ (1961), p. 1718.

40. R. L. Cormia, J. D. Mackenzie, and D. Turnbull, "Kinetics of Melting and Crystallization of Phosphorus Pentoxide", J.A.P., $\underline{34}$ (8) (1963), pp. 2239-48.

41. G. S. Meiling and D. R. Uhlmann, "Crystallization and Melting Kinetics of Sodium Disilicate", Phys. Chem. Glass, $\underline{8}$ (2) (1967), pp. 62-68.

42. G. Tammann, The States of Aggregation, D. Van Nostrand Co., New York (1925), Chapter IX.

43. D. Turnbull and M. H. Cohen, "Concerning Reconstructive Transformation and Formation of Glass", J. Chem. Phys., $\underline{29}$ (5) (1958), p. 1049.

44. D. Turnbull and M. H. Cohen, "Crystallization Kinetics and Glass Formation", Modern Aspects of the Vitreous State, Vol. 1, Butterworth and Co., London (1960), pp. 38-62.

45. V. I. Danilov and V. I. Malkin, Zh. fiz. Khim., $\underline{28}$ (1954), p. 1966.

46. H. Pollatschek, Z. Phys. Chem., $\underline{142}$ (1929), p. 289.

47. K. Neumann and G. Micus, Zeit. fur Physik Chemie., N.F., $\underline{2}$ (1954), pp. 25-39.

48. D. E. Ovsienko and G. A. Alfintsev, Kristallografiya, 8 (19ᵤ3), pp. 796-799.

49. R. L. Cormia, J. D. Mackenzie, and D. Turnbull, "Kinetics of Melting and Crystallization of Phosphorus Pentoxide", J.A.P., 34, 8 (1963), pp. 2239-2244.

50. R. L. Cormia, J. D. Mackenzie and D. Turnbull, "Viscous Flow and Melt Allotropy of Phosphorus Pentoxide", J.A.P., 34, 8 (1963), pp. 2244-2248.

51. R. J. Greet, "Solidification Kinetics of 1,2-Diphenylbenzene", J. Cryst. Gr., 1 (1967), pp. 195-203.

52. J. H. Magill, and D. J. Plazek, "Physical Properties of Aromatic Hydrocarbons. II Solidification Behavior of 1,3,5-Tri-α-Naphthylbenzene", J. Chem. Phys., 46, 10 (1967), pp. 3757-3769.

53. G. S. Meiling and D. R. Uhlmann, "Crystallization and Melting Kinetics of Sodium Disilicate", Phys. Chem. Glasses, 8, 2 (1967), pp. 62-68.

54. G. S. Meiling and D. R. Uhlmann, "Crystallization Kinetics of Sodium Disilicate", pp. 747-756 in Crystal Growth, Proceedings of an International Conference on Crystal Growth, Pergamon Press, Oxford and New York (1967).

55. W. D. Scott and J. A. Pask, "Nucleation and Growth of Sodium Disilicate Crystals in Sodium Disilicate Glass", J. Am. Cer. Soc., 44 (4) (1961), pp. 181-187.

56. A. Leontjewa, "The Linear Speed of Crystallization of Potassium, Sodium, and Lithium Disilicate", Acta Physicochimica U.R.S.S., 16, 1-2 (1942), pp. 97-101.

57. H. R. Swift, "Some Experiments on Crystal Growth and Solution in Glasses", J. Am. Cer. Soc., 30, 6 (1947), pp. 165-174.

58. E. Preston, "The Crystallization Relationship of Soda-Lime-Magnesia-Silica Glass as Used for Drawn Sheet and the Process of Devitrification", J. Soc. Glass Technol., 24 (1940), p. 139.

59. A. J. Milne, "The Measurement of Devitrification Characteristics of Glass", J. Soc. Glass Technol., 36, (1952), pp. 275-286.

60.   F. E. Wagstaff and K. J. Richards, "Kinetics of
       Crystallization of Stoichiometric SiO_2 Glass in
       H_2O Atmospheres", J. Am. Cer. Soc., 49, 3 (1961),
       pp. 118-121.

61.   F. E. Wagstaff, S. D. Brown, and I. B. Cutler,
       "The Influence of H_2O and O_2 Atmospheres on the
       Crystallization of Vitreous Silica", Phys. Chem.
       Glasses, 5, 3 (1964), pp. 76-81.

62.   N. G. Ainslie, C. R. Morelock, and D. Turnbull,
       "Devitrification of Fused Silica", Symposium on
       Nucleation and Crystallization in Glasses and
       Melts, American Ceramic Soc., Columbus (1962).

63.   J. Hlavac and L. Vaskova, "Crystallization of
       Reduced Silica Glass in an Oxidizing Atmosphere",
       Silikaty, 9, 3 (1965), pp. 237-42.

64.   F. E. Wagstaff and K. H. Richards, "Preparation
       and Crystallization Behavior of Oxygen-Deficient
       Vitreous Silica", J. Am. Cer. Soc., 48, 7 (1965),
       pp. 382-3.

65.   S. D. Brown and S. S. Kistler, "Devitrification
       of High-SiO_2 Glasses of the System Al_2O_3-SiO_2",
       J. Am. Cer. Soc., 42, 6 (1959), pp. 263-270.

66.   F. E. Wagstaff, "Crystallization Kinetics of
       Internally Nucleated Vitreous Silica", J. Am. Cer.
       Soc., 5, 8 (1968), pp. 449-452.

67.   N. G. Ainslie, J. D. Mackenzie, and D. Turnbull,
       "Melting Kinetics of Quartz and Cristobalite",
       J. Phys. Chem., 65 (1961), pp. 1718-1724.

68.   F. E. Wagstaff, "Crystallization and Melting Kinetics
       of Cristobalite", (in press).

69.   T. Bell, G. Hetherington, and K. H. Jack, "Water in
       Vitreous Silica. Part 2: Some Aspects of Hydrogen-
       Water-Silica Equilibria", Phys. Chem. Glasses, 3,
       5 (1962), pp. 141-146.

70.   R. F. Strickland-Constable, Kinetics and Mechanisms
       of Crystallization from the Fluid Phase and the
       Condensation and Evaporation of Liquids, p. 7,
       Academic Press, London (1968).

71. A. W. Laubengayer and D. S. Morton, "Germanium XXXIX. The Polymorphism of Germanium Dioxide", J. Amer. Chem. Soc., 54 (1932), pp. 2303-20.

72. Goldschmidt, Naturwissenschaften, 14 (1926), p. 295.

73. Muller and Blank, J. Amer. Chem. Soc., 46 (1924), p. 2358.

74. V. Garino-Canina, "Some Physical Properties Dependent on Defects in Pure Vitreous Germanium Dioxide", J. Phys. Chem. Solids, 20 (1-2) (1961), pp. 110-121.

75. F. A. Trumbore, C. D. Thurmond, and M. Kowalchik, J. Chem. Phys., 24 (1956), p. 1112.

76. N. A. Vasyutinskii, Y. I. Rys'eva, G. I. Petrov, and A. P. Sidorenko, Neogonicheskie Materialy, 1 (7) (1965), pp. 1057-1061.

77. A. D. Mah and L. H. Adami, "Heats and Free Energies of Formation of Germanium Dioxide", Bureau of Mines Report of Investigation # 6034 (1962).

78. L. M. Dennis and A. W. Laubengayer, "Germanium XVII. Fused Germanium Dioxide and Some Germanium Glasses", J. Phys. Chem., 30 (1926), pp. 1510-1526.

79. B. E. Warren, "The Diffraction of X-Rays in Glass", Phys. Rev., 45 (10) (1934), pp. 657-661.

80. J. D. Mackenzie, "Structure of Liquid Germanium Dioxide", J. Chem. Phys., 29 (3) (1958), pp. 605-607.

81. K. K. Kelley and A. U. Christensen, "High Temperature Heat Content and Entropies of Crystalline and Glassy Germanium Dioxide", Bureau of Mines Report of Investigations # 5710 (1961).

82. V. Garino-Canina, "Absorption optique et niveaux d' energie dans l' oxyde de germanium vitreux", Compt. Rend. Acad. Sci. Paris, 248 (1959), pp. 1488-1491.

83. V. Garino-Canina, "Quelques proprietes optiques de l' oxyde de germanium vitreux dans l' ultraviolet, oxyde pur", Compt. Rend. Acad. Sci. Paris, 247 (1958), pp. 593-596.

84. A. J. Cohen and H. L. Smith, "Ultraviolet and Infrared Absorption of Fused Germania", J. Phys. Chem. Solids, 7 (1958), pp. 301-306.

85. R. W. Shaw, "Optical Absorption of Fused Germanium Dioxide from 0.185μ to 8.5μ", Phys. Rev., 51 (1937), p. 146.

86. A. J. Cohen, "Neutron Specific Color Center in Fused Silica and an Impurity Band of Identical Wavelength", Phys. Rev., 105 (4) (1957), pp. 1151-1155.

87. V. Garino-Canina, "Diffusion of Oxygen in Vitreous Germanium Dioxide", Comp. Rend. Acad. Sci. Paris, 248 (1959), pp. 1319-22.

88. V. Garino-Canina and J. Denoncin, "Optical Study of Oxygen Diffusion in Nonstoichiometric Vitreous Germanium Dioxide", Comp. Rend. Acad. Sci. Paris, 250 (1960), pp. 1815-17.

89. V. Garino-Canina, "The 2420Å Absorption Band of Vitreous Silica: Germanium Impurity and Oxygen Defiency", Comp. Rend. Acad. Sci. Paris, 242 (1956), pp. 1982-84.

90. P. J. Vergano and D. R. Uhlmann, 6th International Symposium on Reactivity of Solids, Schenectady (1968) (in press).

91. J. D. Mackenzie, "Structure of Liquid Germanium Dioxide", J. Chem. Phys., 29 (3) (1958), pp. 605-607.

92. C. R. Kurkjian and R. W. Douglas, "The Viscosity of Glasses in the System Na_2O-GeO_2", Phys. Chem. Glasses, 1 (1) (1960), pp. 19-25.

93. C. B. Nemilov and A. O. Ivanov, Zh. prikl. Khim., 36 (11) (1963), pp. 2541-42.

94. E. F. Riebling, "Structure of Molten Oxides I. Viscosity of GeO_2 and Binary Germanates Containing Li_2O, Na_2O, K_2O and Rb_2O", J. Chem. Phys., 39 (7) (1963), pp. 1889-1895.

95. V. Bruckner, Glastech Ber., 413 (9) (1964), pp. 413-425.

96.   E. H. Fontana and W. A. Plummer, "A Study of
       Viscosity-Temperature Relationships in the GeO_2
       and SiO_2 Systems", Phys. Chem. Glasses, $\underline{7}$ (4)
       (1966), pp. 139-146.

97.   J. De Neufville, private communication.

98.   G. B. Harris, "Quantitative Measurement of Preferred
       Orientation in Rolled Uranium Bars". Communication
       from the National Physics Laboratory, Ser. 7, Vol.
       43, no. 336 (1952), pp. 113-123.

99.   D. Turnbull and D. R. Uhlmann, private communication.

100.   D. L. Dexter, "Theory of the Optical Properties of
       Imperfections in Nonmetals", pp. 355-411 in $\underline{Solid}$
       $\underline{State}$ $\underline{Physics}$, Vol. $\underline{6}$, ed. by F. Seitz and
       D. Turnbull, Academic Press, New York (1958).

101.   W. D. Compton and G. W. Arnold, Jr., "Radiation
       Effects in Fused Silica and α-Al_2O_3", Disc.
       Faraday Soc. 31, pp. 130-139 (1961).

APPENDIX A

Crystal Growth and Melting Data

Table A.1

Crystal Growth Data

glass #	temperature $^{\circ}C$	time	crystal thickness (μ's)
1B	700	6 hrs	3.0,3.3
		9	4.9,5.3
		12	3.0,4.8
		15	7.5,9.0
		18	8.7,8.9
1B	750	60 mins	1.8,2.5
		90	2.9,3.5
		120	4.5,4.6
		150	5.6,5.6
		180	6.2,6.5
1B	800	30 mins	2.6,2.7
		45	4.8,5.5
		60	7.5,7.6
		75	8.4
		90	9.2
1B	850	10 mins	2.7,2.8
		14	3.8,3.8
		18	5.9,5.9
		22	7.4,8.0
		26	9.0
1A	850	10 mins	2.9,4.5
		14	3.8,4.0
		18	7.7,8.5
		22	8.4,8.8
		26	10.4,11.0
1A	900	4 mins	2.7,2.9
		6	3.4,4.6
		8	7.5,8.5
		10	8.3,9.3
		12	12.8
1A	950	4 mins	4.1,5.2
		5	5.2,7.0
		6	9.1,11.7
		7	14.9
		8	14.5,17.4

Table A.1 (cont'd)

glass #	temperature °C	time	crystal thickness (μ's)
1A	1000	3.5 mins	10.9
		4	8.1,9.5
		5	16.5,16.6,17.1,19.8
		6	21.1,25.9
		6.5	24.6,26.8
1A	1050	6 mins	16.7,16.9
		9	29.4,32.1
		12	52.5,67.5
		15	64.8,76.1
1A	1100	3.5 mins.	8.3,9.0
		4	10.5,10.5
		5	12.4,12.9,16.0,16.3
2B	800	45 mins	2.4,2.5
		60	3.5,5.4
		75	5.3,5.9
		90	5.8,7.5
		120	9.5,9.6
2B	850	10 mins	2.4,2.5
		18	4.1,4.2
		26	5.8,6.4
		34	8.9,9.4
2B	900	8 mins	4.6,5.6
		10	7.2,8.7
		12	7.2,9.1
		14	11.1,13.3
2B	950	4 mins	2.9,2.9
		6	7.4,7.4
		8	10.6,12.0
		10	13.7,13.9
		12	16.9,18.3
2B	1000	4 mins	5.8,6.3
		5	7.6,8.3
		6	10.4
		7	16.2
		8	21.5

Table A.1 (cont'd)

glass #	temperature °C	time	crystal thickness (μ's)
2A	1050	4 mins	11.6,12.9
		6	18.8,21.5
		8	26.2,32.9
		10	45.7,52.8
		12	37.8,40.2
2A	1093	4 mins	11.1,11.9
		6	15.7,22.2
		8	20.9,24.0
		10	21.9,28.5
		12	38.0,38.9
2A	1097	4 mins	12.2,12.9
		6	12.6,14.7
		8	22.1,22.3
		10	20.3,24.5
		12	30.0,31.6
2A	1102	4 mins	8.9,10.4
		8	15.3,18.6
		12	22.8,26.8
		16	36.4,37.6
		20	40.7,47.9
2A	1107	6 mins	8.5,9.7
		12	7.9,15.7
		18	23.5,24.4
		24	28.0,31.7
		30	37.7,45.0
3D	800	1 hr	3.2,3.7
		2	5.8,8.0
		3	7.8,9.1
		4	12.8,13.2
		5	14.4,14.9
3D	850	20 mins	2.3,3.0
		40	6.4,6.4
		60	7.5,10.2
		70	12.3,13.6
		80	14.4,15.9

Table A.1 (cont'd)

glass #	temperature °C	time	crystal thickness (µ's)
3B	900	8 mins	2.7,3.9
		12	5.8,6.8
		16	6.3,8.7
		20	5.8,8.9
		24	13.5,16.2
3C	950	4 mins	3.0,3.3
		6	4.9,5.4
		10	9.6,9.9
3B	950	4 mins	2.2
		6	2.4
		8	3.9,4.2
		10	4.9,5.4
		12	6.7,8.3
3A	950	4 mins	2.0,2.0
		6	4.0,5.3
		8	9.5,12.4
		10	11.5,12.3
		12	11.6,13.3
3C	1000	4 mins	6.2,10.3
		6	10.1,12.2
		8	20.2
		10	20.1,24.2
3B	1000	4 mins	3.0,3.5
		6	7.2,8.9
		8	9.3,10.0
		10	13.0,13.8
		12	14.2,14.4
3A	1001	4 mins	5.5,5.9
		6	6.8,8.9
		8	10.5,10.9
		10	19.2,21.0
		12	22.4,24.1
3C	1050	4 mins	8.2,8.7
		6	12.2,12.2
		8	18.9,19.8
		10	33.5
		12	36.2,38.2

Table A.1 (cont'd)

glass #	temperature °C	time	crystal thickness (µ's)
3B	1050	4 mins	4.7,5.5
		6	9.0,10.1
		8	14.9,17.3
		10	22.1,24.0
		12	24.5,25.2
3A	1050	4 mins	6.9,7.2
		6	10.3,11.7
		8	14.2,14.8
		10	20.5,22.2
		12	21.6,22.1
3B	1101	4 mins	2.9,3.0
		6	4.3,6.1
		8	5.7,6.3
		10	7.2,7.5
		12	7.2,7.2
3C	1102	6 mins	6.6,9.9
		12	10.5,12.9
		18	18.9,22.4
3A	1101	4 mins	4.2,5.0
		6	8.7,11.0
		8	9.6,10.7
		10	11.6,12.1
3A	1106	4 mins	3.4,3.9
		8	7.2,7.8
		12	7.4,7.8
		16	7.8,11.0
		20	11.2,12.2
3B	1110	6 mins	2.2,2.5
		10	3.2,3.8
		12	6.1,6.8
		14	4.7,5.5
3A	1110	10 mins	3.6
		15	5.2
		20	5.9
		25	8.3

Table A.1 (cont'd)

glass #	temperature °C	time	crystal thickness (μ's)
4A	800	1 hr	3.6
		2	10.3,11.0
		3	14.9,15.3
		4	19.1,21.6
		5	23.5,24.3
4A	850	20 mins	3.9,4.6
		40	8.4,8.5
		60	15.2,15.3
		80	20.8,21.3,22.0,22.1
4B	900	5 mins	1.8,2.3
		10	4.5,6.4
		15	6.9,8.0
		20	10.3,10.5
		25	14.1,14.8
4B	950	4 mins	2.3,4.3
		6	5.8,7.2
		8	7.6,8.2
		10	14.1,17.9
		12	14.1,18.7
4A	1000	4 mins	5.5,7.0,9.2,9.3
		5	7.6,9.2
		6	12.4,13.1
		8	15.1,16.7
		10	20.5,22.2
		12	24.0,25.4
4B	1000	4 mins	9.1,12.4
		6	15.8,18.2
		8	18.9,23.9
		10	27.3,30.9
		12	31.2,37.0
4A	1050	4 mins	8.0,8.7
		6	11.1,12.1
		8	15.5,15.9
		10	23.4,23.7
		12	23.7,23.7

Table A.1 (cont'd)

glass #	temperature °C	time	crystal thickness (µ's)
4A	1094	5 mins	7.5,7.7
		10	11.9,13.0
		15	13.6,16.8
		20	22.1,23.5
		25	27.7,28.0
4A	1099	4 mins	4.9,5.2
		6	6.5,6.8
		8	6.9,8.7
		10	10.2,11.4
		12	10.3,10.4
4A	1105	5 mins	3.5,3.8
		10	6.4,6.6
		15	7.6,7.9
		20	8.9,9.4
		25	12.6,13.4
4A	1111	5 mins	2.6,3.0
		10	3.1,3.9
		15	4.8,5.1
		20	6.0,6.1
		25	6.4,7.7

Table A.2

Melting Data

glass #	temperature °C	time (mins)	melt layer thickness (microns)
1C and 1D	1122	4	4.5,5.3
		6	6.0,10.2
		8	12.3,14.5
		10	14.3,15.2
		12	15.1,18.5
1C and 1D	1127	2	3.5,5.8
		4	8.3,8.5,12.6
		6	15.1,15.3
		8	16.8,20.8,32.5
		10	25.3,29.3
		12	23.0,39.2,42.8
		14	51.4
1C and 1D	1132	2	7.5,8.9
		4	10.5,15.0,19.9
		5	17.6
		6	18.8,26.1,29.6
		7	24.6
		8	22.2,29.2,38.4
		10	46.3
		12	48.8
1C and 1D	1137	2	11.4,12.8,13.3
		3	16.7,20.8
		4	26.5,28.5,29.6
		5	32.1,39.7
		6	30.1,48.0
		7	52.7
		8	47.9
4A	1119	6	2.2,3.3
		9	3.4,5.2
		12	5.2,7.2
4A	1125½	4	3.8,4.1
		6	5.4,7.0
		8	8.9,9.4
		10	9.4,10.0

Table A.2 (cont'd)

glass #	temperature °C	time (mins)	melt layer thickness (microns)
4A	1131	3	3.3,4.2
		4	6.2,6.8
		6	7.0,8.3
		8	12.1,12.9
		10	13.6,15.9
4A	1136	2	2.7,3.3
		4	7.0,9.1
		6	8.7,10.5
		8	12.7,15.8

APPENDIX B

Smakula's Equation

Smakula's Equation relates the concentration of defects, N, to the size of the absorption peak caused by those defects (100):

$$Nf = (1.29 \times 10^{17} \text{ cm}^{-3}) \frac{n}{(n^2 + 2)^2} K_{max} H \qquad (B.1)$$

where N = concentration of defects

f = oscillator strength

n = refractive index

K_{max} = linear absorption coefficient at the peak

H = half-width of the absorption peak

The derivation of Smakula's Equation involves approximations beyond the intent of this thesis; it also involves assuming that the absorption centers do not interact and that the absorption peak is Lorentzian in form*.

In applying this equation here, it is also assumed applicable in amorphous materials. More specific assumptions to be used in the present case are: (1) an oscillator strength of unity**; (2) a refractive index equal to n_{NaD} of 1.60; (3) a symmetrical absorption peak; and (4) a single photon absorption process.

A Typical Calculation of Defect Concentration:

Data for Glass 1A:

peak height (taking 2450 $\overset{o}{A}$ absorption
level of stoichiometric glass as $\quad = \quad$ 3.77
zero)

$$\text{specimen thickness} \quad = \quad 0.025 \text{ cm}$$

$$\text{wavelength at peak} \quad = \quad 2435 \overset{o}{A}$$

$$\text{wavelengths at half height} \quad = \quad 2595 \overset{o}{A} \text{ and } 2275 \overset{o}{A}$$

$$K_{max} \quad = \quad \frac{3.\ddot{7}7}{.025} \text{ cm} \quad = \quad 1.51 \times 10^2/\text{cm}$$

$$H \quad = \quad 12.4 \left(\frac{1}{2.275} - \frac{1}{2.595}\right) \quad = \quad 0.670 \text{ eV}$$

$$Nf \quad = \quad 1.29 \times 10^{17} \times \frac{1.6}{[(1.6)^2 + 2]^2} \times 1.51 \times 10^2 \times 6.70 \times 10^{-1}$$

$$Nf \quad = \quad 8.42 \times 10^{17}$$

assuming $f = 1**$, $N = 8.42 \times 10^{17}$ defects/cm^3.

A Typical Calculation of State of Reduction:

$$\text{Amount of Reduction} \quad = \quad C_o \quad = \quad \frac{N \times \text{molecular weight}}{\text{density} \times \text{Avogadro's number}}$$

$$C_o \quad = \quad \frac{N}{2.07 \times 10^{22} \text{ tetrahedra/cm}^3} \quad = \quad 4.4 \times 10^{-5}$$

*   If it is assumed that the absorption peak is
Gaussian in form, the concentrations computed are smaller
by a factor of 0.675.

**   The only measurement of an oscillator strength in
an oxide material (α-Al$_2$O$_3$) was made by Arnold and Compton([101])
on a peak at 2040 $\overset{o}{A}$ which was introduced by electron irradia-
tion. They computed oscillator strengths of 0.78 or 0.92
depending upon the type of defect assumed. These values are
in the same range as oscillator strengths measured on alkali
halide F centers (anion vacancies), which range from about
0.6 to 1.3.

The value of the oscillator strength of the 2450 $\overset{o}{A}$
germanium dioxide peak was the subject of a thorough
discussion with Professor A. Smakula of M.I.T. He suggested
that the best value of the oscillator strength in this
instance is unity, assuming that the identification of the
defect as an F' center (an anion vacancy with two trapped
electrons) by Garino-Canina([74]) is correct.

APPENDIX C

The Effects of Melting Conditions
on the Stoichiometry of GeO_2 Glass

To determine how the state of reduction of germanium
dioxide glass varies with melting conditions, four 100 gram
batches of stoichiometric glass were prepared from electronic
grade germanium dioxide by holding them at $1150^{\circ}C$ in a
vacuum of approximately 500 microns for eighteen hours in
platinum boats. After quenching to room temperature, each
glass was cut into smaller pieces and these portions were
then subjected to various heat treatments, as listed in Table
C.1. All additional heat treatments were made on pieces which
were initially about 1/4" thick. During heat treatments,
flowing to fill the platinum boat and evaporation reduced the
glass thickness to 1/8" or less in each case.

The ultraviolet absorption spectra for the original
stoichiometric glasses and for the heat treated glasses
were determined with a Cary 14 Spectrophotometer using
polished laths approximately .010" thick. Neutral density
filters were used to extend the range of this instrument
from two to five orders of magnitude.

The ultraviolet absorption spectra of some of the
stoichiometric glasses are presented in Figure C.1. The
ultraviolet cutoff occurs at approximately 2200 $\overset{\circ}{A}$; no peaks
appear in the spectra. Figure C.2 contains the ultraviolet
absorption spectra of germanium dioxide glasses heat treated
in nitrogen. The peak at 2450 $\overset{\circ}{A}$ is associated with the

Table C.1

Heat Treatments

$T, ^\circ C$	atmosphere	time	spec. thick.
1200	N_2	4	.008"
1200	air	4	.008"
1200	air	10	.008"
1200	O_2	4	.008"
1300	N_2	4	.008"
1300	air	4	.009"
1300	O_2	4	.008"
1300	vacuum	4	.006"
1400	N_2	4	.007"
1400	air	4	.009"
1400	O_2	4	.005"
1400	vacuum	0.5	.007"
1500	N_2	1	.012"
1500	air	4	.012"
1500	vacuum	.25	.012"
#1, 1150	vacuum	18	.010"
#2, 1150	vacuum	18	.009"
#3, 1150	vacuum	18	.009"
#4, 1150	vacuum	18	.009"
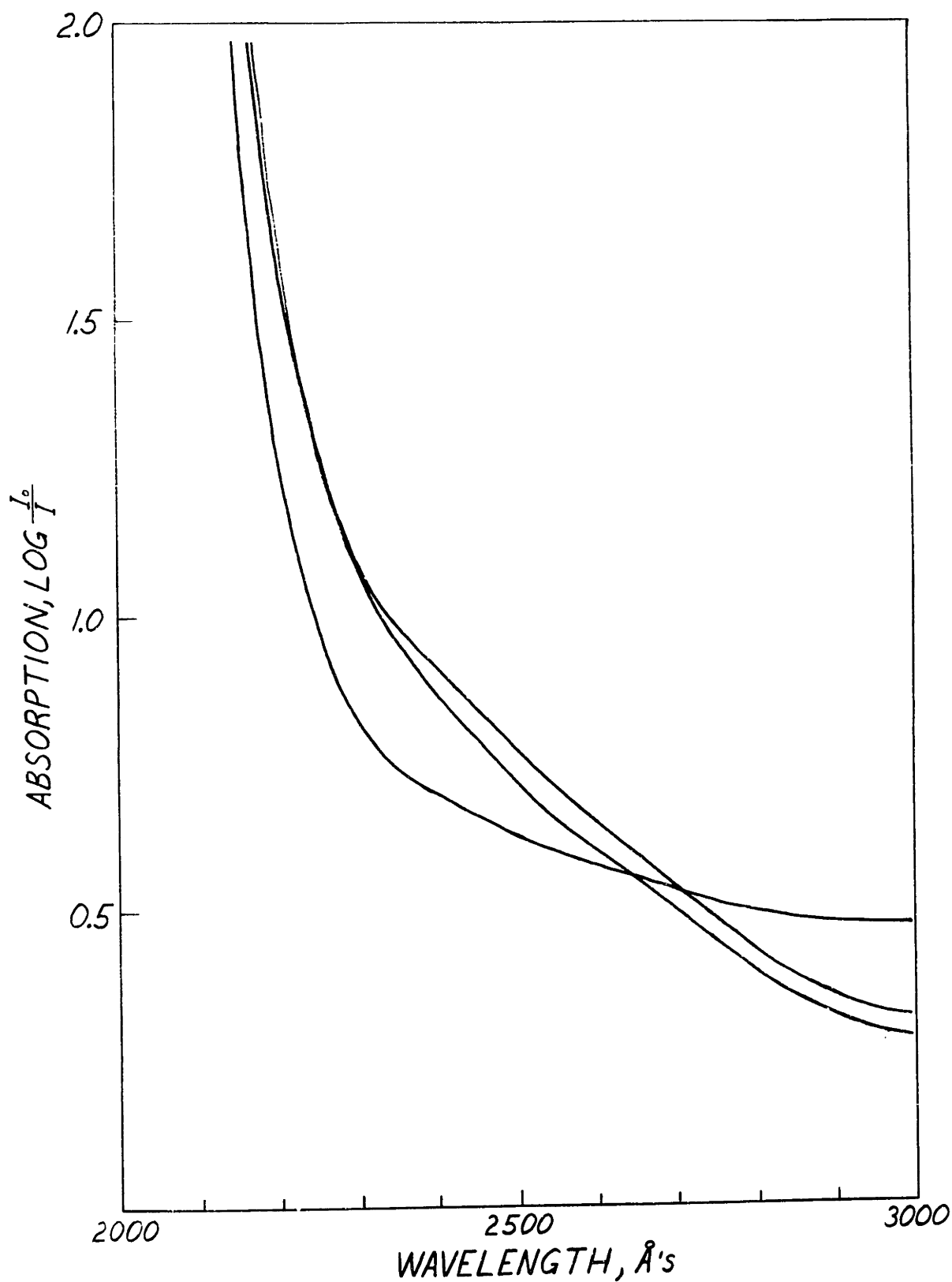
Figure C.1: Ultraviolet absorption spectra of some
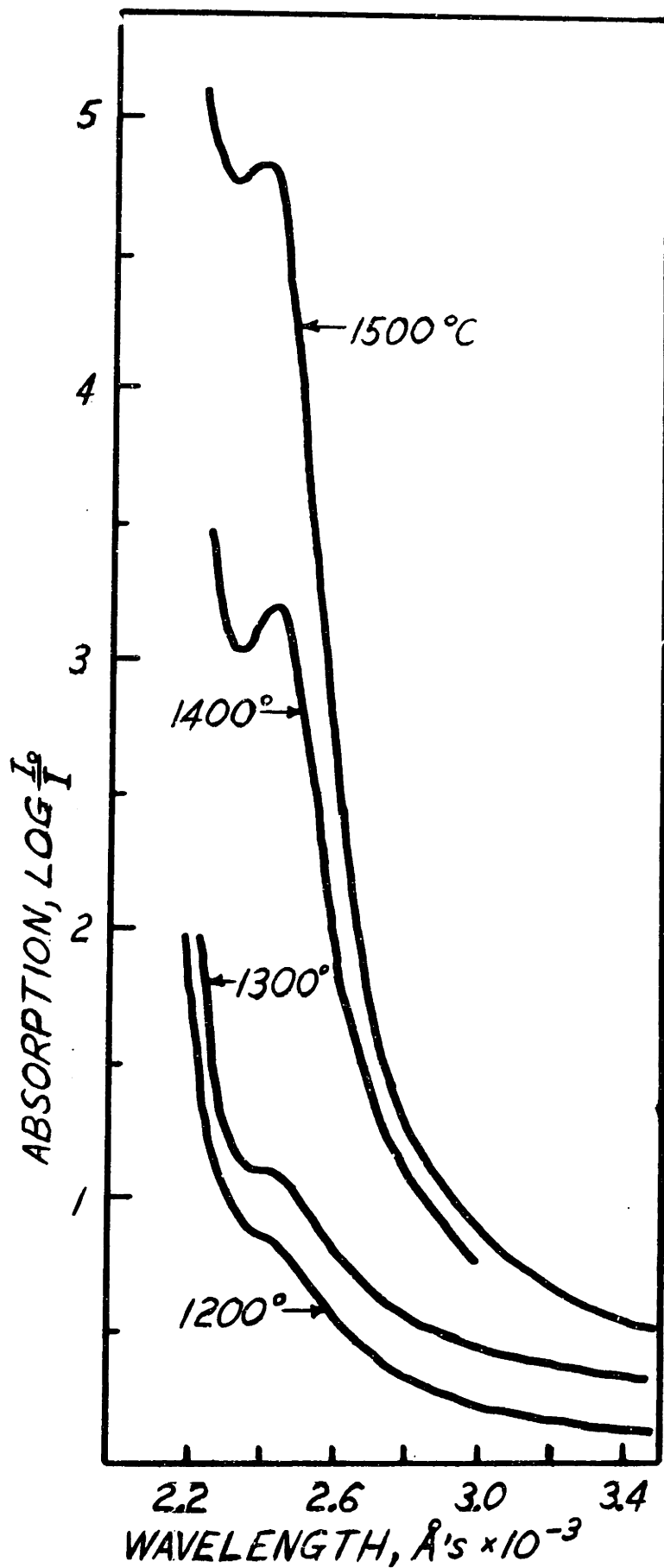stoichiometric glasses.

Figure C.2: Ultraviolet absorption spectra after heat
treatments in nitrogen.

state of reduction of the glass, as discussed in section

II.7.2. In a nitrogen atmosphere, this peak first begins

to appear at 1200°C; its size increases continuously

with increasing melt temperature. In Figure C.3, the ultra-

violet absorption spectra for glasses melted in air also

show the development of the 2450 $\overset{\text{o}}{\text{A}}$ peak; the absorption of

the 1500°C glass at 2450 $\overset{\text{o}}{\text{A}}$ could not be determined due to

"noise" problems in the spectrophotometer at that very low

light intensity. The peak develops less rapidly with

increasing temperature in air than in nitrogen. The 2450 $\overset{\text{o}}{\text{A}}$

peak also appears in glasses melted in oxygen and vacuum,

as seen in the ultraviolet absorption spectra presented in

Figures C.4 and C.5; these peaks are smaller than those

appearing in nitrogen and air at the same temperatures.

The fact that the glasses melted in air, oxygen,

and even in vacuum are reduced by heat treatments of 1400°C

and 1500°C suggests that the glass is more stable in a

slightly reduced condition.

Figure C.6 shows the development of the 2450 $\overset{\text{o}}{\text{A}}$ peak

in glasses heat treated for different lengths of time in dry

nitrogen at 1400°C. Figure C.7 illustrates how the

absorption peak can be bleached by heat treatments in an

oxidizing atmosphere.

The most reduced glass produced in this study, that

melted at 1500°C in nitrogen, is only about .005% reduced;

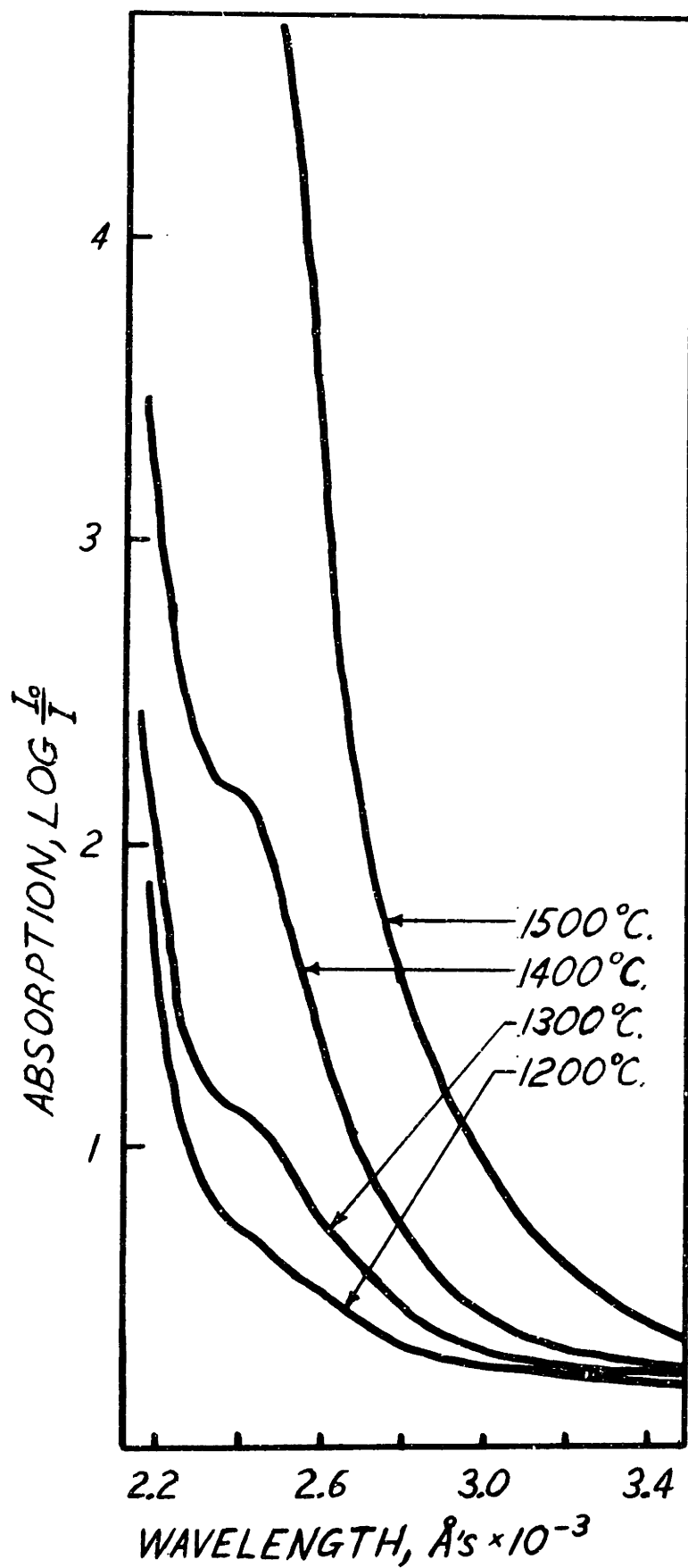this is calculated using Smakula's Equation as described in

Figure C.3: Ultraviolet absorption spectra after heat
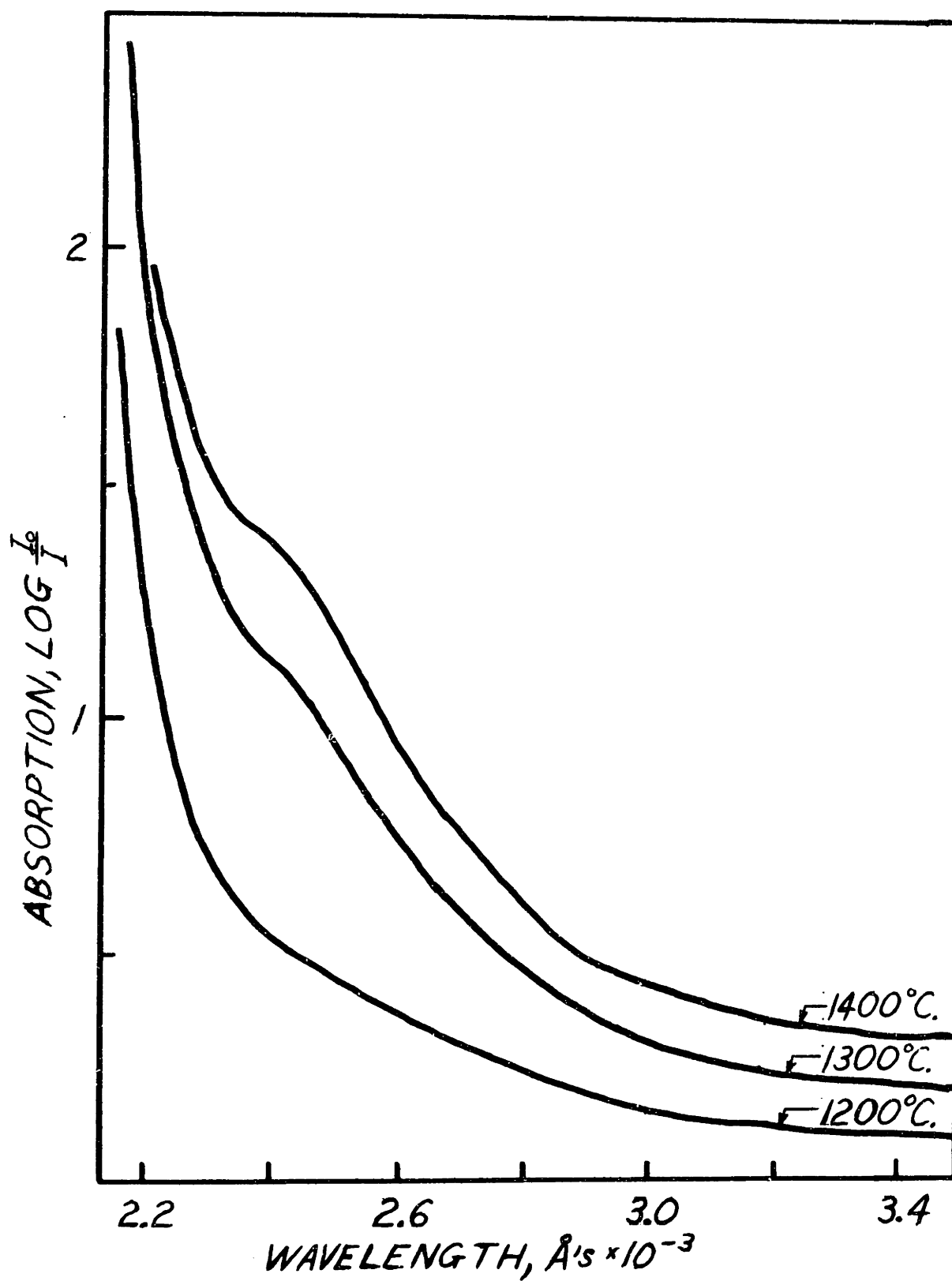treatments in air.

Figure C.4: Ultraviolet absorption spectra after heat
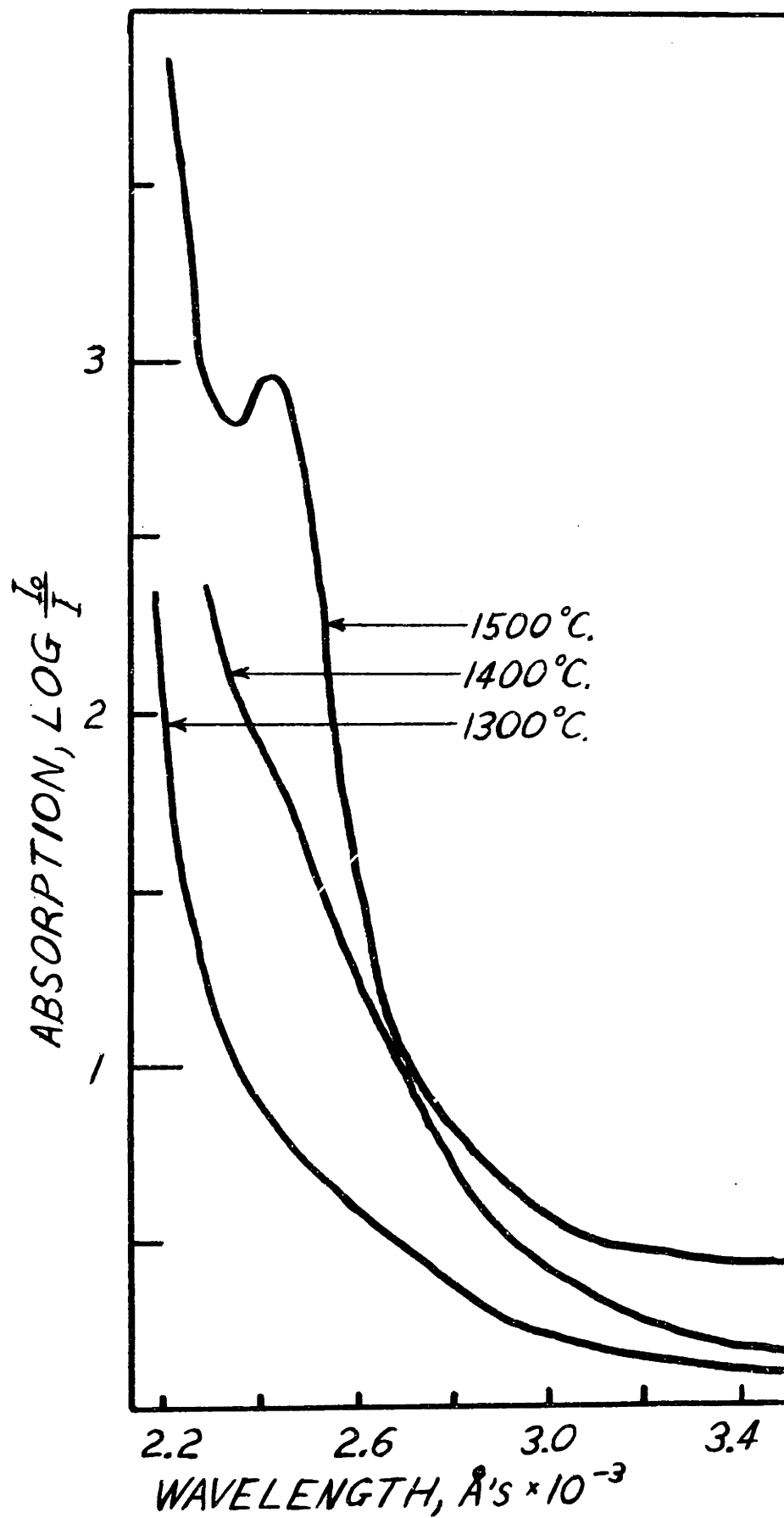treatments in oxygen.

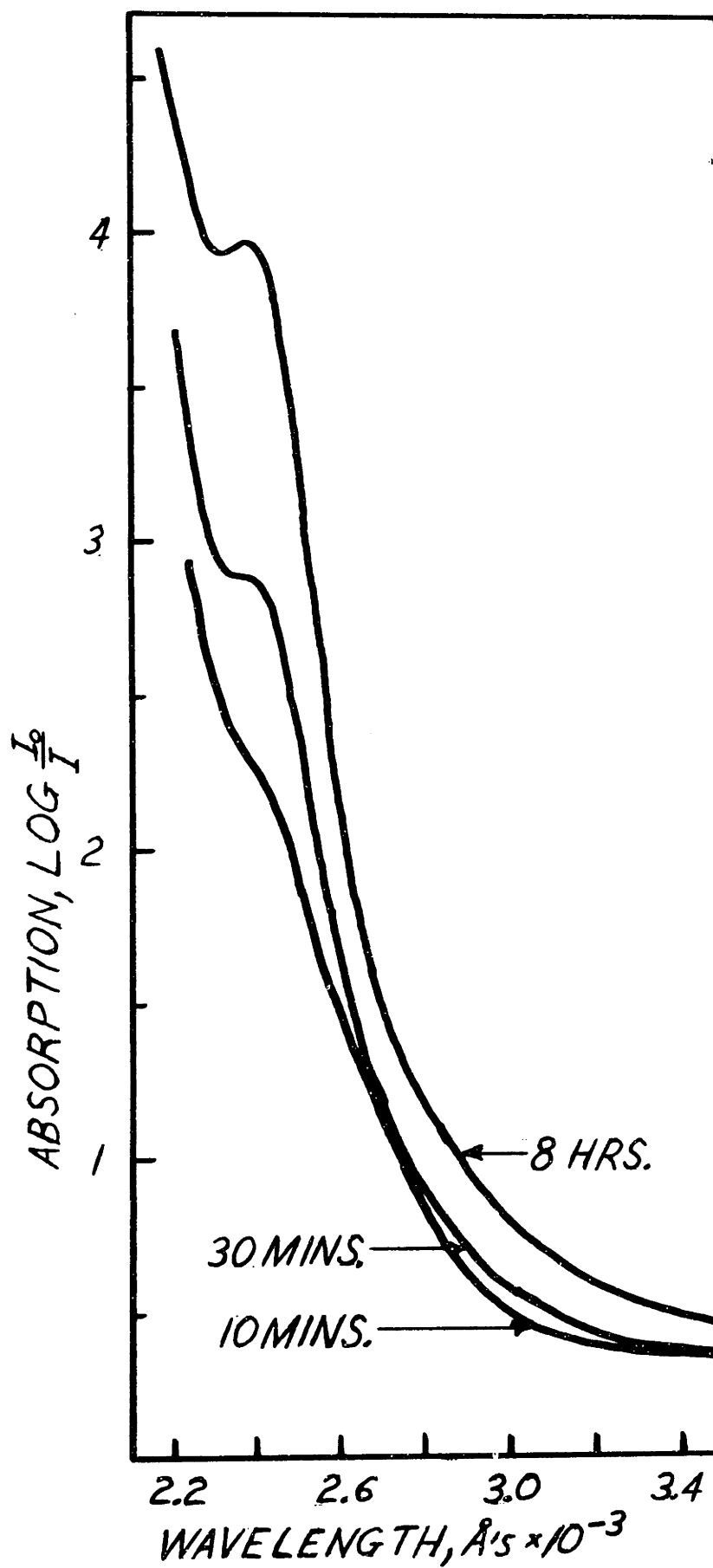Figure C.5: Ultraviolet absorption spectra after heat treatment in vacuum.

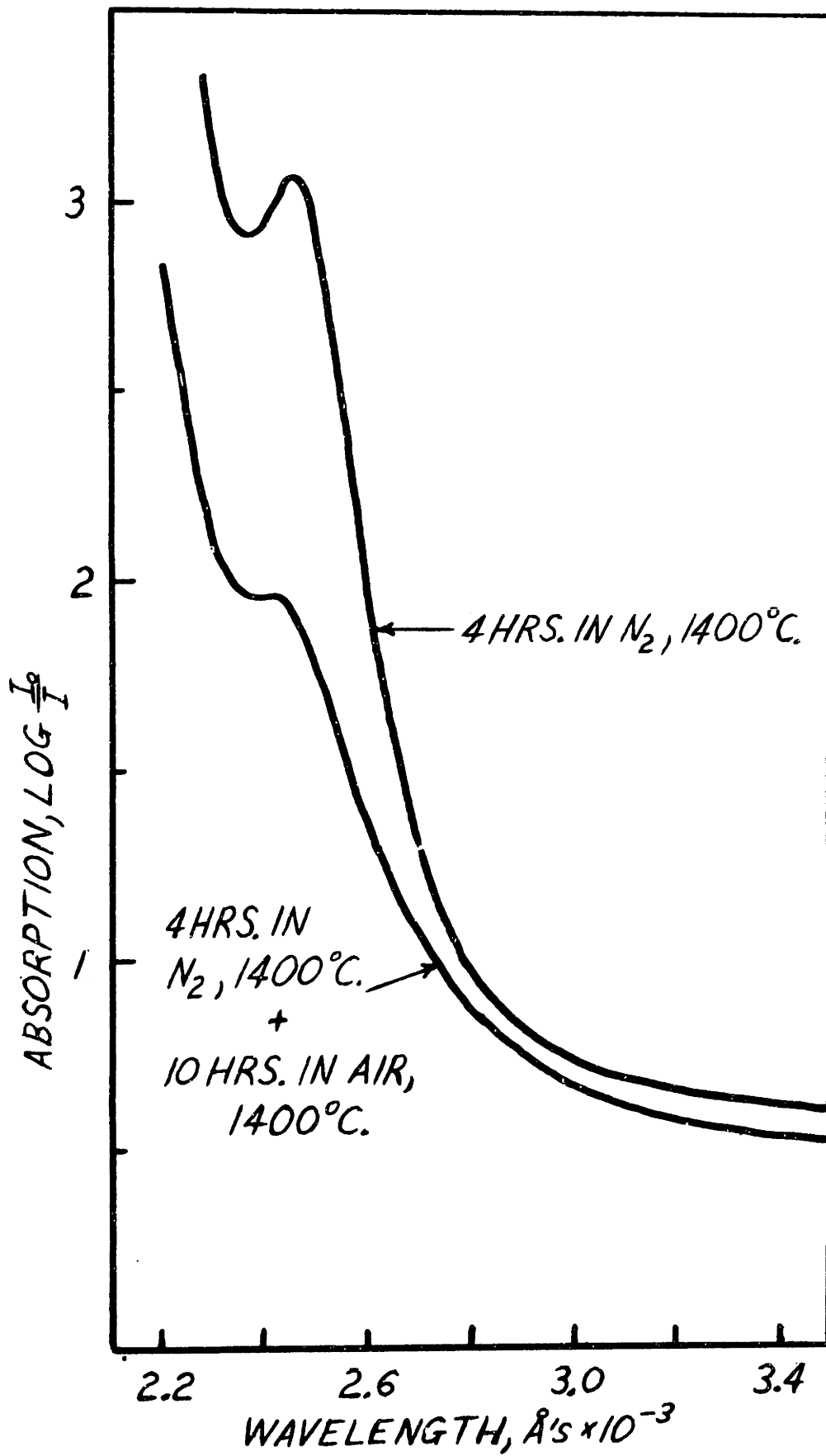Figure C.6: Development of absorption peak with time (1400oC in N_2).

Figure C.7: Bleaching of absorption peak.

Appendix B. The state of reduction of each of the glasses is approximately in proportion with the height of their absorption peaks.

The slight departure from stoichiometry produced by melting germanium dioxide glasses in nitrogen or air is not unexpected, reasoning by analogy with silicon dioxide. The slight reduction produced by melting in oxygen and vacuum was not expected; apparently, these results indicate that the glass is more stable in a slightly reduced condition at higher temperatures.

APPENDIX D

Reduced Growth Rate Variation with Temperature
for Series 2-4 Glasses

The importance of using the correct viscosity data in determining the reduced growth rate variation with temperature is stressed in the Introduction and Discussion sections of this thesis. The plots on the following pages are known to be in error because of the use of viscosity data obtained on a glass differing in its state of reduction. These figures do indicate, however, that the dip in the reduced growth rate values at small undercoolings increases with the likelihood of error introduced in the use of this viscosity data (with increasing difference between the state of reduction of the crystal growth material and that on which viscosity data were obtained).

The overall variation in the reduced growth rate in these cases (a factor of 4 or less) should be viewed in the prospective of the fact that over the range of the growth rate measurements the viscosity varies by more than three orders of magnitude.

The values of the reduced growth and melting rates plotted in Figures D.1 and D.2 are listed in Tables D.1 and D.2. These values were computed using the literature value of $1116^{o}C$ for the melting temperature, rather than the value of $1114^{o}C$ which is more accurate for these glasses, as discussed in Section VI.2.
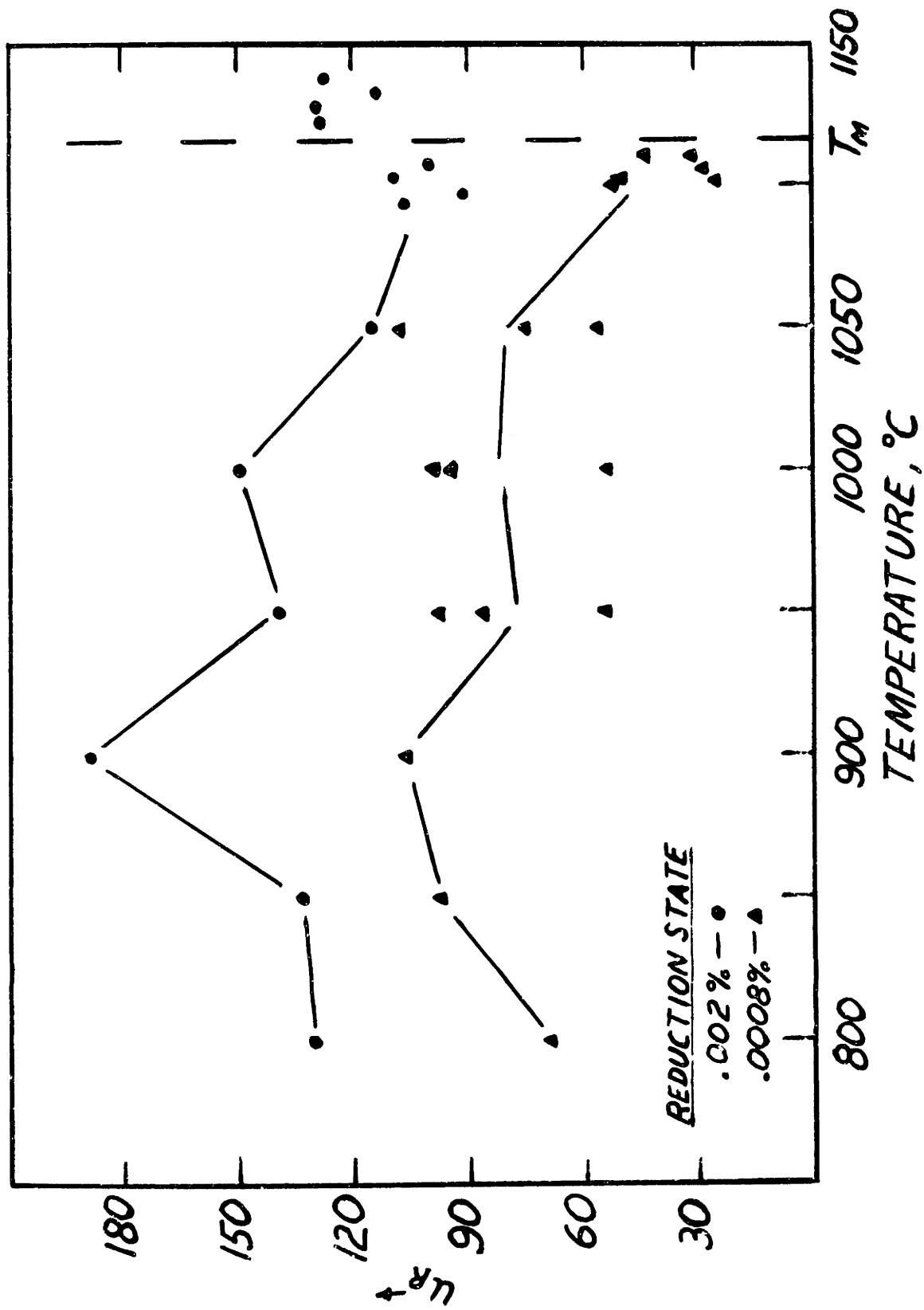
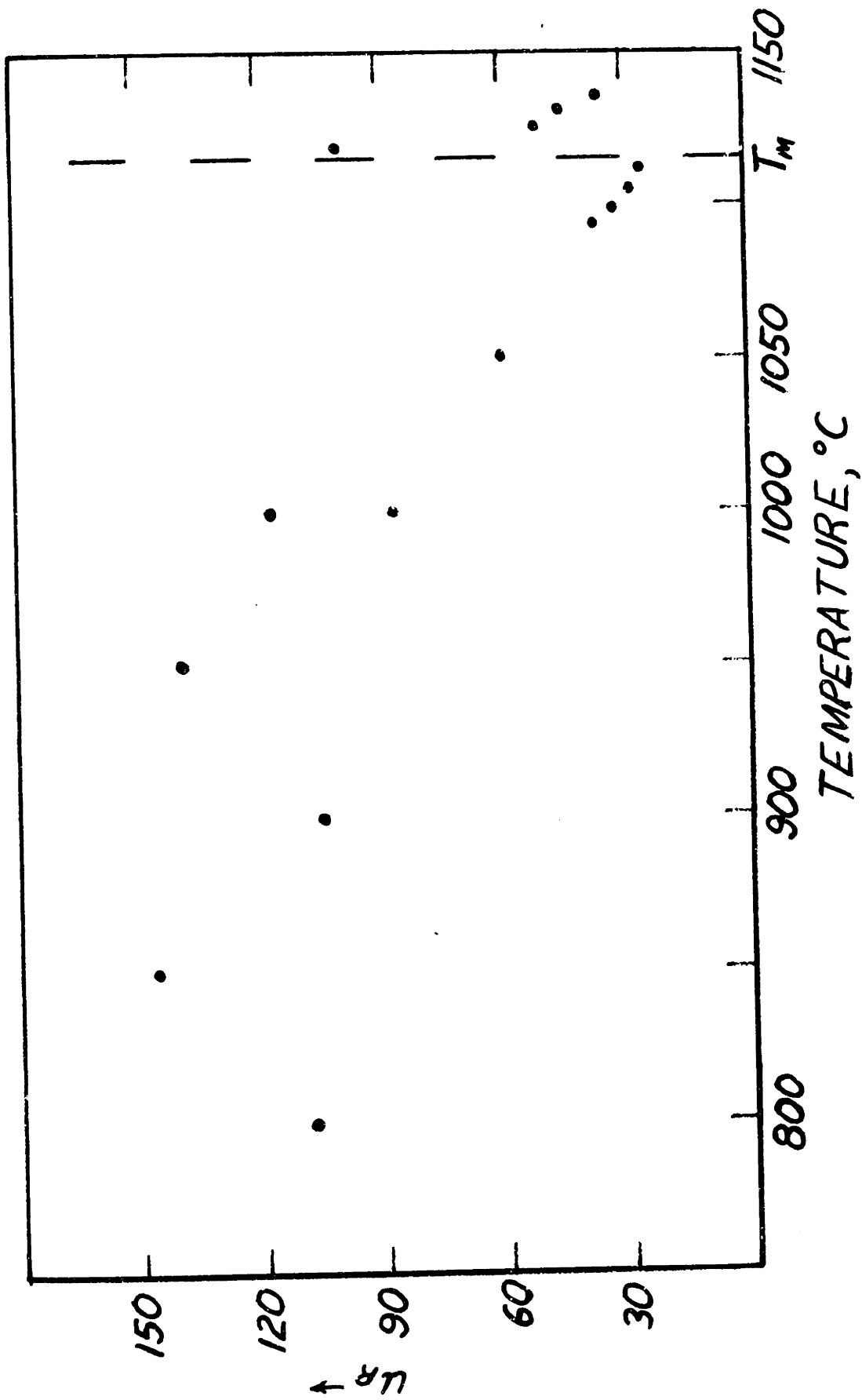Figure D.1: Reduced growth rate variation with temperature for Series 2 and 3 glasses.

Figure D.2: Reduced growth and reduced melting rate variation with temperature for Series 4 glasses.

Table D.1

Reduced Growth Rates of Series 2-4 Glasses

glass	temp., °C	u (cms/sec)	η (poises)	$[1-\exp(\frac{-L\Delta T}{RTT_E})]$	u_R
2A	1107	2.28×10^{-6}	3.71×10^5	0.00848	100
2A	1102	3.70×10^{-6}	3.89×10^5	0.0133	109
2A	1097	3.75×10^{-6}	4.47×10^5	0.181	92
2A	1093	5.00×10^{-6}	4.68×10^5	0.0219	107
2A	1050	6.83×10^{-6}	1.07×10^6	0.063	116
2B	1000	6.27×10^{-6}	2.69×10^6	0.112	150
2B	950	2.97×10^{-6}	7.59×10^6	0.161	140
2B	900	1.79×10^{-6}	2.24×10^7	0.212	189
2B	850	4.58×10^{-6}	7.76×10^7	0.265	134
2B	800	1.51×10^{-7}	2.76×10^8	0.318	131
3A	1110	5.14×10^{-7}	3.45×10^5	0.00470	32
3B	1110	7.20×10^{-7}	3.45×10^5	0.00470	44
3A	1106	7.44×10^{-7}	3.70×10^5	0.00944	29
3C	1102	1.71×10^{-6}	3.89×10^5	0.0133	51
3A	1101	1.83×10^{-6}	4.06×10^5	0.0142	52
3B	1101	8.85×10^{-7}	4.06×10^5	0.0142	25
3A	1050	3.32×10^{-6}	1.07×10^6	0.0630	57
3B	1050	4.40×10^{-6}	1.07×10^6	0.0630	75
3C	1050	6.40×10^{-6}	1.07×10^6	0.0630	109
3A	1000	3.98×10^{-6}	2.69×10^6	0.112	96
3B	1000	2.25×10^{-6}	2.69×10^6	0.112	54
3C	1000	4.12×10^{-6}	2.69×10^6	0.112	99
3A	950	2.34×10^{-6}	7.59×10^6	0.161	98
3B	950	1.15×10^{-6}	7.59×10^6	0.161	54
3C	950	1.84×10^{-6}	7.59×10^6	0.161	87
3B	900	1.01×10^{-6}	2.24×10^7	0.212	107
3D	850	3.33×10^{-7}	7.76×10^7	0.265	98
3D	800	7.88×10^{-8}	2.76×10^8	0.318	68

Table D.1 (cont'd)

glass	temp., °C	u (cms/sec)	n (poises)	$[1-\exp(\frac{-L\Delta T}{RTT})]_E$	u_R
4A	1111	3.67×10^{-7}	3.35×10^{5}	0.00564	26
4A	1105	7.09×10^{-7}	3.81×10^{5}	0.01039	28
4A	1099	1.23×10^{-6}	4.20×10^{5}	0.0160	32
4A	1094	1.69×10^{-6}	4.49×10^{5}	0.0207	37
4A	1050	3.54×10^{-6}	1.07×10^{6}	0.0630	60
4A	1000	3.65×10^{-6}	2.69×10^{6}	0.112	88
4B	1000	4.88×10^{-6}	2.69×10^{6}	0.112	117
4B	950	2.96×10^{-6}	7.59×10^{6}	0.161	139
4B	900	9.88×10^{-7}	2.24×10^{7}	0.212	105
4A	850	4.93×10^{-7}	7.76×10^{8}	0.265	146
4A	800	1.36×10^{-7}	2.76×10^{8}	0.318	108

Table D.2

Reduced Melting Rates

glass	temp., $^{\circ}C$	u (cms/sec)	η (poises)	$[1-\exp(\frac{-L\Delta T}{RTT_E})]$	u_R
1C and 1D	1122	2.52×10^{-6}	2.86×10^5	.00560	129
1C and 1D	1127	5.11×10^{-6}	2.60×10^5	.0102	130
1C and 1D	1132	6.95×10^{-6}	2.42×10^5	.0148	114
1C and 1D	1137	1.12×10^{-5}	2.21×10^5	.0194	128
4A	1119	9.54×10^{-7}	2.95×10^5	.00280	100
4A	1125½	1.68×10^{-6}	2.69×10^5	.00884	51
4A	1131	2.56×10^{-6}	2.42×10^5	.0139	45
4A	1136	2.93×10^{-6}	2.28×10^5	.0185	36

APPENDIX E

Melting Germanium Dioxide Glass

The optimum and very elaborate melt schedule listed below satisfies two conditions important in producing a glass free of extrinsic growth problems: (1) chlorine and water impurities are diminished; and (2) a minimum concentration of new impurities is introduced into the glass.

This melting is carried out in the mullite tube furnace described in Section IV.1 (Figure E.1) with the entrance port for gas flowing into the furnace at the end of the tube opposite that at which vacuum is drawn and with a valve next to the vacuum port which can be opened to flow gas through the furnace. New refractories within the mullite tube should be used for each melt.

Melt Schedule

1. GeO_2 powder heated overnight at $100^{\circ}C$ under a vacuum below 1.0 mm. Hg.

2. Sample heated to $1150^{\circ}C$, taking at least two hours in the temperature range $950^{\circ} - 1116^{\circ}C$, under the same vacuum.

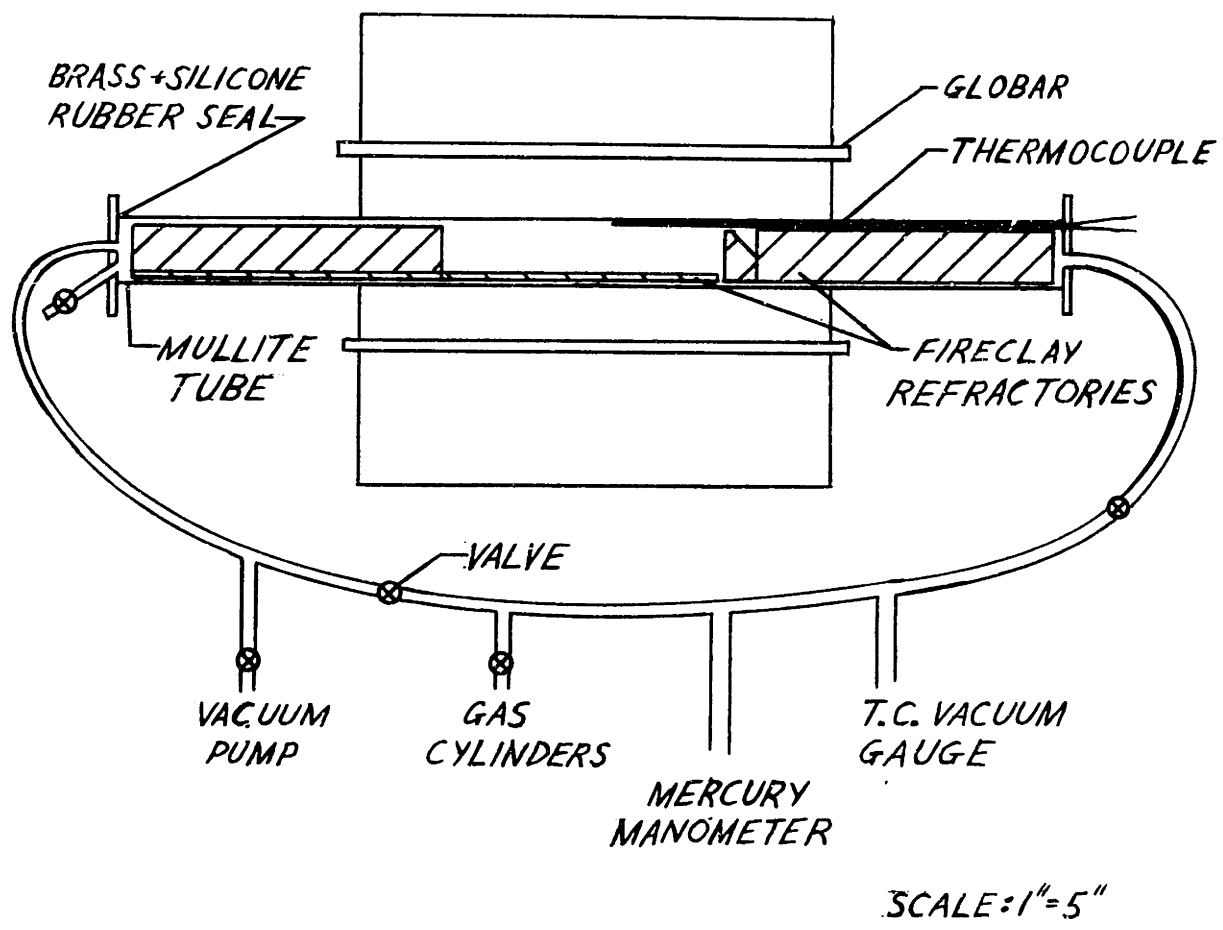3. Sample held at $1150^{\circ}C$ for four hours under the same vacuum.

Figure E.1: Glass-melting furnace (cross-section).

4.   Oxygen or dry nitrogen atmosphere substituted

over the glass at the end of the four hour

soak at 1150°C but before Step (5) commences

(gas flowed through the furnace at a rate of

2-5 ambient temperature cubic feet per hour).

5.   Sample heated to 1400°C with gas flowing.

6.   Sample held at 1400°C overnight with gas

flowing.

7.   Glass quenched to room temperature, then

annealed for two hours at 480°C.

If oxygen is used in melting, the glass produced is
more nearly stoichiometric and no higher in water content.
To produce a perfectly stoichiometric glass, additional
heat treatments in pure oxygen at 1150 - 1200°C are best.

APPENDIX F

Determination of the Temperature of an Advancing
Crystal-Liquid Interface

In order to ascertain that the temperature at the crystal-liquid interface was negligibly different from the furnace temperature during crystal growth in this study, crystals were grown past a thermocouple bead embedded in germanium dioxide glass. A very fine (.001") Pt(10% Rh)-Pt thermocouple was embedded in a glass by remelting laths of Glass 2C with the thermocouple bead placed between them. Melting was done in a small platinum foil boat (1/4" x 1/4" x 1/8" deep) at 1200°C in air for two hours. The thermocouple bead was embedded about 1/16" into the glass.

The glass was crystallized in the same platinum boat in air at 1000°C using the furnace described in Section III.3. The thermocouple leads were only 4" long, so they were joined to chromel wire by crimping with platinum foil; this cold junction was approximately 100° cooler than the furnace hot zone. The chromel wires extended out of the furnace to a Leeds and Northrup Speedomax H Strip Chart Recorder set at its maximum sensitivity (full scale = 0.667 mv.).

The intrinsic crystal growth rate at 1000°C for the glass used is approximately 2 microns/min., near the

maximum intrinsic growth rate measured in this study. The glass was held at $1000^{\circ}C$ for ten hours and was fully crystallized. No crystals nucleated on the platinum foil; the crystals grew from the air interface down. No irregularities in the crystalline morphology were observed around the thermocouple bead.

The recorder plotted the temperature at the thermocouple bead for the full ten hours of the experiment. No abrupt change in the temperature of the thermocouple junction was detectable, either at the time calculated to be that when the interface reached the thermocouple junction, or at any other time in the run. The recorder did show that the temperature within the glass specimen did gradually vary by $\pm 0.5^{\circ}C$ with a period of over one hour; the form of this fluctuation suggests that it is due to gradual changes in temperature either in the hot zone or at the cold junction.

BIOGRAPHICAL NOTE

The author was born in New York City on October 30, 1942. He graduated from Teaneck High School, Teaneck, New Jersey, in 1960. With his completion of a combined engineering-liberal arts program in 1965, the author received a B.S. in Ceramics and an A.B. in Liberal Arts, both with High Honors, from Rutgers University.

Since September, 1965, the author has been a graduate student in the Department of Metallurgy of the Massachusetts Institute of Technology. He is married and the father of a one-year old son.

The author is a member of Keramos, the American Ceramic Society, Tau Beta Pi, and Phi Beta Kappa.

He has reported on this work at the Sixth International Symposium on Reactivity in Solids in August 1968 and at the 1969 Annual Meeting of the American Ceramic Society.